UNIVERSITY OF CALIFORNIA SAN DIEGO

Climate, Circulation, Chlorophyll, and Cetaceans in the California Current

A dissertation submitted in partial satisfaction of the requirements for the degree Doctor of Philosophy

in

Oceanography

by

Kimberly Ashlyn Avery Giddings

Committee in Charge:

Simone Baumann-Pickering, Co-chair
Peter J.S. Franks, Co-chair
Andrew Barton
David Demer
Carolyn Kurle
Jennifer Mackinnon

2022

The Dissertation of Kimberly Ashlyn Avery Giddings is approved, and it is acceptable in quality and form for publication on microfilm and electronically.

University of California San Diego

2022

DEDICATION

To Matt, without whom none of this would have been possible.
And to Tabitha, the best-worst cat/coauthor.

EPIGRAPH

There's nothing wrong with enjoying looking at the surface of the ocean itself,

except that when you finally see what goes on underwater,

you realize that you've been missing the whole point of the ocean.

Staying on the surface all the time is like going to the circus

and staring at the outside of the tent.

---Dave Barry

TABLE OF CONTENTS

LIST OF FIGURES

LIST OF TABLES

ACKNOWLEDGEMENTS

First and foremost, I would like to thank Simone Baumann-Pickering and Peter Franks. I could not have asked for a better pair of advisors! Thank you both for your mentorship and guidance over the past few years. I would not be the scientist I am today if it wasn't for you. I would also like to thank the members of my committee for their help and insightful guidance throughout the thesis process.

My thesis would not have been possible without the hard work of everyone involved in the CalCOFI program, especially the many visual observers who helped us with the marine mammal visual surveys. In particular, thank you to Katherine Whittiker and Arial Brewer for teaching me how to do visual observations at sea, and to Bruce Thayre for helping to wrangle the CalCOFI data into a more manageable form.

A huge thanks goes out to the community of students, scientists, and support staff who make SIO such a supportive space. Thanks to the members of the Franks Lab (Bryce Inman, Jessica Garwood, Eric Orenstein, Mara Freilich, Kelley McBride, Taylor Hernandez, and Shailja Gangrade), the Scripps Acoustic Ecology Lab (Alba Berga, Annebelle Kok, Anne Simonis, Jenny Trickey, Ally Rice, Morgan Ziegenhorn, Natalie Posdaljian, Ella Kim, Michaela Alksne, Anna Krumpel, Shelby Bloom, Catalina Aguilar, and Grace Teller), as well as the broader MBARC group (John Hildebrand, Sean Wiggins, Kait Fraiser, Marie Roch, Josh Jones, Macey Rafter, Regina Guazzo, Rebecca Cohen, Eric Snyder, Vanessa Zobell, Amada Leu, and Eva Hidalgo Pla) for your help!

I owe a huge debt of gratitude to the friends I made during graduate school, especially Sarah Schwenck, Sarah Maher, Eadoh Reshef, Jill Fader, Emilia Chamberlain, and CJ Collins for

support, great memories, game nights and, of course, our snack mountains. And to Camille Pagniello, the best nemesis anyone could ask for.

Thanks to my family, especially my mom, for all your support over the years. Thanks to my husband, Matt, who has been a constant source of strength. Thank you for standing by me through thick and thin; I would not have gotten through this without you. I am looking forward to what comes next for us! And thanks to my cats Tabitha and Ser Pounce. Ser Pounce, thanks for ensuring that I took a break once a day for snuggles. Tabitha, thanks for sitting by me during every zoom meeting and always offering input whenever I typed anything. I didn't always agree with your edits, but I appreciate that you cared enough to try and help me with my work.

Chapter 2, in full, is a reprint of the material as it appears in Giddings, A., Franks, P. J. S. & Baumann-Pickering, S. 2022. Monthly to Decadal Variability of Mesoscale Stirring in the California Current System: Links to Upwelling, Climate Forcing, and Chlorophyll Transport. *J Geophys Res Oceans* 127. The dissertation author was the primary investigator and author of this paper.

Chapter 3, in part, is currently being prepared for submission for publication of the material. Giddings, A., Franks, P. J. S. & Baumann-Pickering, S. The dissertation author was the primary investigator and author of this paper.

Chapter 4, in part, is currently being prepared for submission for publication of the material. Giddings, A., Franks, P. J. S. & Baumann-Pickering, S. The dissertation author was the primary investigator and author of this paper.

VITA

2014 Bachelor of Science, Biochemistry and Biology: Molecular, Cellular, and Developmental
Summa cum laude
University of Washington

2016 Master of Science, Marine Biology
Scripps Institution of Oceanography
University of California San Diego

2022 Doctor of Philosophy, Oceanography
Scripps Institution of Oceanography
University of California San Diego

PUBLICATIONS

Giddings, A., Franks, P. J. S. & Baumann-Pickering, S. 2022. Monthly to Decadal Variability of Mesoscale Stirring in the California Current System: Links to Upwelling, Climate Forcing, and Chlorophyll Transport. *J Geophys Res Oceans* **127**

Thompson, A. R., Bjorkstedt, E., Bograd, S. J., Fisher, J. L., Hazen, E., Leising, A., Santora, J., Satterthwaite, E.V., Sydeman, W. J., Alksne, M., Auth, T.D., Baumann-Pickering, S., Bowlin, N.M., Burke, B., Dewar, H,. Field, J., Garfield, N.T., **Giddings, A**., Georicke, R., Hildebrand, J., Horton, C.A., Jacobson, K., Jacox, M., Jahncke, J., Johns, M., Jones, J., Kudela, R. M., Melin, S., Morgan, C.A., Nickels, C., Orben, R.A., Porquez, J., Portner, E. J,. Preti, A., Robertson, R., Rudnick, D. L., Sakuma, K. M., Schroeder, I.D., Snodgrass, O .E., Thompson, S.A., Trickey, J.E., Warzybok, P., Watson, W., & Weber, E. D. 2022. State of the California Current Ecosystem in 2021: Winter Is Coming?. *Frontiers in Marine Science*, 1721. *In press*

Weber, E.D., Auth, T.D., Baumann-Pickering, S., Baumgartner, T. R., Bjorkstedt, E. P., Bograd, S. J., Burke, B. J., Cadena-Ramírez, J. L., Daly, E. A., de la Cruz, M., Dewar, H., Field ,J. C., Fisher, J. L., **Giddings, A**., Goericke, R., Gomez-Ocampo, E., Gomez-Valdes, J., Hazen, E. L., Hildebrand, J., Horton, C. A., Jacobson, K. C., Jacox, M. G., Jahncke, J., Kahru, M., Kudela, R. M,. Lavaniegos, B. E., Leising, A., Melin, S. R., Miranda-Bojorquez, L. E., Morgan, C. A., Nickels, C. F., Orben, R. A., Porquez, J. M., Portner, E. J., Robertson, R. R., Rudnick, D. L., Sakuma, K. M., Santora, J. A., Schroeder, I. D., Snodgrass, O. E., Sydeman, W. J., Thompson, A. R., Thompson, S. A., Trickey, J. S., Villegas-Mendoza, J., Warzybok, P., Watson, W., & Zeman, S.M. 2021 State of the California Current 2019–2020: Back to the Future With Marine Heatwaves? Front. Mar. Sci. 8:709454. doi: 10.3389/fmars.2021.709454

Cavole, L. ., Demko, A. M. , Diner, R. E. , **Giddings, A.**, Koester, I., Pagniello, C. M. L. S., Paulsen, M.-L. , Ramiirez-Valdez, S. M. , Schwenck, S. M. , Yen, N. K. , Zill, M. E. , and Franks, P. J. S.. 2016. Biological impacts of the 2013-2015 warm-water anomaly in the Northeast Pacific: Winners, losers, and the future. Oceanography 29: 273–285. (*Authors listed alphabetically*)

ABSTRACT OF THE DISSERTATION

Climate, Circulation, Chlorophyll, and Cetaceans in the California Current

by

Kimberly Ashlyn Avery Giddings

Doctor of Philosophy in Oceanography

University of California San Diego, 2022

Simone Baumann-Pickering, Co-chair
Peter J.S. Franks, Co-chair

The California Current System (CCS) is a highly productive Eastern Boundary Upwelling System. Cross-shore transport of recently-upwelled water is driven by horizontal stirring from mesoscale eddies, fronts, and filaments; these shift surface productivity away from the narrow upwelling zone inshore. In addition to driving the cross-shore transport of upwelled water, mesoscale features form pelagic habitats through biophysical coupling, which create regions where the physical convergences and enhanced growth of plankton attract higher trophic levels, forming important foraging habitats for many organisms. Climate variability, such as the El Niño Southern Oscillation, can drive large changes in physical processes such as upwelling that can reverberate through the ecosystem. This dissertation combines a 25-year daily record of finite-size Lyapunov exponents (FSLEs), a measure of mesoscale features and horizontal stirring, with 21 years of

satellite-derived chlorophyll *a* measurements and 18 years of quarterly marine mammal visual surveys in order to investigate the links between mesoscale features, chlorophyll, climate variability, and cetaceans in the CCS. The annual cycle of mesoscale stirring was found to be highly correlated with seasonal upwelling in the CCS. Interannual fluctuations in mesoscale stirring showed 3-12 month lagged responses to climate indices, with the CCS oscillating out of phase with waters west and north. Chlorophyll *a* was positively correlated with FSLE intensity in a meridional band 200-600 km offshore, indicating enhanced offshore transport during periods of intense mesoscale activity. Annual cetacean sightings (scaled for effort) were stable for most species but scaled sightings of Dall's porpoise and Pacific white-sided dolphin decreased over the study period. During the 2014-2016 marine heatwave, scaled sightings of common and Risso's dolphins increased, an effect driven by unusually large groups in the winter and spring of 2015. Scaled sightings of several dolphin species were higher during El Niño events, whereas blue and fin whale summertime scaled sightings were higher during La Niñas. Blue, fin, and humpback whales showed habitat partitioning through geographic separation and species-specific preferences for certain mesoscale features. Dall's porpoises had a strong association with rare, intense FSLEs. These results demonstrate the important couplings of climate, mesoscale dynamics, and organism distributions in the CCS.

Chapter 1
Introduction

The California Current is a highly productive Eastern Boundary Upwelling System, supporting dynamic food webs featuring numerous top predators and commercially important fisheries. The California Current's high production is enabled by nutrient-rich water brought up to the surface from depth through wind-driven upwelling. Starting in March or April, the prevailing alongshore winds shift to the equatorward direction, driving offshore surface Ekman transport, which causes the upwelling of cold, nutrient-rich water at the coast (Chereskin, 1995). Additional upwelling is caused through wind stress curl-driven Ekman pumping (Hickey, 1979; Rykaczewski & Checkley, 2008). Upwelling-favorable winds continue to dominate until the fall.

The upwelled water is advected offshore from the location of upwelling through horizontal stirring by mesoscale features (Chabert et al., 2021). Mesoscale features include fronts, eddies, and filaments that exist on spatial scales from tens to hundreds of kilometers, and on temporal scales on the order of weeks to months (McGillicuddy, 2014). Mesoscale filaments and non-linear eddies entrain and channel upwelled, high-chlorophyll water offshore (Chelton et al., 2011; Chenillat et al., 2016; Combes et al., 2013; Gruber et al., 2011; Nagai et al., 2015; Zaba et al., 2021; Zhao et al., 2021). Thus, mesoscale features expand the geographic influence of coastally upwelled water through cross-shore transport. In addition to driving the cross-shore transport of upwelled water, mesoscale features form pelagic habitats through

biophysical coupling, which creates regions where the physical convergences and enhanced growth of plankton attract higher trophic levels (Godø et al., 2012; Lehahn et al., 2017; Scales et al., 2014). Mesoscale features are therefore important foraging habitats for many organisms.

One method of studying mesoscale features involves the use of Lagrangian coherent structures (LCS), which form a framework of attracting and repelling manifolds (Haller, 2015). LCSs demarcate eddies, fronts, and filaments in the ocean, and thus are a useful tool for studying mesoscale and submesoscale features (Beron-Vera et al., 2008; Harrison & Glatzmaier, 2012; d'Ovidio et al., 2004). In oceanography, two methods are commonly used to find LCSs: finite-time Lyapunov exponents (FTLEs) and finite-size Lyapunov exponents (FSLEs) (Haller, 2015; d'Ovidio et al., 2004). Lyapunov exponents are the rate of exponential separation of fluid parcels that were initially separated by an infinitesimally small distance; this rate of separation is averaged over infinite time (d'Ovidio et al., 2004). Because of the inherent difficulties of averaging over infinite time, finite-time and finite-size Lyapunov exponents are used instead. In oceanography, both are typically calculated from the geostrophic velocity field, based on horizontal gradients of sea-surface height anomalies. In this dissertation, I used FSLEs, which have been shown to be robust to noise in the data and are able to resolve structures at a finer scale than the oceanic velocity field (Haller, 2015; Hernández-Carrasco et al., 2011). FSLEs (λ, equation 1) are computed via the time τ required for particles at position **x**, initially separated by finite distance δ_0 at time t, to separate to finite distance δ_f (d'Ovidio et al., 2004).

$$\lambda(\mathbf{x},t,\delta_0,\delta_f) \equiv \frac{1}{\tau}\log\frac{\delta_f}{\delta_0}$$

FSLE ridges highlight LCSs in the fluid flow (D'Ovidio et al. 2004; Haller 2015). When integrated backwards in time, FSLE ridges show attracting LCSs (areas of high convergence) (Haller 2015), such as eddies, fronts, and filaments.

There has been a recent increase in interest as to how oceanic LCSs structure pelagic ecosystems – from phytoplankton to top predators such as cetaceans and humans. For example, LCSs were correlated with spatial differences in phytoplankton community structure (d'Ovidio et al., 2010) and patch densities among krill (Maps et al. 2015). This spatial structuring of the ecosystem by LCSs is exploited by higher trophic levels. Great frigatebirds in the Mozambique channel tracked LCSs during travel as well as while foraging (Kai et al., 2009), while southern elephant seals tracked LCSs during intense foraging bouts, although not during travel (Penna et al., 2015). LCSs are associated with increased catches and higher profits in certain fisheries such as tuna and swordfish (Scales et al., 2018; Watson et al., 2018). It is therefore not surprising that the risk of fisheries bycatch is increased at LCS (Scales et al., 2018).

Studies have shown that cetaceans, particularly baleen whales, are often associated with LCSs. For example, Mediterranean fin whales are closely associated with LCSs in the summer (Cotte et al., 2011), while the presence of LCSs was correlated with an increase in residence time of fin whales in the California Current (Scales et al., 2017). Large groups of humpback whales off South Africa were associated with LCSs, as were blue whales near Monterey Bay (Cade et al., 2021). Additionally, the feeding rates of blue whales off Monterey Bay were shown to increase at LCSs (Fahlbusch et al., 2022). Studies such as these have primarily been conducted by tracking organisms with satellite tags, which give fine-scale movement information but are limited in duration and sample size: they may miss important long-time-

scale, large-spatial-scale processes that affect both the structure and intensity of mesoscale features, and the associations of top predators with those structures.

Decadal to interannual climate variability such as the Pacific Decadal Oscillation (PDO), the North Pacific Gyre Oscillation (NPGO), and the El Niño Southern Oscillation (ENSO) can drive large changes in ecosystems through physical processes such as changes in upwelling and change in the strength of the California Current (Bograd et al., 2009; Chenillat et al., 2012; Cordero-Quirós et al., 2019; Jacox et al., 2014). These bottom-up effects can reverberate throughout the ecosystem, affecting everything from primary producers to top predators such as cetaceans.

The goal of this dissertation is to understand the links between climate variability, mesoscale features, chlorophyll, and cetaceans. In Chapter 2, 25 years of daily FSLE data and 21 years of satellite-derived chlorophyll data from the California Current System are used to investigate the links between climate variability, mesoscale stirring, and offshore chlorophyll transport. In Chapter 3, correlations between climate variability and cetacean presence are calculated using 18 years of quarterly marine mammal visual surveys, including 9 species of marine mammal. In Chapter 4, the associations of 6 species of cetaceans with mesoscale features are investigated using FSLEs, satellite-derived eddy positions, and marine mammal visual surveys. Each chapter is written as a stand-alone document for publication in a scientific journal and thus there may be repetition within the introduction and methods sections.

Chapter 2

Monthly to decadal variability of mesoscale stirring in the California Current System: links to upwelling, climate forcing, and chlorophyll transport.

The California Current System (CCS) is a highly productive eastern boundary upwelling system. Cross-shore transport is driven by horizontal stirring from mesoscale (and submesoscale) eddies, fronts, and filaments, that shift surface productivity away from the narrow upwelling zone inshore. Using an unprecedented 25-year daily record of finite size Lyapunov exponents (FSLEs), we characterize the spatial and temporal patterns of mesoscale stirring in the entire CCS and quantify correlations of FSLEs with satellite-measured chlorophyll *a* and climate indices. The annual cycle of mesoscale stirring is highly correlated with seasonal upwelling in the CCS, with bands of intense FSLE propagating to the west during the upwelling season. Annual cycles and interannual variability in FSLE intensity were most prominent to the north and inshore of the CCS, and weaker to the south and offshore. Interannual fluctuations in mesoscale stirring showed 3-12 month lagged responses to climate indices, with the CCS oscillating out of phase with waters west and north. Chlorophyll *a* is positively correlated with FSLE intensity in a meridional band 200-600 km offshore, consistent with the hypothesis that increased horizontal stirring increases the export of chlorophyll *a* to offshore waters. When mesoscale stirring intensifies during negative phases of the PDO and

ONI we predict greater offshore transport of organic carbon. Our analyses underscore the predictability of annual and interannual cycles of mesoscale stirring and chlorophyll *a* fluxes in the CCS, and their links with climate indices.

2.1 Introduction

Eastern boundary upwelling systems (EBUS) are among the most productive marine ecosystems in the world (Pauly & Christensen, 1995). This high production is enabled by the wind-driven upwelling of nutrient-rich water from depth into the euphotic zone which stimulates new primary production. This in turn supports dynamic food webs and economically important fisheries. The upwelled water is acted upon by physical forces – advected away from the point of upwelling, subducted away from the euphotic zone, or mixed into other water masses. In EBUS, horizontal stirring – the kinematic mixing of water masses and tracers driven by the flows associated with fronts, filaments, and eddies, and their interactions – moves upwelled water away from its coastal origin, increasing the input of nutrient-rich and high chlorophyll water to oligotrophic waters offshore, while reducing the availability of this nutrient-rich water inshore (Gruber et al., 2011; Rossi et al., 2009). Because of its impact on the spatial distribution of upwelled, highly productive waters, it is critical to understand what drives variability in horizontal stirring in EBUS.

The California Current System (CCS) is a highly productive EBUS off the west coast of Canada, the United States, and Mexico. The upwelling season in the CCS begins in March or April, during the "spring transition" – when winds shift to predominantly upwelling-favorable (equatorward) – and continues throughout the summer until the "fall transition" in October or November, which marks the cessation of mainly upwelling-favorable winds

(Checkley & Barth, 2009). Upwelling-favorable winds drive offshore Ekman transport at the coast, which causes the upwelling of cold, nutrient-rich water (Chereskin, 1995). Offshore, wind stress curl also drives Ekman pumping, which causes additional upwelling (Hickey, 1979; Rykaczewski & Checkley, 2008).

Recently upwelled water does not remain isolated in the narrow band along the coast in which it was upwelled. Instead, horizontal stirring moves the water offshore, increasing the offshore influence of coastally upwelled water (Chabert et al., 2021). Fronts of upwelled water in the CCS tend to be baroclinically unstable, and frequently form both cyclonic and anticyclonic eddies that propagate westward at a speed of approximately 2 km/day (Kurian et al., 2011). This creates a highly nonlinear field of mesoscale features formed by interacting eddies and fronts that drives horizontal stirring (Waugh & Abraham, 2008). Non-linear eddies entrain upwelled, high-chlorophyll waters and advect and stir them westward from the coast throughout the current's domain (Chelton et al., 2011; Chenillat et al., 2016; Combes et al., 2013; Gruber et al., 2011; Zhao et al., 2021). Mesoscale filaments also efficiently channel high-chlorophyll upwelled waters offshore (Nagai et al., 2015; Zaba et al., 2021). As the recently upwelled water is advected offshore, fixed organic carbon is exported out of the euphotic zone (Chabert et al., 2021). Thus, these mesoscale features are the sites of enhanced carbon sequestration and fluxes of food to the deep sea, far away from where the production initially occurred (Chabert et al., 2021; Stukel et al., 2017).

Beyond inducing cross-shore transport of upwelled water, mesoscale features function as important pelagic habitats. Biophysical coupling at mesoscale fronts and eddies creates regions where the physical convergences and enhanced growth of plankton attract higher

trophic levels (Godø et al., 2012; Lehahn et al., 2017; Scales et al., 2014). Thus, mesoscale features are important foraging habitat for many organisms, including endangered and commercially important species.

There are several ways to quantify horizontal stirring and mesoscale activity. In this study, we use finite size Lyapunov exponents (FSLEs), a Lagrangian technique for measuring horizontal stirring in the ocean (d'Ovidio et al., 2004, 2009). Briefly, FSLEs (λ, equation 1) are computed as the time τ required for particles at position x, initially separated by finite distance δ0 at time t, to separate to a final finite distance δf:

$$\lambda(\mathbf{x},t,\delta_0,\delta_f) \equiv \frac{1}{\tau}\log\frac{\delta_f}{\delta_0}$$

When calculated backwards-in-time, FSLE values show areas of high horizontal convergence characteristic of fronts, filaments, and the edges of eddies (d'Ovidio et al., 2004, 2009). Thus, FSLEs serve as both a measure of stirring in the ocean and as a measure of mesoscale activity.

Because FSLEs are calculated from currents derived from cloud-penetrating satellite altimetry, they are particularly useful for detecting fronts and eddies in cloudy regions where other methods of front or eddy detection (such as ocean color or sea surface temperature gradients) would result in missing data. FSLEs have been shown to be robust to noise in the data and are able to resolve structures at a finer scale than the oceanic velocity field from which they are calculated (Haller, 2015; Hernández-Carrasco et al., 2011). Furthermore, FSLEs are ecologically relevant markers. For example, FSLEs were correlated with spatial differences in

phytoplankton community structure (d'Ovidio et al., 2010), and have been shown to correlate with important foraging habitat for top predators such as frigatebirds in the Mozambique channel (Kai et al., 2009), fin whales in the Mediterranean (Cotte et al., 2011), and elephant seals in the Southern Ocean (Della Penna et al., 2015).

Past studies have examined horizontal stirring or mesoscale activity in the CCS. Rossi et al. (2009) investigated the correlations between horizontal stirring in the CCS and chlorophyll from 2000-2005 using FSLEs. Keister and Strub (2008) characterized mesoscale activity in the northern and central CCS from 1992-2006 using sea surface height anomalies. More recent research by Martínez-Moreno et al. (2021) used sea surface height and eddy kinetic energy to investigate mesoscale activity over the entire north Pacific but did not isolate the CCS for analysis. Other research on mesoscale activity in the CCS has quantified specific mesoscale features such as fronts (Kahru et al., 2018) or eddies (Chenillat et al., 2018; Kurian et al., 2011; Stegmann & Schwing, 2007) in isolation, rather than exploring mesoscale activity as a whole.

Our study builds upon previous work by investigating horizontal stirring and mesoscale activity over larger spatial and longer temporal domains in order to answer the following questions: (1) What are the spatial and temporal patterns in mesoscale horizontal stirring in the CCS? (2) What drives mesoscale horizontal stirring on an annual basis? (3) What drives interannual variability in mesoscale horizontal stirring? (4) Does mesoscale horizontal stirring increase carbon export from the nearshore to the offshore region?

Here we analyze a daily 25-year record (1994-2018) of FSLE intensities over the entire CCS (20°N to 51°N and -110°W to -133°W). Our analyses reveal a strong link of FSLE

intensity to the annual cycle of coastal upwelling. We found considerable spatial and temporal variability in horizontal stirring throughout the CCS at annual and sub-annual timescales. We show that FSLE intensity positively correlated with chlorophyll *a* approximately 200-600 km offshore along the study domain. Our study also revealed that the coupled FSLE-chlorophyll *a* system has a predictable, lagged response to climate indices, with important implications for predictions of offshore carbon export.

2.2 Materials and Methods

2.2.1 Data

We obtained backwards-in-time FSLEs from Archiving, Validation, and Interpretation of Satellite Oceanography (https://www.aviso.altimetry.fr/). FSLE intensities were calculated based on the methodology of d'Ovidio et al. (2004) using geostrophic velocity fields calculated from satellite altimetry. In the FSLE dataset, the initial separation δ0 is 0.02 degrees and the final separation distance δf is 0.6 degrees. The maximum integration window is 200 days; if the separation time exceeds this window, a value of 0 is given. The FSLEs are run backwards-in-time to show regions of convergence. The FSLE fields have a temporal resolution of 1 day and a spatial resolution of 0.04°.

We analyzed a time series of daily FSLEs spanning a twenty-five-year period from January 1, 1994 through December 31, 2018. We restrict our analyses to the CCS region, which we defined as the area from 20°N to 51°N and -110°W to -133°W.

Monthly composite chlorophyll concentration measurements from satellite observations were obtained as the reprocessed L4 (ESA-CCI) monthly product from Copernicus Marine

Environment Monitoring Service (https://marine.copernicus.eu/). This dataset spans September 1997 through December 2018 and has a 4 km spatial resolution.

The Coastal Upwelling Transport Index (CUTI) was used to estimate upwelling. The CUTI gives estimates of vertical transport into and out of the surface mixed layer using regional ocean reanalysis products (Jacox et al., 2018). The CUTI is given every 1° of latitude from 31°N to 47°N in the CCS. We obtained the monthly means of daily CUTI values maintained by Mike Jacox (https://mjacox.com/upwelling-indices/).

Three monthly climate indices were used in this study: the Pacific Decadal Oscillation (PDO), the North Pacific Gyre Oscillation (NPGO), and the Ocean Niño index (ONI). The PDO is defined as the first mode of variability of sea surface temperature and reflects a basin-wide pattern of climate variability in the north Pacific (Mantua et al., 1997). The PDO index was created using the Extended Reconstructed Sea Surface Temperature (ERSST) dataset. We obtained the time series of the PDO from the NOAA National Centers of Environmental Information (https://www.ncdc.noaa.gov/teleconnections/pdo/).

The NPGO is defined as the second mode of variability in sea surface height anomaly. Reflecting variations in the intensity of North Pacific gyre circulation, it is correlated with variation in salinity, nitrogen, and chlorophyll *a* concentrations in the North Pacific (Di Lorenzo et al., 2008). We obtained the NPGO time series from (http://www.o3d.org/npgo/npgo.php) maintained by Emanuele Di Lorenzo.

The Oceanic Niño Index (ONI) is defined as the 3-month running mean of ERSST.v5 SST anomalies in the Niño 3.4 region (5°N – 5°S and 120° – 170°W). The ONI is a measure of

the El Niño Southern Oscillation (ENSO) events, El Niño and La Niña, which have far-reaching consequences in the CCS (Checkley & Barth, 2009). We obtained the ONI record from the NOAA National Weather Service Climate Prediction Center (https://origin.cpc.ncep.noaa.gov/products/analysis_monitoring/ensostuff/ONI_v5.php).

2.2.2 Methods

2.2.2.1 Empirical orthogonal functions

We used empirical orthogonal functions (EOFs) to analyze spatial modes of variability in FSLEs. EOFs reduce data complexity and extract dominant modes of spatial variability along with the principal components (PCs) of the time series. The total variance in the dataset is given by the sum of the EOFs, with the number of modes equal to the length of the timeseries. We calculated EOFs in MATLAB using scripts from the Climate Data Toolbox (Greene et al., 2019). We averaged the FSLEs spatially into 1°x1° bins and into annual averages before computing the EOFs in order to focus on interannual variability. The 1°x1° spatial averages were sufficient for identifying the relevant spatial patterns of variability. EOFs with finer spatial and temporal resolution are provided in the supplemental materials (Supplemental Figure 1). Similar overall patterns were seen in EOFs 1 and 2 when calculated with higher spatial resolution (Supplemental Figure 2.1, a and b), but differences in EOF 2 were seen when calculated with higher temporal resolution (Supplemental Figure 2.1, f and j).

2.2.2.2 Regions

To analyze trends in FSLEs in both space and time, we defined 3°x3° regions within the CCS based on the spatial patterns of variability shown in the annual EOFs. We selected eight

illustrative regions: four inshore-offshore pairs within the CCS, centered at 45.5°N, 38.5°N, 31.5 °N and 27.5°N. Inshore regions were centered at 126.5°W, 126.5°W, 119.5°W, and 116.5°W, respectively and offshore region were centered at 129.5°W, 129.5°W, 122.5°W, and 119.5°W, respectively (Figure 2.1a). The four northern regions (45.5°N inshore & offshore; 38.5°N inshore & offshore) straddle the regions where EOF 1 oscillated out of phase to the north and south of a node. Two other pairs of regions (38.5°N inshore & offshore; 31.5°N inshore & offshore) were chosen in the areas where the phase of EOF 2 differed inshore and offshore at those latitudes. The southernmost boxes (27.5°N inshore & offshore) were chosen to explore the temporal patterns off Punta Eugenia and to compare those FSLE fluctuations with those to the north. Analyses were performed with more comprehensive spatial coverage of 3°x3° regions, but were not included in the main text, as they did not provide additional insight (Supplemental Figures 2.2 and 2.3).

2.2.2.3 Wavelet analysis

We conducted wavelet analyses to decompose the regional FSLE timeseries in both time and periodicity. As a signal-processing technique for the analysis of non-stationary timeseries data (Grinsted et al., 2004; Torrence & Compo, 1998), wavelets allow us to quantify the local intensities of given periodicities throughout the timeseries. We used the continuous wavelet transform from the cross wavelet and wavelet coherence toolbox (Grinsted, 2021) with a Morlet wavelet with 1/12 octave. This was applied to the daily timeseries of FSLEs averaged within each 3° x 3° region defined above.

2.2.2.4 Correlation analysis with climate indices and chlorophyll a

To quantify spatial correlations between FSLE and the CUTI, we calculated the average FSLE intensity within 1°x1° regions for each month to obtain a single annual cycle for each region. We calculated the correlations between average FSLE intensity in each region and the average CUTI for that month at the corresponding latitude. Because the CUTI is given only from 31°N to 47°N, we restricted our analysis to these latitudes.

To quantify spatial correlations between FSLE and the three climate indices, and between FSLE and the chlorophyll *a* time series, we calculated monthly averages of the absolute value of the FSLE intensity within 1° x 1° regions. Correlations between the monthly time series of FSLE intensity for each region and the monthly climate index or the monthly average chlorophyll *a* concentration were obtained using MATLAB. We also calculated the monthly anomalies of the absolute value of FSLE intensity and chlorophyll *a* concentration by subtracting the mean monthly values from the monthly time series. Correlations between monthly FLSE intensity anomalies and monthly chlorophyl a anomalies were obtained using MATLAB.

2.2.2.5 Lagged correlation analysis with climate indices

To quantify potential lags in the response of FSLE to climate forcing, we explored the cross-correlations of the 1° x 1° binned, monthly averaged FSLE from 2.2.4 with monthly values of the ONI, PDO and NPGO indices. All time series were de-meaned, and normalized by their standard deviations to give approximately normal distributions with zero mean and standard deviation of one. Cross-correlations were run using “xcorr” from MATLAB, with the

"unbiased" flag. Confidence limits were calculated by running cross-correlations of 1000 iterations of pairs of normally distributed random time series the same length as the data (300 months). These time series were also de-meaned and normalized by their standard deviations. The cross-correlations were sorted at each time lag to find the central 95% of the data , giving the upper 97.5 percentile, and the lower 2.5 percentile for each lag. These values were used to detect significant departures from random cross-correlations at the 5% level in the FSLE and climate data.

Because we were exploring FSLE responses to climate indices, we only quantified lags that showed the FSLE to follow the climate index. We found the first significant correlation (positive or negative) at a lag equal to or greater than 0 months. The lag (months) and the correlation were then plotted as maps in the study region.

All maps were plotted using the "M_Map" package in MATLAB (Pawlowicz, n.d.).

2.3 Results

2.3.1 Average spatial patterns

The 25-year mean intensity of FSLE had an alongshore maximum approximately 50-250 km offshore in a band extending from 24°N to 43°N (Figure 2.1b). This alongshore region of elevated mean FSLE intensity showed regionally intensified maxima west of Oregon and northern California (35°N to 43°N), and off Punta Eugenia (27°N) in Baja. South of 34°N the mean FSLE was less intense than off Oregon and northern California. Persistently low mean FSLE values formed in the Southern California Bight (30°N to 33°N), and north of 44°N.

Offshore of the band of enhanced mean FSLE intensity, mean FSLE values were persistently low. Inshore of the intense FSLE band, within approximately 50 km of the coast, mean FSLE values were relatively low; this was particularly evident south of Point Conception and in the Southern California Bight. The variance of FSLE followed the spatial pattern of the mean FSLE, showing that regions with the highest mean FSLE values also had the highest variance of FSLE (Figure 2.1c).

The first two EOFs explained 30.6% of the variance of the annual-averaged 1° x 1° FSLE (Figure 2.1e and f). EOF 1 showed two regions of high amplitude. The first, a region extending from 24° N to 43° N, coincided with the high mean FSLE and the core of the CCS (Figure 2.1e). As we show later, the zero contour of EOF 1 provides a robust demarcation line of the response of FSLE intensity to climate indices. We thus define a boundary we call "$EOF1_0$" as the zero contour of EOF 1. The FSLEs in waters to the north, west, and south of $EOF1_0$ fluctuated out of phase with the FSLEs within the $EOF1_0$ contour. EOF 2 showed two regions of high FSLE fluctuation amplitude that oscillated out of phase: one north of 40°N extending west from the coast, and one south of 26°N and west of 126°W (Figure 2.1f). In the study region, EOF 2 showed more spatial variability than EOF 1. There was a general trend of positive EOF 2 along the coast, with highest values to the north, interspersed with regions oscillating out of phase. EOF 2 tended to be negative offshore, but there were regions in the Southern California Bight and west of northern California that were also negative.

A similar overall pattern was seen in the first EOF calculated with higher spatial and temporal resolution (Supplemental Figure 2.1a, e, and i), although each individual EOF explained a lower percentage of the variability in the system as spatial and temporal resolution

increased. The second EOF calculated with daily temporal resolution (Suplemental Figure 2.1f and j) showed an inshore and offshore region that both oscillate out of phase with a central region. Differences of this pattern from the EOF 2 derived from annually-averaged data likely reflect the influences of seasonal or other short-term variability.

2.3.2 FSLE annual variability

FSLE intensity had a strong annual cycle (Figure 2.2a-d; Supplemental Figure 2.4). Mean FSLE intensity increased rapidly from April to May. This springtime increase in the FSLE intensity began inshore, with local regions of particularly enhanced FSLE off Northern California and Oregon (35° N to 43° N), and separately to the south off Punta Eugenia (27° N). This coastal region of high FSLE activity intensified over the summer, spreading westward (offshore), and to the north and south. The FSLE intensity and spatial extent reached a maximum in September, particularly in the two regions of persistently enhanced FSLE. After September, the FSLE intensities across the region slowly decreased to their minima, found between February and April. In the southwest corner of our study domain, FSLE intensity remained relatively low throughout the year. The annual cycle of FSLE intensity in this region was out of phase with that of the CCS, with intensity peaking in April-May, and decreasing through November.

2.3.3 FSLE and upwelling

To quantify the relationship of the CUTI and FSLE intensity at a given latitude, we averaged the monthly FSLEs in 1° x 1° regions into a single annual cycle (Figure 2.2e-h; Supplemental Figure 2.5) and calculated correlations of the CUTI and FSLE over a range of

monthly time lags. FSLE intensity near the coast was positively correlated with the mean CUTI from one month prior (Figure 2.2e). This band of intense positive correlation detached from the coast and moved westward (offshore) as we increased the time lag between the FSLEs and the CUTI. A band of intense negative correlation forms near the coast with a six-month lag when the CUTI and mean FSLE intensity are out of phase. This band likewise propagates westward behind the band of positive correlation.

2.3.4 FSLE seasonal-interannual variability

Guided by the EOFs (Figure 2.1e and f), we selected eight regions for detailed analysis of the seasonal to interannual variability of FSLE intensities. Each region was 3° x 3°, with pairs of regions "inshore" and "offshore" at a given latitude. Regions were designated by latitude at the center of the region (45.5°N, 38.5°N, 31.5 °N and 27.5°N), and inshore ("I", centered at 126.5°W, 126.5°W, 119.5°W, and 116.5°W, respectively) or offshore ("O" centered at 129.5°W, 129.5°W, 122.5°W, and 119.5°W, respectively) (Figure 2.1a). Within each region we created time series of the absolute value of the average monthly FSLE intensity and the average monthly chlorophyll *a* concentration (Figure 2.3, d-k), for comparison to time series of climate indices.

Mean FSLE intensity was greater in the inshore region than in the offshore region of a given latitude. This difference was greatest between the inshore and offshore regions centered at 38.5°N. In contrast, mean FSLE intensity in 31.5-I was only slightly stronger than in 31.5-O. The region with highest FSLE intensity was 38.5-I (Figure 2.3f). However, the region with the highest chlorophyll *a* was the northernmost inshore region, 45.5-I (Figure 2.3d). A strong

annual periodicity in FSLE intensity was evident in regions 38.5-I and 38.5-O whereas the time series in the other regions showed less consistent annual periodicities.

To quantify the relative contributions of different periodicities to the observed FSLE fluctuations, we used continuous wavelet transforms of the daily time series of spatial-averaged FSLE intensity in each region (Figure 2.4). The wavelet transforms showed that FSLE fluctuations in the northern inshore region 38.5-I (Figure 2.4d) were continuously dominated by the annual cycle, as expected from examination of the time series. This annual cycle was present farther to the north in region 45.5-I (Figure 2.4b), but less consistently than at 38.5-I. Interannual (longer period) variability was significant for only a brief period (1997-2009) in region 45.5-I but was never statistically significant in region 38.5-I during the study period.

To the south, 31.5-I and 27.5-I (Figure 2.4f and h) had times when the annual cycle dominated. However, strong annual periodicity at 31.5-I and 27.5-I was not continuous throughout the time series: the annual cycle consistently dominated at 31.5-I before 2013, and consistently after 2005 at 27.5-I. During other times, the fluctuations of FSLE at the annual period were weaker in power or not statistically significant. Fluctuations with periods shorter than one year were often statistically significant, but periods greater than one year rarely reached statistical significance in these regions.

Offshore, the annual cycle was less evident than in the inshore regions, with FSLE fluctuations spread over both shorter (seasonal) and longer (interannual) periods. That being said, the two northernmost offshore regions, 45.5-O and 38.5-O (Figure 2.4a and c), showed a pronounced and continuous annual cycle in addition to longer- and shorter-period fluctuations.

There was no pronounced annual cycle at either of the southern regions (31.5-O, 27.5-O, Figure 2.4e and g).

The continuous wavelet transforms showed similar patterns in regions beyond the eight presented in the main text (Supplemental Figures 2.2 and 2.3). The strong annual signal appeared in the regions north of 37°, while to the south the intensity of the annual cycle was variable. In general, offshore regions had greater power at periods longer than one year compared with the corresponding inshore region, although this discrepancy was less evident south of 26.5°N.

2.3.5 FSLE variability and relation to climate indices: zero time lag

We compared monthly and 1° x 1° averaged FSLE data to monthly averaged climate indices: ONI, PDO and NPGO (Figure 2.5a-c). The ONI was positively correlated with FSLE intensity north of 43°N (Figure 2.5a) with small, scattered regions of positive correlation south of 43°N.

The FSLE fluctuations were positively correlated with the PDO north of 43°N; patches of negative correlation with the PDO were found south of 43°N (Figure 2.5b). Small, local positive correlations between the PDO and FSLEs were found in offshore waters to the southwest of the study domain. Regions of statistically significant negative correlation between the FSLE and NPGO were found offshore near the northern and southern boundaries of the study domain west of 125°W (Figure 2.5c). Statistically significant positive correlations were limited largely to the central offshore region of the CCS east of 128°W.

2.3.6 FSLE variability and relation to climate indices: lagged response

Time lags in the response of FSLE to climate forcing were quantified as the first time lag showing significant correlation (positive or negative) in cross-correlations of the 1° x 1° binned, monthly averaged FSLE and monthly values of the ONI, PDO and NPGO indices. Only lags with the FSLE following changes in the climate index were explored. We plotted the maps of the first significant lag (Figure 2.5d-f) as well as the correlation between the FSLE and climate indices at this lag (Figure 2.5g-i) with the $EOF1_0$ boundary superimposed.

The correlation and time-lag maps of FSLE with climate indices showed persistent spatial patterns that were highly correlated with the FSLE EOF 1 pattern (Figure 2.5d-i). We found the $EOF1_0$ contour to accurately bound regions of similar correlation sign and lag (Figure 2.5). We therefore define three regions containing similar climate-related variability (Figure 2.1c): the CCS (inshore of $EOF1_0$), the Western Offshore Region (west of $EOF1_0$), and the Northern Region (north of $EOF1_0$, approximately 43°N).

In the CCS, fluctuations of FSLE were negatively correlated with the ONI, with a ~1 year lag (Figure 2.5d and g). The Western Offshore Region had similar lags, but a positive correlation with the ONI, showing that the CCS and Western Offshore Region oscillated exactly out of phase with each other. The Northern region was strongly positively correlated with the ONI, but at shorter (~3-7 month) lags than in the CCS or Western Offshore Region.

The spatial correlation patterns of FSLE with the PDO were similar to the ONI: negative in the CCS, and positive in the Western Offshore and Northern Regions (Figure 2.5e and h).

However, the lags in the CCS and Western Offshore Region were shorter than with the ONI – about 3-6 months, with the CCS and Western Offshore Region again fluctuating out of phase with each other. The Northern Region was strongly positively correlated with the PDO at ~1 year lags – longer than the lags in the CCS or Western Offshore Region.

The lagged correlations of the FSLE intensities in CCS with the NPGO were largely non-significant, though the significant correlations were positive, with 2-3 month lags (Figure 2.5f and i). FSLE fluctuations in the Western Offshore and Northern Regions were negatively correlated with the NPGO at 4-5 month lags – the opposite pattern to those seen with the ONI and PDO.

The general patterns of the spatial correlations showed the CCS and Western Offshore regions to fluctuate out of phase with each other: high FSLE intensity in the CCS correlated with low FSLE intensity in the Western Offshore Region. The time lags in these two regions were similar for a given climate index, with the FSLEs showing longer lags to the ONI than the PDO. The Northern Region fluctuated in phase with the Western Offshore Region, but with different time lags to a given climate index.

2.3.7 Relationship of FSLE with remotely sensed chlorophyll *a*

Mean chlorophyll *a* was highest within 200 km of the coast in the study domain, with decreased values along the coast of the Southern California Bight, south to Punta Eugenia (approximately 34°N to 29°N, Figure 2.6a). The high chlorophyll *a* values extended farther offshore (more than 200 km) north of Point Conception (34.5°N) than to the south (less than 100 km). Chlorophyll *a* variance was highest along the coast, with the smallest offshore extents

found from the Southern California Bight south to Punta Eugenia (Figure 2.6b). A region of high mean chlorophyll *a* and chlorophyll *a* variability separated from the coast at Point Conception, extending southeast, following the direction of the coast from the north.

Significant high, positive correlations between monthly chlorophyll *a* concentration and monthly FSLE were found in a meridional band extending about 200-600 km from the coast (Figure 2.6c). Significant negative correlations were found close to the coast along the Baja Peninsula, extending north into the Southern California Bight, and ending at Point Conception. A region of weaker negative correlation of chlorophyll *a* and FSLE intensity was found in the Western Offshore Region.

Monthly FSLE and chlorophyll *a* anomalies showed a region of significant positive correlation over a similar region as above, from approximately 200-600 km offshore (Figure 2.6d). The majority of the area with positive correlations was inshore of $EOF1_0$ in the CCS, though this band of positive correlation extended to the south of $EOF1_0$. The region of positive correlation was sparser in the Northern Region than the correlations without the seasonal cycles removed. The significant correlations between the FSLE and chlorophyll *a* anomaly time series were strongest and covered the greatest spatial extent with no time lag; time lags greater than 2 months resulted in very few areas with statistically significant correlations (Supplemental Figure 2.6).

2.4 Discussion

In this study, we have used a 25-year time series of daily FSLE intensities to investigate spatial and temporal variability of horizontal stirring in the CCS. We built upon the results of

other studies that have analyzed horizontal stirring or mesoscale activity in the CCS, though they used smaller spatial and shorter temporal domains than this study (e.g., Chabert et al., 2021; Chenillat et al., 2016; Combes et al., 2013; Keister & Strub, 2008; Rossi et al., 2009).

The spatial pattern of the first EOF of FSLE intensity led us to define three large regions in our study domain that behaved similarly on interannual time scales; these regions were bounded by the zero contour of EOF 1, denoted $EOF1_0$. The CCS was found inshore of $EOF1_0$; the Western Offshore Region was offshore to the west, and the Northern Region to the north of ~43°N. $EOF1_0$ bounded a domain similar to the region of maximum of mean eddy kinetic energy calculated by Combes et al. (2013) from satellite-measured sea surface height. We showed that this spatial pattern also accurately describes the spatial patterns of correlations and time lags of FSLE intensity with the ONI, PDO, and NPGO climate indices.

Within the CCS, the annual cycle of FSLE intensity has a seasonal low in late winter (January-February) and a seasonal high in late summer (August-September), matching the seasonal pattern in mesoscale activity found through other methods (Keister & Strub, 2008). Although other work has suggested that the relationship between upwelling and mesoscale activity is complex and non-linear (Keister & Strub, 2008), we found the annual cycle of FSLE intensity in the CCS to be highly linearly correlated with cycles of upwelling intensity.

Our analyses identified considerable spatial heterogeneity of seasonal-annual fluctuations of FSLE within the CCS. This spatial heterogeneity did not align with the traditional divisions of the CCS into the northern, central, and southern California Current (e.g., Checkley & Barth, 2009). North of ~36°N, FSLE variability showed a persistently strong

annual cycle; the dominance of the annual periodicity broke down south of 36°N, where its intensity varied considerably with time (see Supplemental Figures 2.2 and 3 for additional regions). The timings of the loss of strong annual periodicity were not obviously related to fluctuations of climate indices. This spatial and temporal variability in the seasonal-annual periodicities of horizontal stirring is lost when data are aggregated over the entire domain (e.g., Rossi et al., 2009). Therefore, it is important to be careful with generalizations regarding mesoscale stirring when considering large areas: important variability at smaller spatial and temporal scales may be overlooked.

The northern extent of the CCS defined by $EOF1_0$ was found at ~43°N – the latitude of Cape Blanco (Figure 2.1b). This confirms prior work that found low mesoscale activity north of Cape Blanco (Combes et al., 2013; Keister & Strub, 2008), but intense stirring to the south. Cape Blanco is an important topographic feature in the CCS, marking the separation point of the coastal upwelling jet from the coast (Barth et al., 2000; Checkley & Barth, 2009). South of this point, the narrow coastal jet moves offshore and becomes unstable with increasing meanders and mesoscale features (Checkley & Barth, 2009). This separation may be due to changes in upwelling at the cape: upwelling strength is lowest to the north of Cape Blanco and has decreased over time from 1988-2010. South of Cape Blanco upwelling is much stronger and has increased in strength over the same time period (Jacox et al., 2014). It is likely that the spatial patterns of mean FSLE intensity – high to the south of Cape Blanco, low to the north – are driven by the changes in upwelling dynamics north and south of Cape Blanco.

We found persistent spatial variability in the correlations between horizontal stirring, chlorophyll *a*, and climate forcing. Consistent with the hypothesis that horizontal stirring

increases primary productivity in offshore waters (Chabert et al., 2021; Chenillat et al., 2016), chlorophyll *a* was positively correlated with FSLE intensity in a meridional band approximately 200-600 km offshore. This band of high positive correlation is apparent both with and without the annual cycles of FSLE and chlorophyll *a*, consistent with stronger offshore advection of chlorophyll *a* during times of intense FSLE activity. These were well predicted by lagged responses of the CCS FSLE intensity to the ONI and PDO: negative ONI and PDO led to stronger FSLE activity and more extensive offshore advection of chlorophyll *a*.

2.4.1 FSLE and the annual upwelling cycle

Seasonal variation in horizontal stirring and mesoscale activity (FSLE intensity) in the CCS mirrors seasonal variation in the upwelling cycle (Checkley & Barth, 2009). There are two annual transitions in the CCS: a "spring transition" in March-April that marks the onset of persistently upwelling-favorable winds, and a "fall transition" in October-November which marks the cessation of upwelling-favorable winds (Checkley & Barth, 2009). This cycle was clearly reflected in the seasonal pattern of FSLE intensity (Figure 2.2a-d). FSLE intensity increased within a month following the spring transition; the intensity of FSLE decreased following the fall transition as the wind-driven energy dissipated.

Much of the mesoscale activity in the CCS is forced through baroclinic instability, a process that converts the potential energy of a stratified fluid to kinetic energy that drives mesoscale activity (Marchesiello et al., 2003). We hypothesized that if mesoscale features were primarily caused by baroclinic instabilities in the upwelling front, as suggested by the seasonal pattern of FSLE intensity as well as previous studies (Marchesiello et al., 2003; Narimousa &

Maxworthy, 1989), we would see a straightforward relationship of the correlations of FSLE intensity and upwelling (as measured by the CUTI) at increasing time lags with increasing distance from shore as the mesoscale features propagated westward. That is, the farther from shore, the greater the time lag needed to find a positive correlation between the CUTI and FSLE intensity. This is precisely the relationship that we found (Figure 2.2e-h). Close to the shore, FSLE intensity is highly correlated with the CUTI from 1-month prior (Figure 2.2e). At larger time lags between the CUTI and the FSLE intensity, the band of high positive correlation separates from the shore and moves westward, expanding north and south in the process (Figure 2.2f-h). At a seven-month lag, FSLE intensities nearshore are out of phase with the CUTI and have strong negative correlations (which also propagate westward through time). This suggests that the annual FSLE cycle is initiated by the onset of upwelling-favorable coastal winds, consistent with the hypothesis that baroclinic instabilities in the upwelling front are a primary source of mesoscale features in the CCS. This coastal band of high mesoscale activity then propagates westward, approximately at the speed of a Rossby wave (Chelton & Schlax, 1996), leading to the westward-propagating band of high lagged correlation between the FSLE and CUTI.

2.4.2 FSLE variability and climate indices

The spatial pattern of EOF 1 showed the CCS to fluctuate out of phase with the Western Offshore Region and the Northern Region. The east-west change in the sign of EOF 1 could be interpreted as a standing wave, with a node where EOF 1 = 0. When EOF 1 is positive in the CCS, it is negative offshore and to the north, and vice versa. In our analyses of FSLE correlations with climate indices, it became apparent that the spatial correlation and lagged

correlation patterns were very similar to EOF 1. Indeed, the nodal contour of EOF 1 = 0 (which we call $EOF1_0$) accurately reproduced the zero-correlation contour of FSLE and climate indices, showing a persistent pattern of opposite correlation sign in the CCS relative to the Western Offshore and Northern Regions. This correlation pattern is consistent with a standing-wave response of FSLE intensity in the CCS relative to offshore and northern waters: as FSLE intensity increases in the CCS, it decreases in offshore and to the north, oscillating around the $EOF1_0$ contour.

While the CCS has considerable heterogeneity at seasonal and annual timescales (as seen in our wavelet analysis, Figure 2.4), at interannual timescales the CCS appears to be coherent, with consistent responses to climate forcing (Figure 2.5; Table 1). The CCS and Western Offshore Region oscillated out of phase with each other but responded to climate forcing on similar time scales. In contrast, the Northern Region oscillated out of phase with the CCS, and responded at different time lags than the CCS to both the ONI and the PDO. Although the zero-lag correlations of climate indices with FSLE intensity were non-significant over most of the study domain, the positive and negative correlation patterns that were significant largely matched the time-lagged spatial correlation patterns and FSLE EOF 1.

The correlation pattern between FSLE intensity and the NPGO is opposite those found with both the PDO or ONI. The PDO has been in a negative (cool) phase for most (1998-2014) of the 25-year timeseries (1994-2018) under investigation. Keister and Strub (2008) found that mesoscale energy was low during years of negative PDO, despite strong upwelling-favorable winds, in the area of 35°-50°N, an area that overlaps with the regions we call the northern CCS and the Northern Region. Their result is consistent with the positive correlations we observed

between the PDO and FSLE intensity in the Northern Region; however, it is inconsistent with the negative correlation we saw in the CCS. Fluctuations in the NPGO are associated with changes in physical and biological parameters in the CCS, such as salinity, nutrient concertation, and chlorophyll *a* (Di Lorenzo et al., 2008). A recent study by Chabert et al. (2021) found that the NPGO was positively correlated with the advection of upwelled water offshore in the central CCS, which they hypothesized was due to the influence of climate forcing on mesoscale activity. We found positive correlations in some areas of the central CCS, although the correlations in the CCS region were largely non-significant. The negative correlation between lagged FSLE intensity and the ONI index in the CCS is consistent with prior studies showing that mesoscale activity is lower in the CCS during El Niño events (strongly positive ONI values), and higher during La Niña events (strongly negative ONI values) (Chabert et al., 2021).

One hypothesis for the difference in time lags between FSLE and ONI in the Northern Region compared with the CCS and Western Offshore Region is that these regions are influenced by different ENSO forcing mechanisms. ENSO events can affect the northeastern Pacific through atmospheric teleconnections (which drive local forcing through changes in wind patterns and operate on daily or weekly timescales), or through oceanic teleconnections (Kelvin-wave driven remote forcing which operates on timescales of weeks to months) (Alexander et al., 2002; Sprintall et al., 2020). Modelling work has suggested that ENSO effects in the Northern Region are driven primarily through local forcing from atmospheric teleconnections (Hermann et al., 2009), whereas remote forcing is more important for the physical response in the CCS (Frischknecht et al., 2015). Because responses to local forcing

would tend to be more rapid, we would anticipate shorter time lags to the ONI in the Northern Region relative to the CCS or Western Offshore regions – which is what we observed.

2.4.4 Cross-shore advection of chlorophyll *a*

Horizontal stirring by mesoscale features will tend to advect upwelled, high-chlorophyll *a* waters offshore, which increases the horizontal spatial extent of upwelled waters (Chabert et al., 2021; Combes et al., 2013; Rubio et al., 2018; Zhao et al., 2021). We found that FSLE intensity is positively correlated with chlorophyll *a* offshore in the CCS. Given that both FSLEs and chlorophyll *a* have an annual cycle, we tested these correlations using data both with (Figure 2.6c) and without (Figure 2.6d) the annual cycle. The positive correlation regions were almost identical, supporting the hypothesis that horizontal stirring advects high-nutrient, high-chlorophyll *a* water offshore: intense horizontal stirring results in increased carbon export offshore, regardless of periodicity.

Previous studies have shown that the advection of upwelled water by mesoscale features and horizontal stirring reduces primary production nearshore in EBUS as nutrient-rich water is advected offshore from the location of upwelling (Gruber et al., 2011; Hernández-Carrasco et al., 2014; Rossi et al., 2009). We thus expected to see a region of negative correlation between FSLE intensity and chlorophyll *a* near the coast, reflecting the reduction in primary productivity due to horizontal stirring. Instead, we found that the corelations between FSLE intensity and chlorophyll *a* nearshore were largely non-significant. We found three locations with negative correlations between FSLE intensity and chlorophyll *a*: the Southern California Bight, Baja California, and the Western Offshore Region (Figure 2.6c). We believe that these patterns are

due to time lags in the annual cycle of FSLEs and chlorophyll *a* in these regions: the correlations were non-significant with the annual cycle removed (Figure 2.6d). It is worth noting that the FSLEs used in this study were calculated from satellite altimetry, which has poor performance in the coastal zone (Vignudelli et al. 2019); this may obscure the relationship between horizontal stirring and chlorophyll *a* within 20 km or less of the coast.

One important caveat with the satellite-measured chlorophyll *a* concentrations used in this study is that remote sensing can only detect chlorophyll shallower than the first optical depth of the ocean; this depth depends on the vertical light attenuation in the water column at that location (Blondeau-Patissier et al., 2014). In oligotrophic waters, the subsurface chlorophyll maximum is often near the base of the euphotic zone (~4.6 optical depths) and therefore invisible to satellite-based observations of ocean color (Blondeau-Patissier et al., 2014; Cullen, 2015). In these waters, fluctuations in primary production driven by mesoscale features are often greatest near the base of the euphotic zone (Chenillat et al., 2015) and undetectable by satellites. Zhao et al. (2021) estimated that mesoscale eddies trap and transport up to half of the global chlorophyll *a*, but that much of this transport occurs subsurface; relying only on satellite-derived estimates of chlorophyll *a* reduced their modeled chlorophyll *a* concentration by more than half. There may be important correlations between FSLEs and subsurface chlorophyll *a* that cannot be detected using satellite data. Data acquired by underwater gliders (e.g., California Underwater Glider Network [CUGN]) will help to increase our understanding of the mechanisms coupling horizontal stirring with fluctuations in subsurface primary productivity.

Given our findings linking climate indices to FSLE intensity and FSLE intensity to chlorophyll *a,* we can predict how climate variability will impact the offshore advection of high-chlorophyll *a* waters, and thus carbon export (Table 1). Positive ONI will lead to a decrease in horizontal stirring in the CCS 9-12 months later, and thus a reduction in carbon export to the open ocean. Positive PDO will also lead to a decrease in horizontal stirring in the CCS, but with only a 3-6 month lag. We expect that the positive phase of the NPGO will lead to increased horizontal stirring in the CCS, although the effect may be weak, and not present throughout all areas of the CCS. While these correlations hold for the time period in question, care is warranted when predicting responses of chlorophyll *a* to changes in climate indices because of potential nonstationarities in the underlying climate variability due to climate change (Litzow et al., 2020).

2.4.3 FSLE variability and the strength of the CCS

Flow into the CCS is modulated by the strength of the North Pacific Current (NPC); when the westward-flowing NPC nears the North American continent, it bifurcates into the Alaska Current (AC) to the north and the CCS to the south. Flow through the CCS is modulated both by the overall strength of the NPC as well as the percentage of the NPC that flows into the CCS relative to the AC (Freeland, 2006). The flow varies both seasonally and interannually. One intriguing possibility suggested by our data is that there is a link between interannual fluctuations in the strength of the flow in the CCS as shown by the climate indices, and interannual fluctuations in the intensity of mesoscale activity in the CCS.

Seasonally, transport to the CCS from the NPC is greatest in August and September and weakest in January-February (Hristova et al., 2019). Seasonal fluctuations of the relative flow of the NPC into the CCS vs the AC match well with the seasonal FSLE intensity data: greater flow from the NPC into the CCS corresponds with the time period of greatest FSLE intensity and spatial extent, while greater flow into the AC relative to the CCS corresponds with the time period of lowest FSLE intensity and spatial extent in the CCS.

Interannually, the NPC can vary in strength (the so-called 'breathing mode') or vary in the relative partitioning of water between the AC and the CCS (the so-called 'bifurcation mode') (Freeland, 2006). The positive phase of the PDO is associated with an increase in flow from the NPC into the AC relative to the CCS; a similar phenomenon occurs during El Niño events (positive ONI) (Hristova et al., 2019). Fluctuations in the NPGO reflect fluctuations in the volume transport of the NPC, driving correlated fluctuations in transport in both the AC and the CCS (Lorenzo et al., 2008). Though the mechanisms through which they influence transport in the CCS vary, a positive NPGO and a negative PDO are both associated with increased transport volume in the CCS and are both correlated with increased FSLE intensity in CCS. Conversely, a positive NPGO and a negative PDO are both associated with decreased FSLE intensity in the Northern Region, where the NPC bifurcates into the CCS and the AC. We hypothesize that an increase in transport to the CCS may be associated with lower FSLE intensities in the Northern Region but higher FSLE intensities in the CCS.

Unfortunately, the dynamic connections between the volume of transport in the CCS and mesoscale activity have not been extensively researched; most research has focused on wind-driven coastal upwelling as the driver of mesoscale dynamics in the system (e.g., Keister

& Strub, 2008). Most of the mesoscale activity in the CCS is thought to be caused by baroclinic instabilities in the current (Capet et al., 2008; Marchesiello et al., 2003). These baroclinic instabilities convert mean potential energy to the eddy kinetic energy that drives mesoscale stirring; strong currents have high eddy kinetic energy (Capet et al., 2008; Ferrari & Wunsch, 2009). Thus, changes in the mean flow through the CCS have the potential to modulate mesoscale stirring through changes in potential and kinetic energy, and may be a source of interannual variability. Flow into the CCS from the NPC is predicted to increase by 2100 (Toste et al., 2019); if transport into the CCS is related to the intensity of horizontal stirring, we would likewise expect an increase in FSLE intensity and horizontal stirring in the CCS over time. An increase in horizontal stirring could lead to an increase in carbon export from the coastal ocean as nutrient-rich waters are advected away from coastal upwelling zones (Chabert et al., 2021). Research is required to determine what influence, if any, the volume of transport has on horizontal stirring and mesoscale activity in the CCS.

2.5 Conclusions

In this study we have documented the spatial and temporal variability of horizontal stirring in the CCS using a 25-year data set of daily FSLE intensities. The mean intensity of FSLEs over the study period had a maximum approximately 50-250 km offshore from 34°N to 43°N, with a secondary area of high intensity off Punta Eugenia (27°N). Low mean FSLE intensities were seen in the Southern California Bight, 30°N to 33°N, as well as north of 43°N. Mean FSLE values were persistently low farther offshore as well as close to the coast. EOF analyses showed that the first two EOFs explained 30.6% of the annual-averaged spatial and temporal variance.

FSLE intensity is strongly seasonal over the entire spatial domain, but the seasonal cycle was particularly apparent in the CCS. FSLE intensity was lowest in the late winter (February-March) and highest in the late summer/early fall (August-September). FSLE intensity began to increase starting in the inshore region in April and May; the region of intensified FSLEs spread westward as the overall FSLE intensity increased, until September, when both the overall intensity and the spatial extent of intense FSLEs peaked.

The annual cycle of FSLE intensity is highly correlated with upwelling as measured by the CUTI. The region of positive FSLE-CUTI correlation propagates westward (offshore) with increasing time lags between the CUTI and FSLEs. After a seven-month lag, FSLE intensities nearshore are out of phase with the CUTI and have negative correlations (which also propagate westward through time).

At seasonal to annual periods, fluctuations in FSLE intensity were heterogeneous in the study domain. The annual cycle was the dominant period of variability in the north of the CCS across the entire time series, but was only intermittently prominent in the southern CCS. The timing of the disappearance of the annual periodicity in FSLE intensity was not correlated among subregions of the CCS, and was not obviously correlated with fluctuations in climate indices.

Chlorophyll *a* was positively correlated with FSLE intensity approximately 200-600 km offshore, both with and without the annual cycle. This is consistent with the hypothesis that increased horizontal stirring drives increased offshore transport of chlorophyll *a* in EBUS.

In response to fluctuations in climate indices, the CCS and Western Offshore Regions fluctuated out of phase, like a standing wave, with shorter lags to the PDO than the ONI. Negative ONI and PDO were correlated with more intense FSLE activity in the CCS, and greater offshore transport of chlorophyll *a*. This relationship may be driven by interannual variations of the flow into the CCS from the North Pacific Current.

2.6 Acknowledgments

The authors would like to thank the anonymous reviewers whose suggestions greatly improved the manuscript. The authors declare no conflicts of interest. Partial support for this project was provided by the US Office of Naval Research, Michael Weise; and the US Pacific Fleet, Chip Johnson.

Chapter 2, in full, is a reprint of the material as it appears in Giddings, A., Franks, P. J. S. & Baumann-Pickering, S. 2022. Monthly to Decadal Variability of Mesoscale Stirring in the California Current System: Links to Upwelling, Climate Forcing, and Chlorophyll Transport. *J Geophys Res Oceans* 127. Used with permission. The dissertation author was the primary investigator and author of this paper.

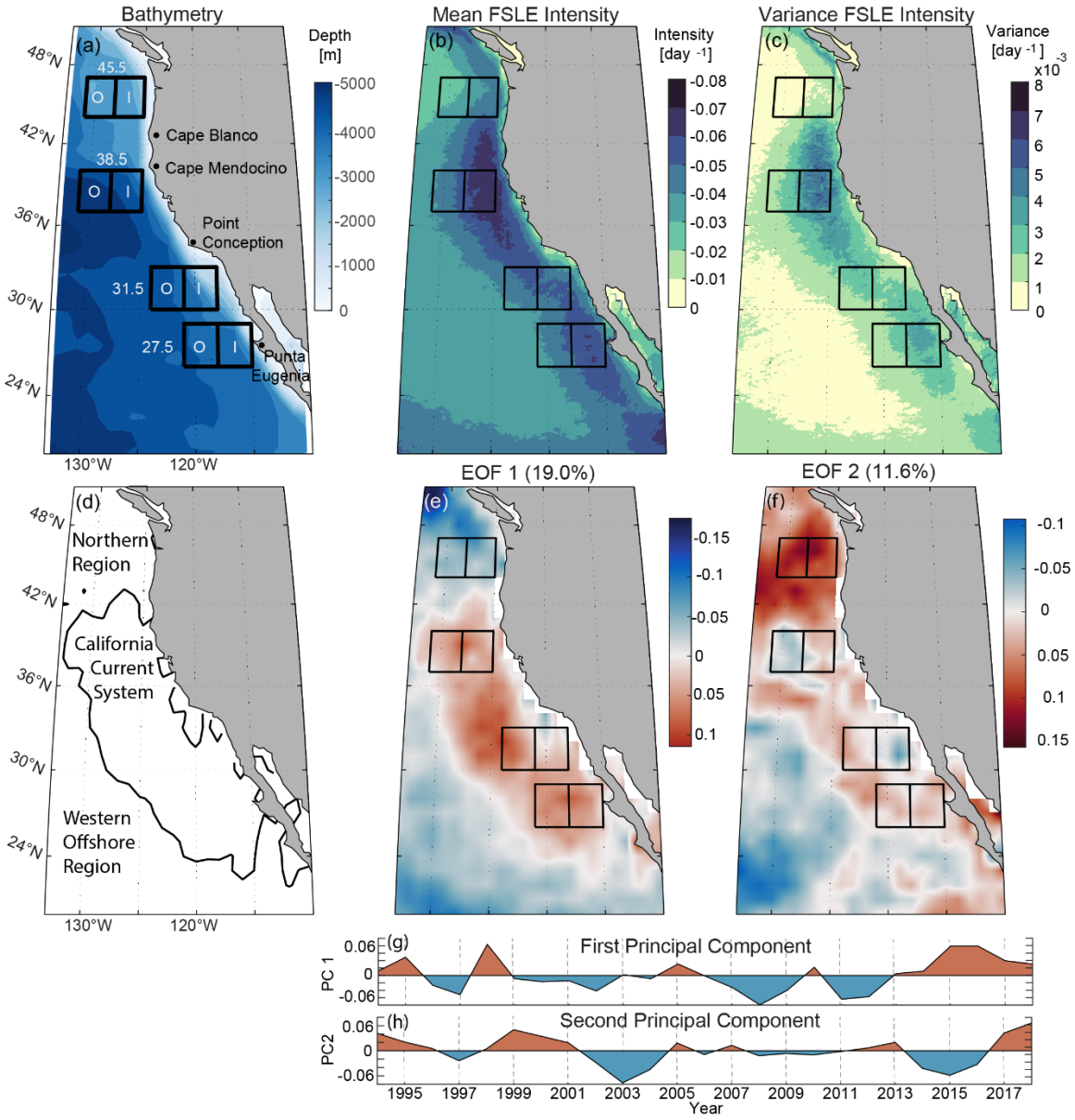

Figure 2.1: Mean FSLE intensity, variance, and dominant modes of variability. (a) Bathymetry. Boxes indicate regions used in subsequent analyses. (b) Mean FSLE intensity, 1994-2018. For these backwards-in-time FSLEs, stronger horizontal convergences are more strongly negative. Mean intensity is highest from 43°N to 34°N. (c) Variance of FSLE intensity, 1994-2018. Variance follows a similar pattern to that of the mean FSLE intensity. (d) The three regions discussed in the text. The black line demarcating the regions is the EOF 1 = 0 contour. (e) EOF 1 and (f) EOF 2, the first two modes of variability, respectively. Regions in red and blue are out of phase with each other. (g) Principal component 1 and (h) principal component 2. These correspond to EOF 1 and EOF 2, respectively.

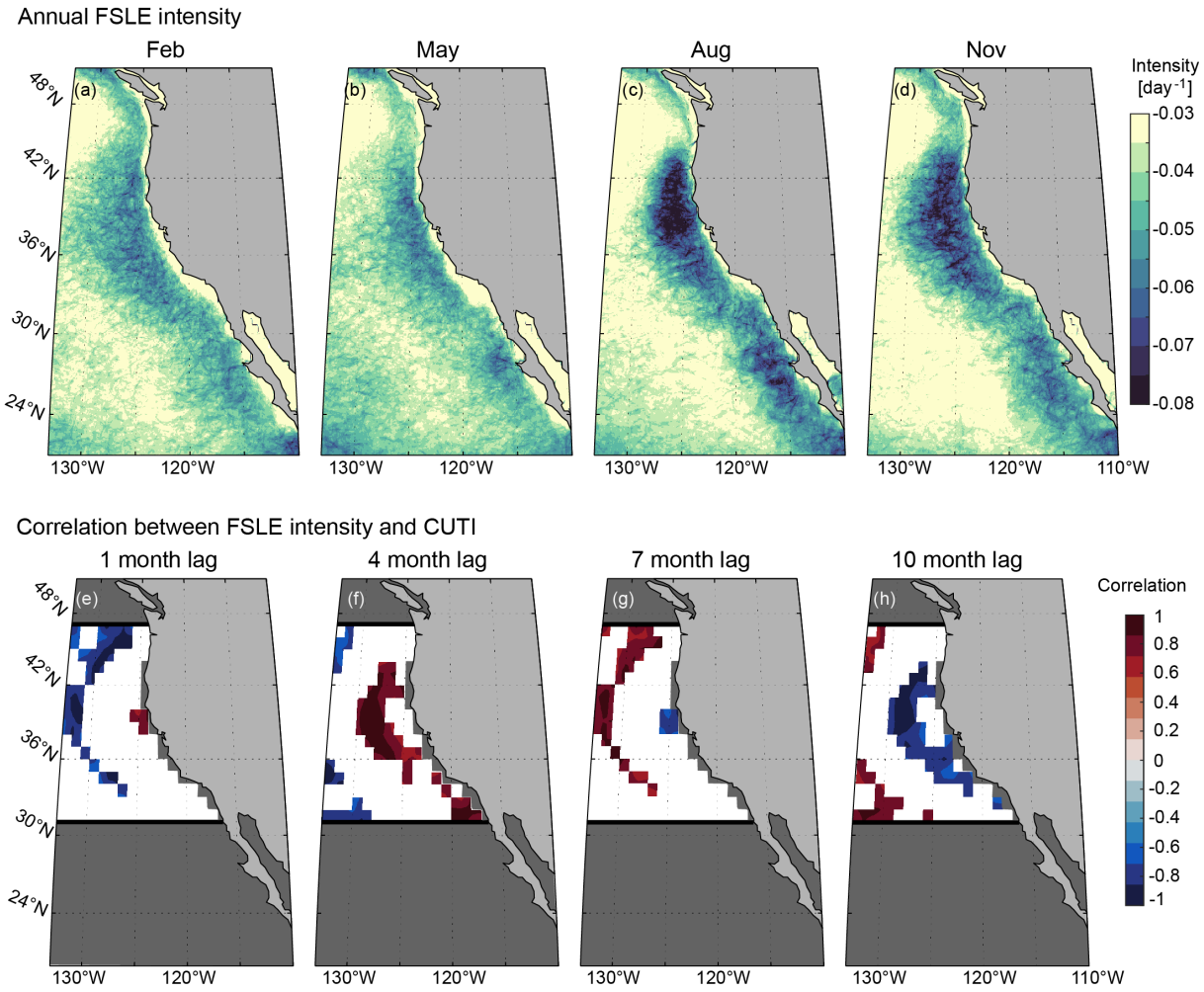

Figure 2.2: FSLE intensity starts to increase near the coast beginning in May, broadens in spatial extent and intensity until September, before decreasing again. (a-d) Mean FSLE intensity. Each month represents the average of that month over the entire twenty-five-year period. (a) February (b) May (c) August (d) November. (e-h) Correlation between the annual cycle of FSLE intensity averaged over 1°x1° regions and the annual cycle of CUTI with different lags: (e) Correlation of FSLE intensity with CUTI from 1-month prior (f) 4-months prior (g) 7-months prior (h) 10 months prior. The CUTI has values every 1° latitude from 31°N to 47°N. Analysis was restricted this region (between the black horizontal bars). Within the analysis region, gray indicates no data and areas shown in color have correlations with $p < 0.05$.

Figure 2.3: Time series of climate indices, FSLE intensity, and chlorophyll a concentration. (a-c) Times series of climate indices. (a) ONI (b) PDO (c) NPGO. (d-k) Time series of monthly averaged FSLE intensity (left y-axis, magenta) and monthly chlorophyll a concentration (right y-axis, green) in the 8 regions. (d) 45.5-I (e) 45.5-O (f) 38.5-I (g) 38.5-O (h) 31.5-I (i) 31.5-O (j) 27.5-I (k) 27.5-O

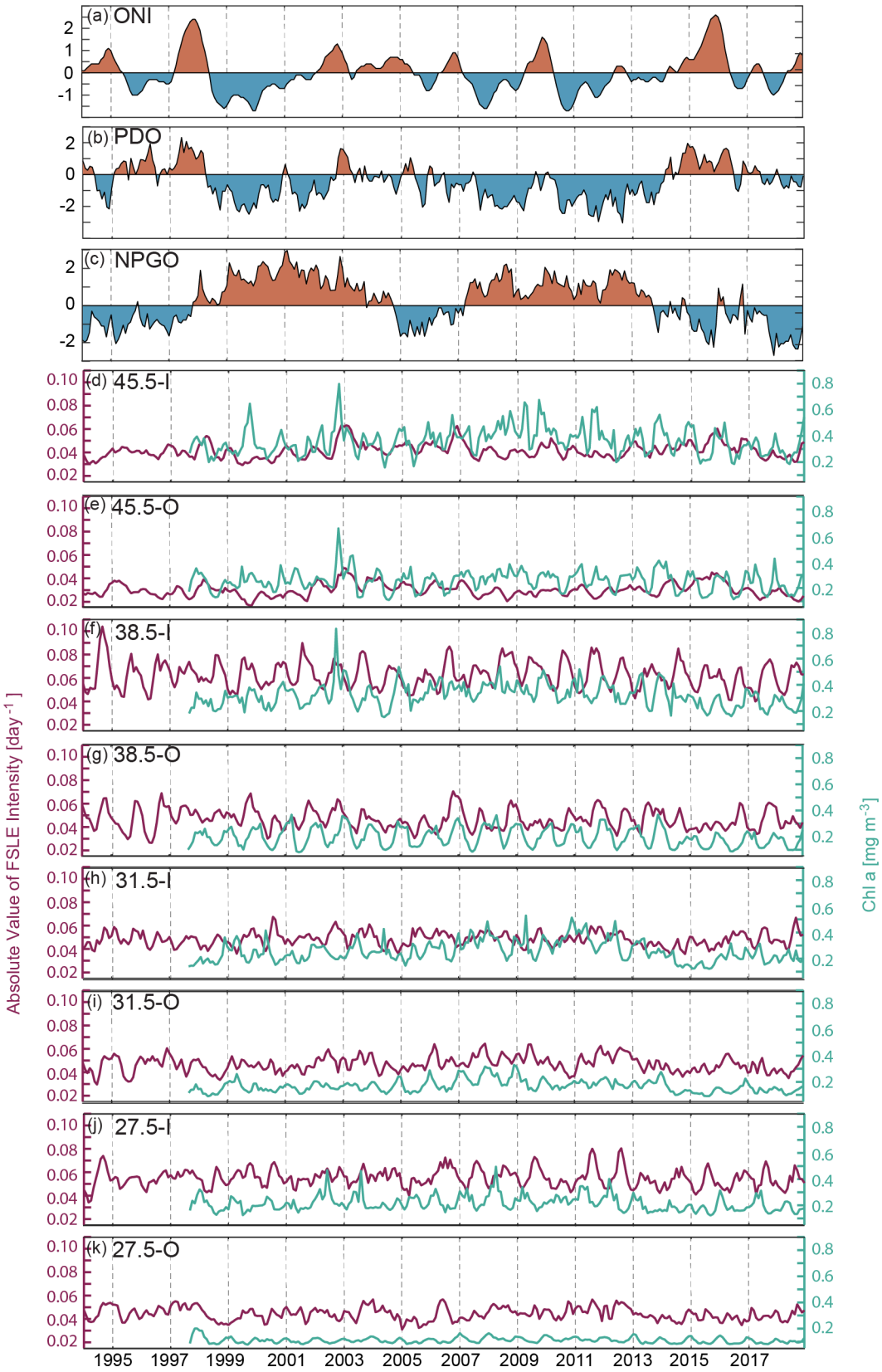
(a) ONI
(b) PDO
(c) NPGO
(d) 45.5-I
(e) 45.5-O
(f) 38.5-I
(g) 38.5-O
(h) 31.5-I
(i) 31.5-O
(j) 27.5-I
(k) 27.5-O
Absolute Value of FSLE Intensity [day^{-1}]
Chl a [mg m^{-3}]
1995 1997 1999 2001 2003 2005 2007 2009 2011 2013 2015 2017

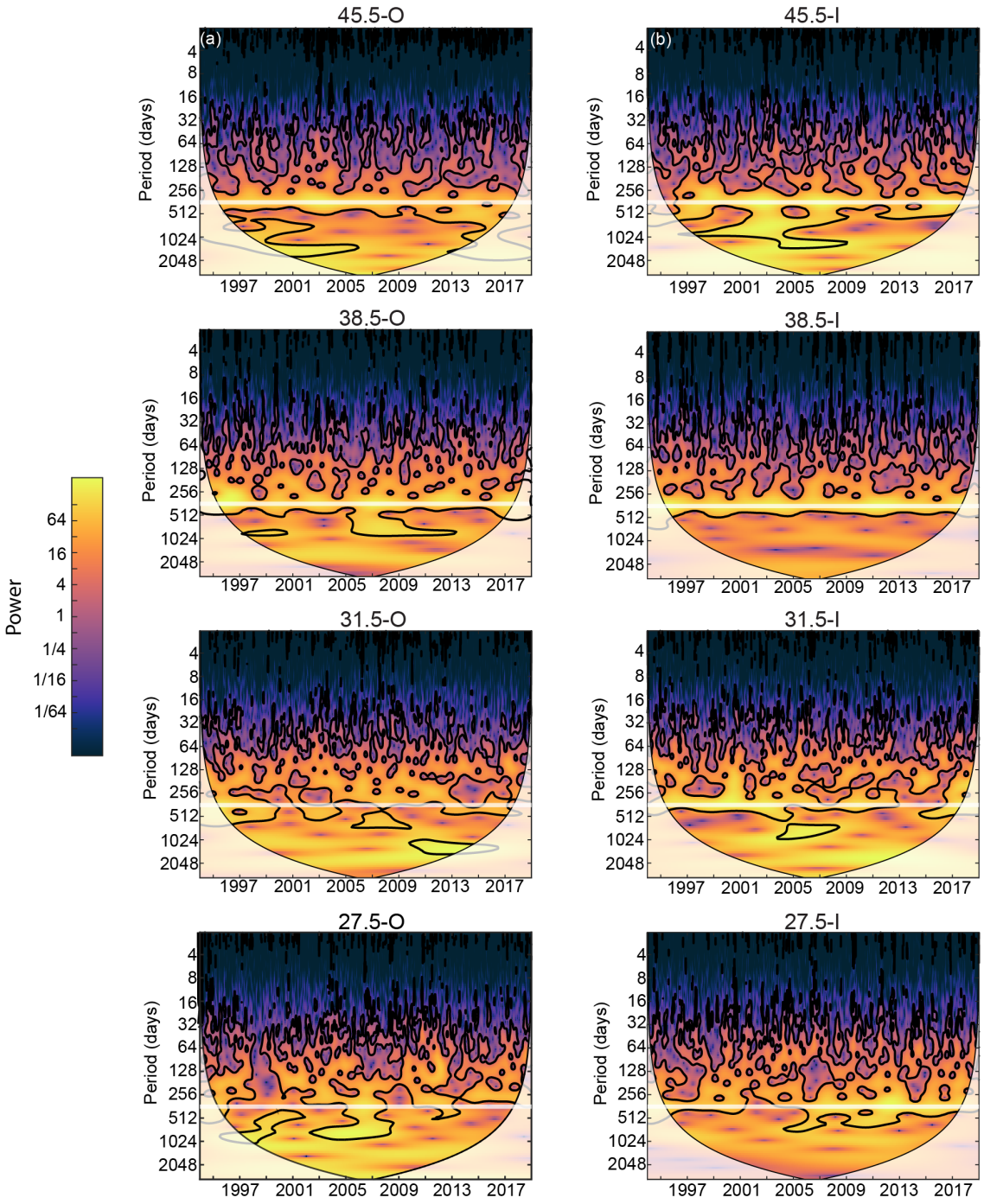

Figure 2.4: FSLE activity in the California Current varies in both space and time. Continuous wavelet transforms for the regions shown in Figure 1a. Rows top to bottom: 48.5°N, 38.5°N, 31.5°N, 27.5°N; left column: offshore (O); right column: inshore (I). Areas where edge artifacts occur due to the wavelet interacting with the ends of the time series are denoted by the shaded 'cone of influence' on each plot. Black contours demarcate the 5% significance level against red noise (Grinsted et al., 2004), showing that significant periodicities vary in time and space. Color bar indicates power. White horizontal line indicates a period of 365 days.

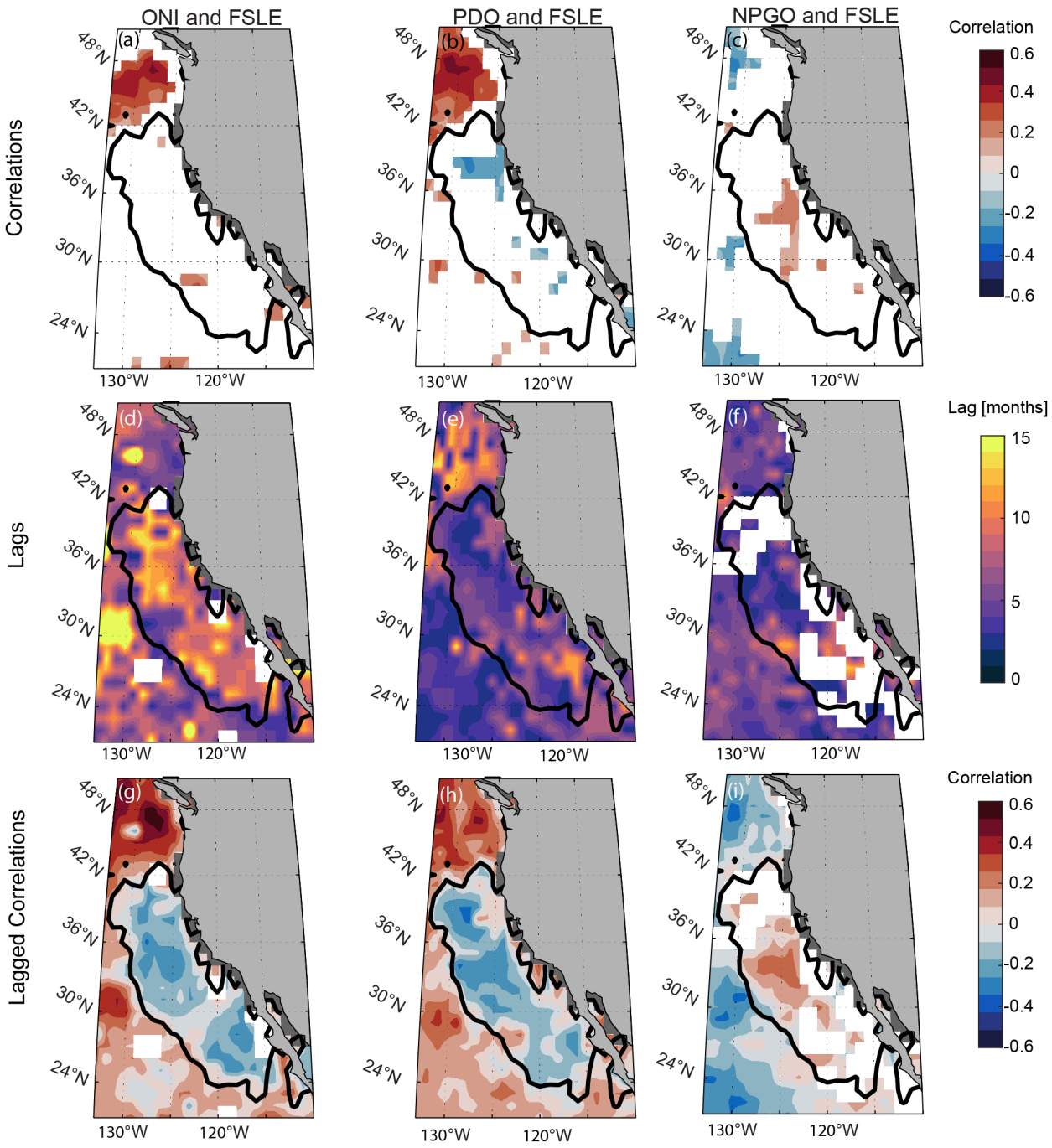

Figure 2.5: FSLE correlations and lagged correlations with climate indices vary spatially. (a-c) Correlation between the absolute value of monthly average FSLE (1° resolution) and (a) ONI, (b) PDO, and (c) NPGO. Regions shown in color have correlations with $p < 0.05$. (d-f) First statistically-significant lag between the absolute value of monthly average FSLE (1° resolution) and (d) ONI, (e) PDO, and (f) NPGO. Regions shown in white were non-significant at any lag. (g-i) Lagged correlation between the absolute value of monthly average FSLE (1° resolution) and (g) ONI, (h) PDO, and (i) NPGO at the lags shown in panels (d-f). Regions shown in white were non-significant at any lag. In all panels, gray indicates no data.

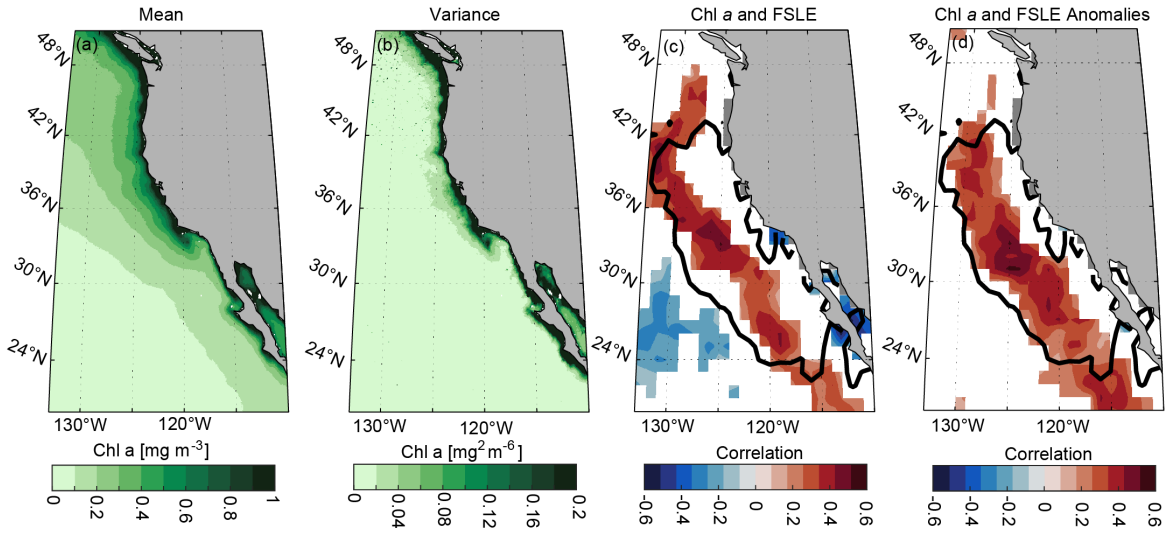

Figure 2.6: FSLEs are strongly correlated with surface chlorophyll a concentration offshore. (a) Mean chlorophyll *a* concentration (b) Variance of chlorophyll *a* concentration. (c) Correlation between the absolute value of monthly average FSLE and chlorophyll *a* (1° resolution). Note that these data retain the seasonal cycles of both FSLE and chlorophyll *a.* (d) Correlation between the absolute value of the FSLE anomalies from the monthly averages, and chlorophyll *a* anomalies from the monthly averages (1° resolution) to reveal relationships between non-seasonal, interannual fluctuations in these properties. In panels (c) and (d), gray indicates no data. Regions shown in color have correlations with $p < 0.05$.

Table 2.1: Response of FSLE Intensity and Offshore Transport of Chlorophyll a (Chl) to Increases in Climate Indices in the Different Regions Delimited by $EOF1_0$. Thick arrows (🡅) indicate strongly significant responses; thin arrows (↑) indicate weakly significant responses. WOR is the Western Offshore Region, and NR is the Northern Region, as defined in the text.

	🡅 ONI	🡅 PDO	🡅 NPGO
CCS FSLE	🡇 (9-12 month lag)	🡇 (3-6 month lag)	↑
WOR FSLE	🡅 (9-12 month lag)	🡅 (3-6 month lag)	🡇
NR FSLE	🡅 (3-7 month lag)	🡅 (8-12 month lag)	🡇
Offshore Chl transport	🡇	🡇	↑

2.7 Supporting Information

2.7.1 Data

We obtained backwards-in-time FSLEs from Archiving, Validation, and Interpretation of Satellite Oceanography (https://www.aviso.altimetry.fr/). FSLE intensities were calculated based on the methodology of d'Ovidio et al. (2004) using surface velocity fields calculated from satellite altimetry. In the FSLE dataset, the initial separation δ_0 is 0.02 degrees and the final separation distance δ_f is 0.6 degrees. The maximum integration window is 200 days; if the separation time exceeds this window, a value of 0 is given. The FSLEs are run backwards-in-time to show regions of convergence. The FSLE fields have a temporal resolution of 1 day and a spatial resolution of 0.04 degrees. We analyzed a time series of daily FSLEs spanning a twenty-five-year period from January 1, 1994 through December 31, 2018. We restrict our analyses to the California Current region, which we defined as the area from 20°N to 51°N and -110°W to -133°W.

The Coastal Upwelling Transport Index (CUTI) was used to estimate upwelling. The CUTI gives estimates of vertical transport into and out of the surface mixed layer using regional ocean reanalysis products (Jacox et al., 2018). The CUTI is given every 1° of latitude from 31°N to 47°N in the CCS. We obtained the monthly means of daily CUTI values maintained by Michael Jacox (https://mjacox.com/upwelling-indices/).

2.7.2 Methods

We used empirical orthogonal functions (EOFs) to analyze spatial modes of variability in FSLEs (Supplemental Figure 2.1). EOFs reduce data complexity and extract dominant modes of spatial variability along with the principal components (PCs) of the time series. The total variance

in the dataset is given by the sum of the EOFs or PCs, with the number of modes equal to the length of the timeseries. We calculated EOFs in MATLAB using scripts from the Climate Data Toolbox (Greene et al., 2019). We averaged the daily FSLEs spatially into either 0.04° x 0.04° bins or 1°x1° bins before computing the EOFs.

To investigate the annual pattern of FSLE intensity, we calculated the mean FSLE intensity over the 25-year data record for each month in order to obtain a single annual cycle (Supplemental Figure 2.2).

To quantify spatial correlations between FSLE and the CUTI, we calculated the average FSLE intensity within 1°x1° regions for each month to obtain a single annual cycle for each region (Supplemental Figure 2.3). We calculated the correlations between average FSLE intensity in each region and the average CUTI for that month at the corresponding latitude. Because the CUTI is given only from 31°N to 47°N, we restricted our analysis to these latitudes.

To analyze trends in FSLEs in both space and time, we defined 3°x3° regions within the California Current, separated by 0.05° latitude (Supplemental Figures 2.4 and 2.5). We conducted wavelet analyses to decompose the regional FSLE timeseries in both time and frequency space. Wavelets can be applied as a signal-processing technique for the analysis of non-stationary timeseries data (Grinsted et al., 2004; Torrence & Compo, 1998). This technique allows us to quantify when the dominant periods of variability change throughout the timeseries. We used the continuous wavelet transform from the cross wavelet and wavelet coherence toolbox (Aslak Grinsted, 2021) with a Morlet wavelet with 1/12 octave. This was applied to the daily timeseries of FSLEs averaged within each 3° x 3° region defined above.

To quantify spatial correlations between FSLE and the chlorophyll *a* time series, we calculated monthly averages of the absolute value of the FSLE intensity within 1° x 1° regions. We calculated the monthly anomalies of the absolute value of FSLE intensity and chlorophyll a concentration by subtracting the mean monthly values from the monthly time series. Correlations between monthly FLSE intensity anomalies and monthly chlorophyl *a* anomalies were obtained using MATLAB.

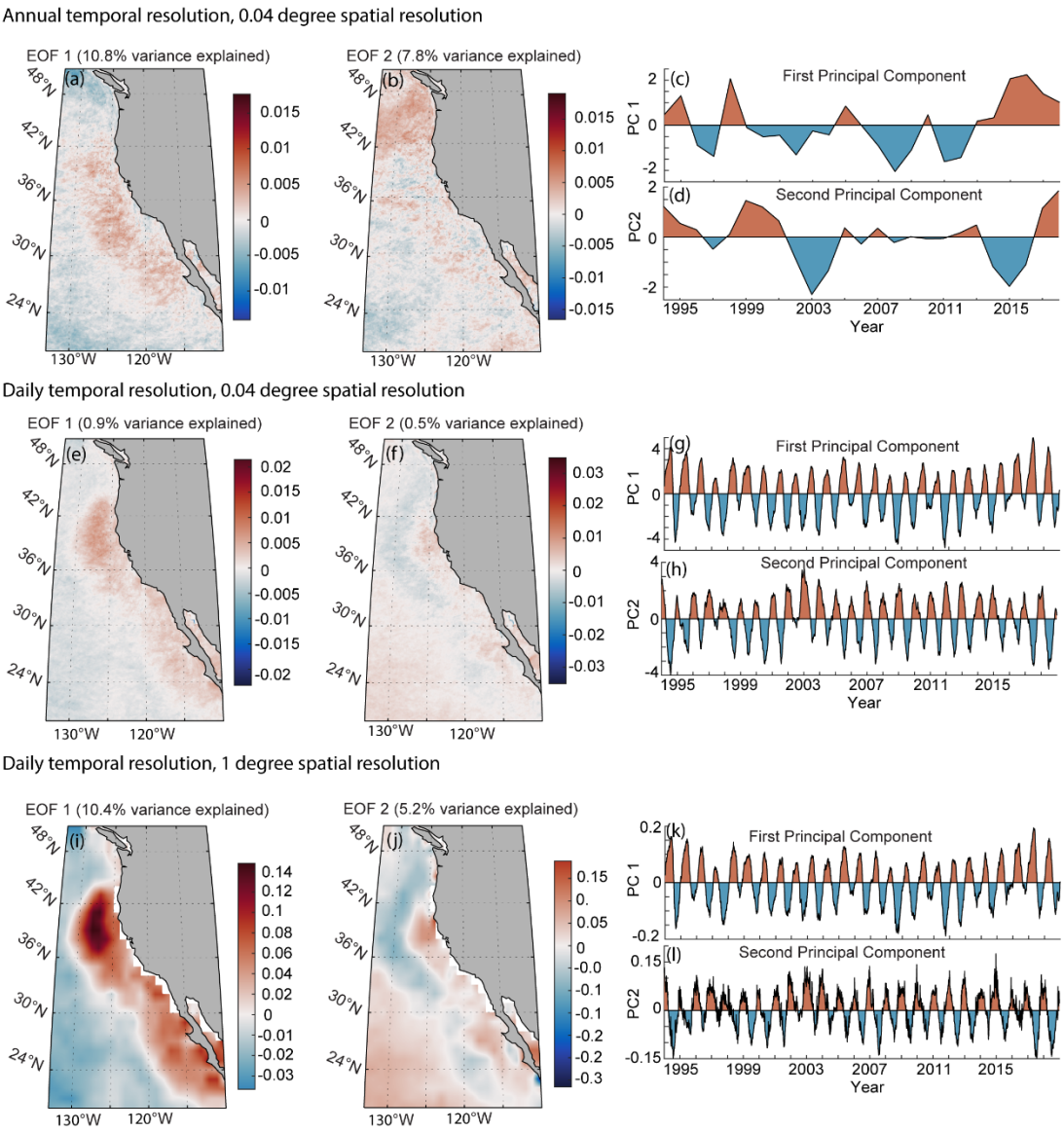

Supplemental Figure 2.1: Empirical Orthogonal Functions with varying spatial and temporal resolutions. (a) EOF 1 and (b) EOF 2, the first two modes of variability, respectively, and their corresponding principal components, (c) principal component 1 and (d) principal component 2, for FSLE intensity data with 0.04° spatial resolution and annual temporal resolution. (e-h) Same as in (a-d) but with daily temporal resolution and 0.04° spatial resolution. (i-l) Same as in (a-d) but with daily temporal resolution and 1° spatial resolution. Regions in red and blue are out of phase with each other.

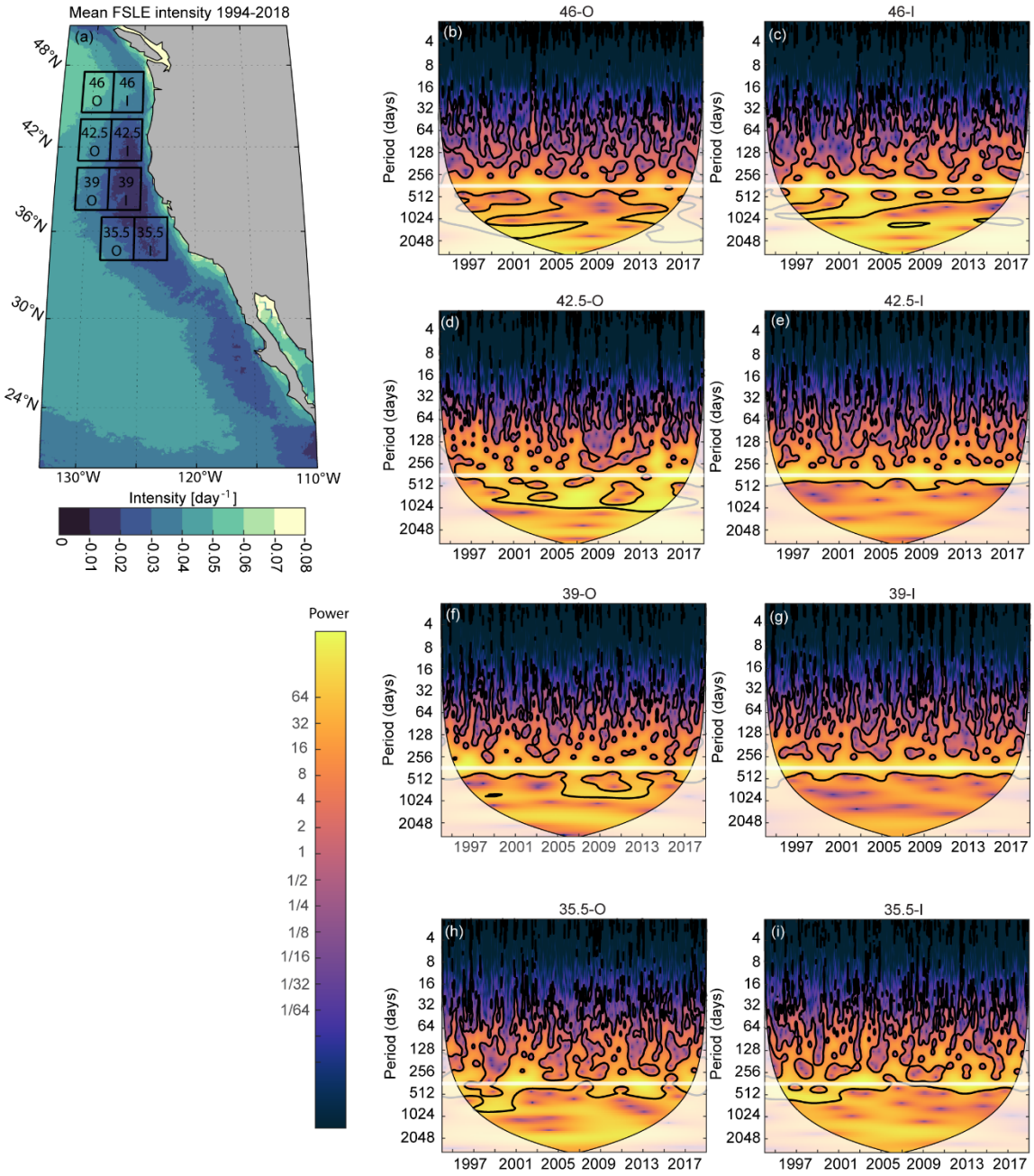

Supplemental Figure 2.2: FSLE activity in the northern California Current System varies in both space and time. (b-i) Continuous wavelet transforms for the regions shown in (a). Rows top to bottom: 46°N, 42.5°N, 39°N, 35.5°N; left column: offshore (O); right column: inshore (I). Areas where edge artifacts occur due to the wavelet interacting with the ends of the time series are denoted by the shaded 'cone of influence' on each plot. Black contours demarcate the 5% significance level against red noise (Grinsted et al., 2004). Color bar indicates power. White horizontal line indicates a period of 365 days.

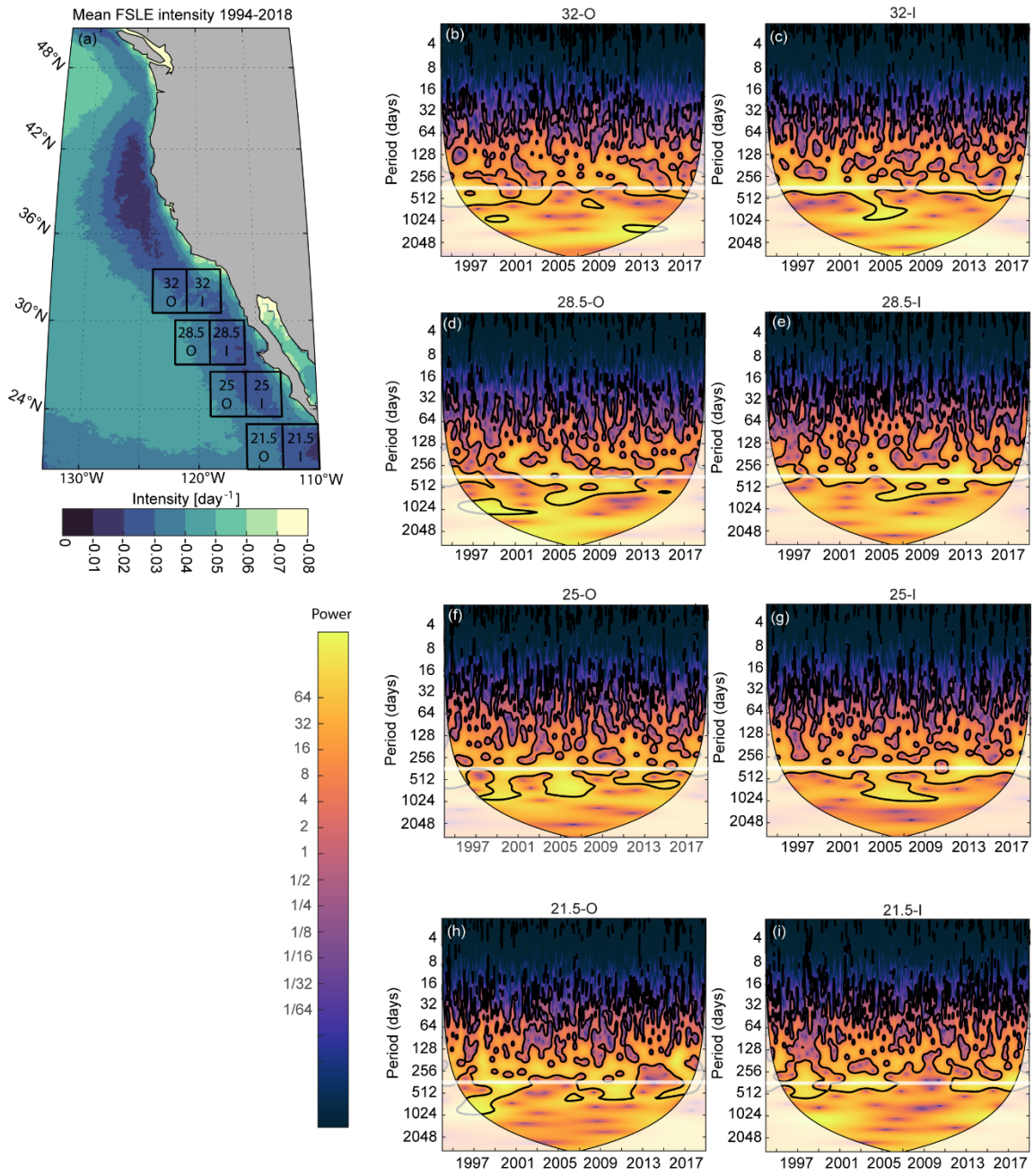

Supplemental Figure 2.3: FSLE activity in the southern California Current System varies in both space and time. (b-i) Continuous wavelet transforms for the regions shown in (a). Rows top to bottom: 32°N, 28.5°N, 25°N, 21.5°N; left column: offshore (O); right column: inshore (I). Areas where edge artifacts occur due to the wavelet interacting with the ends of the time series are denoted by the shaded 'cone of influence' on each plot. Black contours demarcate the 5% significance level against red noise (Grinsted et al., 2004). Color bar indicates power. White horizontal line indicates a period of 365 days.

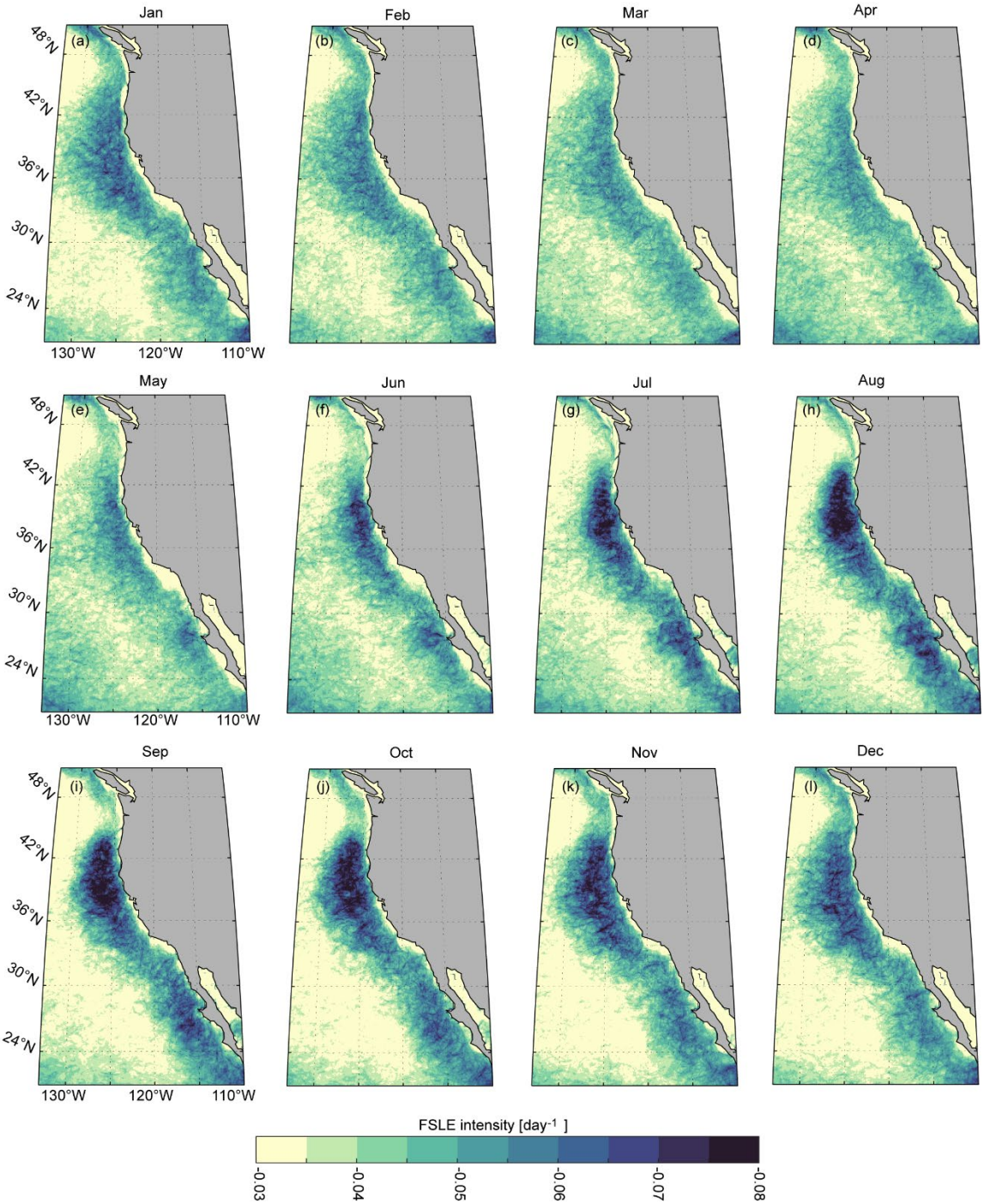

Supplemental Figure 2.4: FSLE intensity starts to increase near the coast beginning in May, broadens in spatial extent and intensity until September, before decreasing again. Each month represents the mean FSLE intensity of that month over the entire 25-year period.

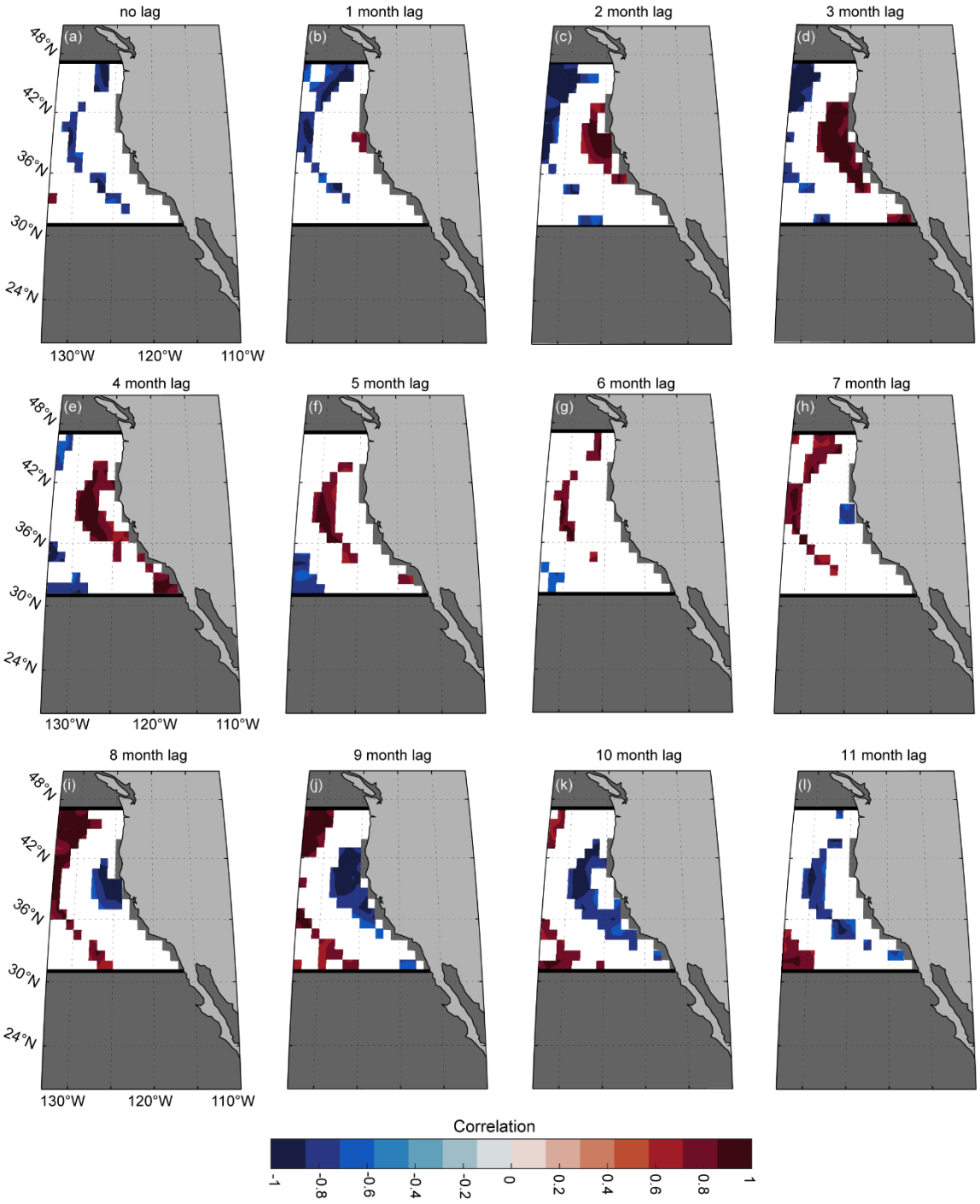

Supplemental Figure 2.5: The annual cycle of FSLE intensity is correlated with the annual cycle of upwelling (CUTI). Correlation between the annual cycle of FSLE intensity averaged over 1°x1° regions and the annual cycle of CUTI with different lags. The CUTI has values every 1° latitude from 31°N to 47°N. Analysis was restricted to this region (between the black horizontal bars). Within the analysis region, gray indicates no data, and areas shown in color have correlations with $p < 0.05$.

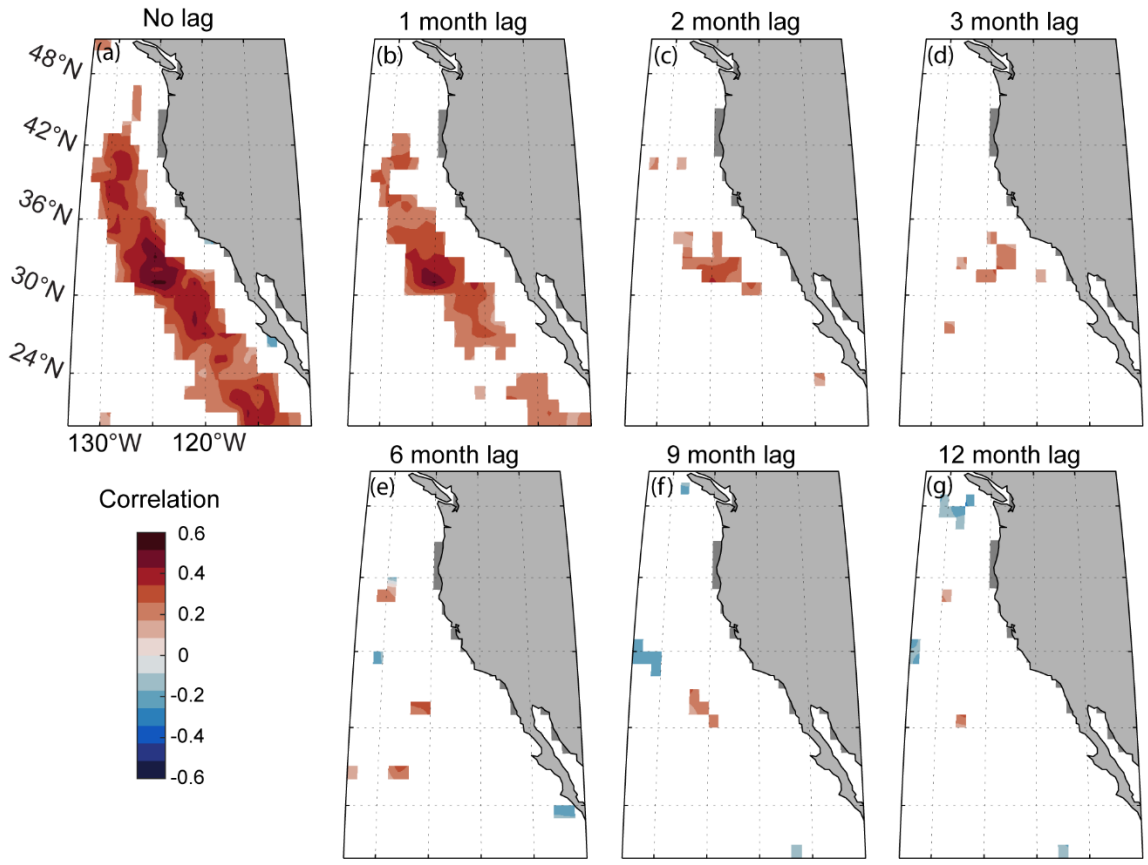

Supplemental Figure 2.6: FSLE and chlorophyll *a* anomalies are positively correlated at short time lags. (a-g) Correlations between the absolute value of monthly FSLE intensity anomalies and chlorophyll *a* anomalies (1° resolution). Gray indicates no data and areas shown in color have correlations with $p < 0.05$. (a) No lag between the two time series. Chlorophyll *a* lags FSLE intensities by (b) 1 month (c) 2 months (d) 3 months (e) 6 months (f) 9 months (g) 12 months.

Chapter 3

Cetacean densities, trends, and climate forcing in the Southern California Current Ecosystem

The California Current is a productive marine ecosystem which supports a diverse group of top predators including many cetacean species. Recently, the California Current has experienced several marine heatwaves, including the record-breaking 2014-2016 north Pacific marine heatwave. Marine heatwaves, along with other modes of climate variability such as the El Niño Southern Oscillation, can lead to profound changes within ecosystems. The impact of marine heatwaves and climate variability on cetacean species in the CalCOFI region on seasonal timescales is unknown. Here, we use data from visual surveys conducted on sixty-four quarterly California Cooperative Oceanic Fisheries Investigations (CalCOFI) cruises during 2004-2021 to (1) provide updated seasonal and overall density estimates for nine of the most abundant cetacean species and to (2) examine interannual trends on an annual and per-season basis and relate those trends to climate variability and marine heatwaves. We found that while annual cetacean sightings (scaled for effort) were stable for most species, scaled sightings of Dall's porpoise and Pacific white-sided dolphin decreased over the study period. The marine heatwave had more statistically-significant correlations with cetacean sightings than any other climate correlate tested. During the largest marine heatwave, scaled sightings of short- and long-beaked common dolphins and Risso's dolphins increased, an effect driven by large groups of each species in the winter and spring of 2015. We also found that blue and fin whale summertime scaled sightings were higher during La

Niña conditions whereas scaled sightings of several dolphin species were higher during El Niño events. Our study shows that climate variability and marine heatwaves are associated with changes in cetacean sightings in the CalCOFI region. In addition, our work highlights the importance of frequent surveys over long periods in order to ascertain seasonal and inter-annual trends.

3.1 Introduction

The California Current is a productive eastern boundary upwelling system that supports numerous commercially important fisheries (Carr, 2001) and top predators such as cetaceans. These marine mammals influence marine ecosystems through both top-down effects via predation and bottom-up effects through the vertical and horizontal transport of nutrients (Kiszka et al., 2022; Roman et al., 2014; Roman & McCarthy, 2010). Cetaceans in the California Current have been estimated to consume ~12% of the net primary productivity, although other recent work suggests this may be an underestimate (Barlow et al., 2008; Savoca et al., 2021). Given their ecological influence, knowledge of cetacean ecology is vital to understanding ecosystem functioning within the California Current.

Marine ecosystems are being impacted by climate change (Poloczanska et al., 2016). Climate variability and climate change can lead to regime shifts in marine ecosystems (Francis et al., 1998; Jiao, 2009), which can lead to population declines of vulnerable species, including cetaceans, and present a challenge for conservation of threatened and endangered species (e.g., Meyer-Gutbrod et al., 2021). There is evidence that some cetacean species have altered their migration timing or shifted their distribution poleward in response to climate change (Weelden et al., 2021). However, knowledge gaps remain and additional research on how cetaceans respond to climate change is needed (Poloczanska et al., 2016; Weelden et al., 2021). Decadal to interannual

climate variability such as the Pacific Decadal Oscillation (PDO), the North Pacific Gyre Oscillation (NPGO), and the El Niño Southern Oscillation (ENSO) can drive large changes in ecosystems through physical processes such as changes in upwelling, carbon export, and mesoscale stirring (Bograd et al., 2009; Chenillat et al., 2012; Cordero-Quirós et al., 2019; Giddings et al., 2022; M. G. Jacox et al., 2014). To fully understand how climate change will impact ecosystem functioning within the California Current ecosystem, it is necessary to understand how cetaceans within the California Current respond to both cyclical climate variability and climate change.

Marine heatwaves, discrete periods of persistently elevated ocean temperature, have become more frequent over the past century, increasing in both duration and intensity (Frölicher et al., 2018; Oliver et al., 2018). This trajectory is expected to continue under future climate change (Frölicher et al., 2018). Marine heatwaves have profound impacts on ecosystems and are a threat to biodiversity (Smale et al., 2019). The 2014-2016 marine heatwave in the north Pacific was the largest ever recorded (Frölicher & Laufkötter, 2018) and had large impacts on the north Pacific ecosystems, including the California Current (Cavole et al., 2016; Suryan et al., 2021). Many marine species expanded their ranges, for example shifting northward or contracting inshore, resulting in significant changes to community composition and species diversity and richness (Cavole et al., 2016; Nielsen et al., 2021; Walker et al., 2020). Temperature-mediated habitat compression during the heatwave increased the spatial overlap between whales and fisheries, resulting in an increase in entanglement-caused mortality (Santora et al., 2020). The marine heatwave also caused a large bloom of the toxic diatom *Pseudo-nitzschia*, which poisoned seabirds and marine mammals throughout the California Current and led to several fisheries closures (McCabe et al., 2016). Recent habitat modelling suggested that several species of cetacean in the

southern California Current could have shifted their habitat in response to the 2014-2016 marine heatwave, but this work was based on limited surveys conducted only in the summer and fall with gaps of up to four years between surveys (Becker et al., 2022).

The California Current Oceanic Fisheries Investigation (CalCOFI) conducts quarterly cruises in the southern California Current. Dedicated visual surveys for marine mammals have been conducted since 2004, enabling us to quantify seasonal and interannual trends in cetacean presence in this region. Such frequent (~seasonal) sampling over a broad spatial scale is rare in marine mammal monitoring and improves our ability to detect and understand temporal trends in distribution and abundance (Taylor et al., 2007). Here, we use data from 64 quarterly cruises from 2004-2021 to (1) provide updated seasonal and overall density estimates for nine of the most abundant cetacean species and (2) examine interannual trends on an annual and per-season basis and relate those trends to marine heatwaves and cyclical climate variability.

3.2 Methods

Visual surveys of marine mammals were conducted on quarterly California Cooperative Oceanic Fisheries Investigations (CalCOFI) cruises according to the protocols outlined in Campbell et al. (2015). The data analyzed here include sightings from the CalCOFI "standard grid" of six cross-shore transect lines comprising 75 stations. The southernmost line (line 93.3) originates at San Diego, California, while the northernmost line (line 76.7) originates at Avila Beach, north of Point Conception, California (Figure 3.1).

Visual surveys were conducted during daylight transits between CalCOFI oceanographic stations by two observers (except for the fall 2019 cruise, where only one observer was present) using 7x50 Fuijinon binoculars. Sightings were logged systematically and included supporting

information such as Beaufort sea state. Visual observations were conducted on each quarterly CalCOFI cruise from the summer of 2004 to fall of 2021. No visual survey was conducted on the spring 2010 cruise; no visual surveys were conducted from spring 2020 through spring 2021 due to COVID-related restrictions.

3.2.1 Density estimates

Abundances and density estimates of the target species were calculated for the southern CalCOFI region using distance sampling techniques with the 'distance' package in R (Miller et al., 2019). The analysis included only sightings that were "on-effort" as well as "on-transect" as per the criteria in Campbell et al. (2015). Transects were defined as segments between oceanographic stations on lines perpendicular to the coast and did not include coast-parallel transits between CalCOFI lines (Figure 3.1). To fit a detection function, a minimum of 60 "on-effort" and "on-transect" sightings is recommended (Buckland et al., 2001). When detections were pooled across all CalCOFI cruises, eight species met this requirement: blue whale (*Balaenoptera musculus*), fin whale (*Balaenoptera physalus*), humpback whale (*Megaptera novaeangliae*), gray whale (*Eschrichtius robustus*), common dolphin (*Delphinus delphis*), Pacific white-sided dolphin (*Lagenorhynchus obliquidens*), Risso's dolphin (*Grampus griseus*), and Dall's porpoise (*Phocoenoides dalli*). Although gray whales met the 60-sighting requirement for detection function fitting, they only passed through the region during migration to and from their breeding grounds in Baja California and therefore were not included in this paper's analyses. A ninth species (bottlenose dolphin *Tursiops truncates*) was also analyzed, although only 59 sightings met the "on-effort" and "on-transect" requirements. Bottlenose dolphins in the Southern California Bight exist as two different ecotypes: a coastal ecotype (generally found within 1 km of shore) and an offshore

ecotype (Perrin et al., 2011); the sightings used in this study to estimate abundance are for the offshore ecotype. Common dolphin taxonomy has been highly debated, with recent genetic analysis suggesting that previous divisions between long-beaked and short-beaked common dolphins into separate species were not warranted (Cunha et al., 2015). However, there is genetic evidence that the long-beaked common dolphin in the Northeast Pacific is genetically distinct from the short-beaked common dolphin and is currently classified as a distinct sub-species. (Cunha et al., 2015; Rosel et al., 1994). Therefore, in our analysis common dolphins were split into two subspecies: long-beaked common dolphin (*D. delphis bairdii)* and short-beaked common dolphin (*D. delphis delphis*).

Because the group sizes of common dolphins vary widely – and this could have an impact on detection probability – short-beaked common dolphins were further divided based on group size: less than or equal to 20 dolphins or greater than 20 dolphins per group. Results from each were combined to give a total abundance for short-beaked common dolphins. Such group-sized stratification was not possible with long-beaked common dolphins because very few sightings occurred with groups smaller than 21 dolphins.

Truncation was selected using the Cramér-von Mises goodness-of fit (CvM) test and was based on either distance to the sighting (e.g., truncation of sightings farther than 2400 m away), or data percentage (e.g., truncating data farther away than 90% of the recorded observed distances; Supplemental Table 1). Truncation was used to determine the effective strip width (Buckland et al., 2001). Sea state, season, and group size were investigated as covariates (Marques et al., 2007). Detection function models were selected using the Akaike information criterion (AIC) and CvM tests. Pacific white-sided dolphin, Dall's porpoise, bottlenose dolphin, and common dolphin have

all been shown to have responsive movement (e.g., ship attraction), which can cause a positive bias in density and abundance estimation. Hazard-rate models for these species exacerbate this positive bias with a large spike at low detection probabilities. To counteract this issue, we restricted our analyses to half-normal models for these species. Confidence intervals were calculated using a log-normal distribution.

CalCOFI surveys are conducted in "passing mode," with the ship remaining on the transect line throughout the survey. This results in larger numbers of unidentified individuals than using other survey designs. To counteract the potential negative bias to our abundance estimates, we applied a correction factor following the protocol in (Becker et al., 2017):

$$c = 1 + \frac{t_{unid}}{t_{tgt}+t_{oth}} \quad (1)$$

In this equation, t_{tgt} is the number of identified individuals of the target species, t_{oth} is the number of identified individuals of closely related species, and t_{unid} is the number of unidentified individuals in the species group (Becker et al., 2017). We used this correction factor for two groups: unidentified large baleen whales (either blue, fin, or humpback whales), and common dolphins not identified at the subspecies level (either long-beaked or short-beaked common dolphins). This correction factor *c* was then multiplied by the abundance estimate *D* (Becker et al., 2017; Buckland et al., 2001),

$$D = \frac{n \cdot s \cdot c}{L \cdot ESW \cdot g(0)} \quad (2)$$

which generates the densities from the distance sampling protocol for large whales (blue, fin, and humpback whales) and for common dolphins (long- and short-beaked common dolphins). Here *D* is the density (animals per km^2), *s* is the mean group size, *c* is the unidentified animal correction

factor (equation 1), L is the length surveyed, ESW is the effective strip width, and $g(0)$ is the probability of detection on the track line. We were unable to measure the detection probability directly on the track line and thus relied on previous estimates of track line detection probability ($g(0)$) in the region (Jay Barlow & Forney, 2007). It is worth noting that these estimates were calculated for observers using greater magnification (25x vs 7x in the present study) and thus are likely to have some positive bias.

We calculated 95% log-based confidence intervals using the following equations from Buckland et al. (Buckland et al., 2001), where $\widehat{D}$ is the estimated abundance and cv is the coefficient of variation:

$$C = \exp\{1.96 * \sqrt{\ln\left(1 + cv\left(\widehat{D}\right)^2\right)}\}$$

$$Upper\ Confidence\ Interval = \widehat{D} * C$$

$$Lower\ Confidence\ Interval = \widehat{D}/C$$

3.2.2 Scaled Sightings

Distance sampling and resulting density estimation works best with large numbers of sightings, which required us to pool our survey results over all available surveys. In order to investigate the response of cetaceans to climate variability and marine heatwaves on an annual or seasonal basis, we used the number of animals seen while on-effort and on-transect, scaled per 1000 km of survey track covered. We therefore avoided issues with small sample sizes (exacerbated by data truncation) that would reduce the performance of density estimates on short temporal scales.

3.2.3 Climate variables

We investigated associations of cetacean scaled sighting fluctuations with three climate variables in this study (Figure 3.2a-c): the North Pacific Gyre Oscillation (NPGO), the Pacific Decadal Oscillation (PDO), and the Multivariate ENSO Index Version 2 (MEI) (Figure 3.2). The NPGO is defined as the second Empirical Orthogonal Function of sea surface height anomaly; we obtained the NPGO time series from (http://www.o3d.org/npgo/npgo.php) maintained by Emanuele Di Lorenzo; (Di Lorenzo et al., 2008). The PDO is defined as the first Empirical Orthogonal Function of sea surface temperature; we obtained the time series of the PDO from the NOAA National Centers of Environmental Information (https://www.ncdc.noaa.gov/teleconnections/pdo/) (Mantua et al., 1997). The MEI is a measure of the El Niño Southern Oscillation (ENSO) phenomenon which is defined as the first combined Empirical Orthogonal Function of five variables in the tropical Pacific (30°S-30°N and 100°E-70°W): sea level pressure, sea surface temperature, surface wind zonal and meridional components, and outgoing longwave radiation; we obtained the MEI time series from the NOAA Physical Sciences Laboratory (https://psl.noaa.gov/enso/mei/).

To investigate the relationship of marine heatwaves and cetacean scaled sightings in the CalCOFI region, we used the California Current Marine Heatwave Tracker, developed by the Environmental Research Division of NOAA Fisheries Southwest Fisheries Science Center. The heatwave tracker follows Hobday et al.'s (2016) guidelines which define a marine heatwave as a period of at least five contiguous days during which the temperature exceeds 90% of the measured temperatures at that location and Julian day. The Marine Heatwave Tracker modifies this protocol by first standardizing sea surface temperature anomalies (from 1984-present) by their standard

deviation; a modified sea surface temperature anomaly greater than 1.29 is equivalent to the 90% threshold and is used as the cutoff for marine heatwaves. This product was downloaded from ERDDAP (https://oceanview.pfeg.noaa.gov/erddap/info/cciea_OC_MHW_regions/index.html) for the 'socal' region on 2022-06-23. This region overlaps substantially, but not perfectly, with the southern CalCOFI region. At the time of this analysis, the Marine Heatwave Tracker was available only through 2020-12-31, so we did not include the two 2021 cruises in our heatwave analysis. While the Marine Heatwave Tracker contains several measures of heatwave extent and intensity, we found that they were tightly correlated with one another. In our analysis we used marine heatwave spatial extent as our marine heatwave metric (Figure 3.2d), which is the percentage of the southern California region that is experiencing a marine heatwave at a given time.

3.2.4 Climate analyses statistics

The three climate variables were available as monthly datasets, while the marine heatwave index was available with daily resolution. To standardize our analysis, we calculated the average monthly marine heatwave extent. An annual mean was calculated for each of the climate variables for examining the correlations between annual sightings and climate indices. We restricted our analyses to the years in which visual surveys occurred on all four seasonal CalCOFI cruises to minimize the impact of missing cruises on annual sighting data.

We created seasonal time series by separating the per-cruise visual sightings scaled by effort into four seasonal time series for each of the focus species. We then calculated two sets of linear correlations. The first compared the climate variable value for the month of a given cruise to that cruise's scaled sightings. This owed detection of relationships between cetacean presence and climate variability without any delays or lags. However, since cetaceans are predators that

forage at trophic levels which may have varied response times to environmental conditions, we used a second linear correlation that compared cetacean scaled sightings to the value of a given climate variable averaged over the previous 12 months (e.g., for an August cruise, data were averaged from September of the previous year to August of the current year). This allowed detection of relationships of cetacean presence with the averaged environmental conditions over the preceding year.

We used the 'fitlm' command in MATLAB to fit a linear model to the data; to test for non-linear relationships, we fit quadratic models to the data using the same command. In most cases, both the linear and quadratic models had similar levels of statistical significance, though the quadratic model included one more parameter. We chose the most appropriate model (linear or quadratic) by selecting the model with the lowest AIC.

We used a two-sample t-test to assess whether the month a cruise was conducted impacted the mean scaled sightings within a season (e.g., whether a cruise occurring primarily in October led to significantly different scaled sightings than a cruise occurring primarily in November). As there was only one cruise which occurred in June, we limited our summer tests to differences between July and August.

3.3 Results

3.3.1 Survey effort and summary of sightings

Visual surveys were conducted on 64 quarterly CalCOFI cruises from 2004 through 2021 (Figure 3.1). Cruises occurred four times per year: once each in winter, spring, summer, or fall, although the precise month varied. In this study, 14 of the 18 years were complete, with visual surveys being conducted in each of the four quarters. In 4 years, one or more quarters were missed.

In 2004, visual surveys were conducted only in summer and fall. In 2010, no visual survey was conducted during spring. Due to the Covid-19 pandemic, visual surveys were only conducted during the winter of 2020 and during the summer and fall of 2021.

Our study focuses on the nine most frequently encountered cetacean species in the southern CalCOFI region (Table 1). We found no differences in the mean number of animals seen per 1000 km of effort (hereafter "scaled sightings") between months within a given season, with two exceptions: for Dall's porpoise and long-beaked common dolphins, mean scaled sightings were significantly greater in March than in April (Dall's porpoise: $p = 0.0048$; long-beaked common dolphin: $p = 0.037$). March cruises only occurred in three years: 2008, 2009, and 2012; all other spring cruises occurred in April.

3.3.2 Density estimations: overall and per season

Detection function models were selected based on the AIC and CvM tests (Supplementary Table 1). The half-normal model was selected for blue whales, Pacific white sided dolphins (with sea state as a covariate), and long beaked common dolphins. Half-normal models with a cosine adjustment term of order 2 were selected for humpback whales and Dall's porpoises. For bottlenose dolphins and short beaked common dolphins with group sizes both less than or equal to 20 and greater than 20, a half-normal model with two cosine adjustment terms of orders 2 and 3 were selected. Hazard-rate models with sea state as a covariate were selected for fin whales and Risso's dolphins.

Some species are known to be ship-attracted, which violates the assumption in distance sampling that animals are distributed independently of the transect line. In this case, there will be

a sharp increase in sightings at short distances. Four species showed evidence of ship attraction in this study: Pacific white sided dolphins, Dall's porpoise, bottlenose dolphins, and short-beaked common dolphins (Supplemental Figure 3.1). In these cases, hazard-rate models may have lower AIC scores than half-normal models but show sharp jumps in detectability at short distances, leading to potential overestimation of abundance of the species. To correct this bias, model selection was limited to half-normal models for these species.

Fin whales were the most abundant baleen whale species in the CalCOFI region with an overall density estimate of 6.15 animals per 1000 km^2 (Table 2, CV=0.43). Fin whales were most present in the summer, with a seasonal density estimate of 11.11 animals per 1000 km^2, CV=0.23, and least present in the winter, with 2.28 animals per 1000 km^2, CV=0.28. Humpback whales had the second-highest abundance of baleen whales in the CalCOFI region, with an estimated overall density estimate of 2.87 animals per 1000 km^2 (Table 2, CV=0.29). They are most abundant in spring, with an estimated seasonal density of 5.65 animals per 1000 km^2, CV=0.23; they have the lowest density during summer (1.96 animals per 1000 km^2, CV=0.48). Blue whales were the third-most abundant baleen whale species in the CalCOFI region, with an overall density estimate of 2.61 animals per 1000 km^2 (Table 2, CV=0.71). Blue whales show strong seasonal variation in the CalCOFI region, being most abundant during the summer, with a seasonal density estimate of 6.50 animals per 1000 km^2, CV=0.16. However, during the study period they were only seen during the winter in 2017 and during the spring in 2011 and 2016.

The most abundant toothed whale species in the CalCOFI region is the common dolphin, which has two subspecies: short-beaked and long-beaked. The short-beaked common dolphin is the more common subspecies. Densities of short-beaked common dolphins were estimated

separately for animals with group sizes of less than or equal to 20 individuals (hereafter "small groups") vs. groups larger than 20 individuals (hereafter "large groups") due to increased detectability of large dolphin schools (Jay Barlow & Forney, 2007). The estimated density of short-beaked common dolphins in small schools was 140 animals per 1000 km^2, CV=0.18; for large schools the estimated density was 1404 animals per 1000 km^2, CV=0.34, leading to an overall total density estimate of 1544 animals per 1000 km^2 (Table 2). Short-beaked common dolphins were more abundant in the winter (density estimates for small groups: 174 animals per 1000 km^2, CV=0.16; large groups: 2502 animals per 1000 km^2, CV = 0.32; total: 2676 animals per 1000 km^2). Summer showed the lowest densities overall (small groups: 171 animals per 1000 km^2, CV=0.16; large groups: 953 animals per 1000 km^2, CV = 0.25; total: 1124 animals per 1000 km^2); these densities were largely driven by animals in large groups. Density estimates for animals in small groups were similar in winter and summer (174 and 171 animals per 1000 km^2, respectively, CV = 0.16). Large groups showed similar estimated densities during spring and fall (1226 and 1204 animals per 1000 km^2, CV = 0.32 and 0.21, respectively), as did small groups (128 and 107 animals per 1000 km^2, CV = 0.19).

Long-beaked common dolphins were less abundant than short-beaked common dolphins but were more abundant than the other toothed whales in the study. Their overall estimated density was 380 animals per 1000 km^2, CV=0.50. Long-beaked common dolphin density was highest in the winter (814 animals per 1000 km^2, CV=0.67), and lowest in the spring (72 animals per 1000 km^2, CV=0.47).

The third-most abundant toothed whale in this study was the Pacific white-sided dolphin, with an estimated overall density of 31.38 animals per 1000 km^2, CV=0.33. Pacific white-sided

dolphins were most abundant in spring (density estimate: 60.01 animals per 1000 km^2, CV=0.29) and least abundant in the fall (density estimate: 9.94 animals per 1000 km^2, CV=0.72). Bottlenose dolphins were the fourth-most abundant toothed whale in the CalCOFI region with an estimated density of 29.95 animals per 1000 km^2 (CV=0.32). Bottlenose dolphins were most abundant in the winter (density estimate: 49.08 animals per 1000 km^2, CV=0.38), and least in the spring (density estimate: 8.96 animals per 1000 km^2, CV=0.68). The fifth-most abundant toothed whale in the CalCOFI region was the Risso's dolphin, with an estimated density of 14.66 animals per 1000 km^2 (CV=0.30). Seasonal densities were highest in the spring (27.47 animals per 1000 km^2, CV=0.68), and lowest in the winter (9.49 animals per 1000 km^2, CV=0.33), although summer densities were almost as low (9.89 animals per 1000 km^2, CV=0.40). The least-abundant toothed whale in this study was Dall's porpoise (density estimate:13.81 animals per 1000 km^2, CV=0.66). Dall's porpoises were most abundant in the spring (density estimate: 39.80 animals per 1000 km^2, CV=0.26) and least abundant in the summer (density estimate: 0.64 animals per 1000 km^2, CV=0.64).

3.3.3 Sighting trends: annual and seasonal

Although fin and humpback whale scaled sightings (Figure 3.3a-d) fluctuated over the course of the 18-year time series, there was no statistically significant temporal trend in either species during the survey record (Figure 3.5). Annual scaled sightings of fin whales for years in which all four surveys were conducted ranged from a low of 1.94 animals per 1000 km in 2019 to a high of 12.65 animals per 1000 km in 2018 (Figure 3.3b). While 2010 and 2021 had higher sightings (18.28 and 22.93 animals per 1000 km, respectively), the lack of survey coverage during all four seasons reduces the accuracy due to potential seasonal effects. Humpback whale annual

sightings during complete survey years ranged from a low of 0.82 animals per 1000 km in 2012 to a high of 10.19 animals per 1000 km in 2018 (Figure 3.3d). While 2010 had lower scaled sightings, the lack of data from the spring CalCOFI cruise, which is the season of greatest humpback whale presence, artificially decreased the annual totals.

Blue whales had an increasing trend over time during the summer season (Figures 3.3e and 5, $r^2 = 0.294$, $p = 0.087$). Annual blue whale scaled sightings for years in which four surveys were conducted ranged from a low of 0.30 animals per 1000 km in 2007 to a high of 7.54 animals per 1000 km in 2011 (Figure 3.3f). No sightings of blue whales occurred during 2020; however, due to the COVID-19 pandemic, only the winter visual survey was conducted, when blue whales are rare in the CalCOFI region. When considering the complete record, the highest scaled sightings of blue whale occurred in 2021: 31.78 animals per 1000 km. Because visual surveys were only conducted in summer and fall of 2021 – the seasons when blue whales have the highest abundance in the CalCOFI region – the annual scaled sightings number is inflated. However, the summer cruise of 2021 had the highest number of effort-adjusted sightings of any cruise in the 18-year record, with scaled sightings (54.91 animals per 1000 km) twice that of the next-highest cruise (summer 2011: 26.90 animals per 1000 km; Figure 3.3e). The high number of blue whales seen during the summer 2021 cruise resulted in a positive correlation between summer scaled sightings and time.

Short-beaked common dolphins had a significant overall decline in summertime scaled sightings (Figure 3.4a and 3.5, $r^2 = 0.327$, $p=0.017$) but an increase in wintertime scaled sightings ($r^2 = 0.214$, $p=0.072$). Annual scaled sightings of short-beaked common dolphins in years with complete surveys ranged from a low in 2011 (Figure 3.4b, 364 animals per 1000 km) to a high in

2015 (1330 animals per 1000 km). Annual scaled sightings in 2020 and 2021 (Figure 3.4b) were more extreme due to having data only from the most abundant season (2020) or two least abundant seasons (2021).

Contrary to the closely related short-beaked common dolphin, long-beaked common dolphin scaled sightings during the summer increased over time (Figure 3.4c and 3.5, $r^2 = 0.630$, p=0.00094); no other temporal trend of long-beaked common dolphin sightings was statistically significant. Annual scaled sightings of long-beaked common dolphins ranged from a high in 2015 of 1517 animals per 1000 km to a low in 2006 of 3.36 animals per 1000 km (Figure 3.4d).

Scaled sightings of Pacific white-sided dolphins decreased over the study period on an annual basis (Figure 3.4f and 3.5, $r^2 = 0.253$, $p = 0.067$) and on a seasonal basis in the wintertime (Figure 3.4e and 3.5, $r^2 = 0.244$, $p= 0.052$). Annual scaled sightings ranged from a low of 1.01 animals per 1000 km in 2019 to a high of 54.41 animals per 1000 km in 2006 (Figure 3.4f). There were no on-effort, on-transect sightings of Pacific white-sided dolphins in 2020 or 2021; however, both years lack survey effort during the spring, the season with highest Pacific white-sided dolphin abundance in the area.

While bottlenose dolphins showed no annual temporal trend, their scaled sightings increased over time in both winter (Figure 3.4g and 3.5, $r^2 = 0.217$, $p = 0.069$) and summer (Figure 3.4g and 3.5, $r^2 = 0.324$, $p = 0.065$). Greater-than-usual scaled sightings in winter 2019 and summer 2016 and 2021 drove these trends. Annual scaled sightings for years in which all four seasons were sampled ranged from a high of 70.9 animals per 1000 km in 2016 to a low of 0 in 2017, the only year with no on-effort, on-transect sightings of bottlenose dolphins (Figure 3.4g). Annual scaled sightings were higher in 2020 and 2021, years which lacked spring surveys. Because bottlenose

dolphins are least abundant in the CalCOFI region during the spring, this inflates the annual numbers.

Risso's dolphin fall scaled sightings increased over the study period (Figure 3.4i and 3.5, $r^2 = 0.262$, $p = 0.036$). Annual scaled sightings for Risso's dolphin were highest in 2015 and 2016 (Figure 3.4j, 81.60 and 82.95 animals per 1000 km, respectively). There were no on-effort, on-transect sightings of Risso's dolphins in either 2017 or in the incomplete survey years of 2004 and 2010, which are missing data from the spring – the season of greatest Risso's dolphin abundance in the region.

Dall's porpoise showed a strong annual decline in scaled sightings over the study period (Figure 3.4l and 3.5, $r^2 = 0.574$, $p = 0.0017$); this decline was particularly apparent starting in 2014. This was driven by a decline in spring scaled sightings, the season during which Dall's porpoise is most abundant (Figure 3.4k and 3.5, $r^2 = 0.406$, $p = 0.014$). Dall's porpoise spring scaled sightings were significantly greater during the three March cruises (in 2008, 2009, 2012) than during the eleven April cruises (all other years); the statistically significant decline in spring scaled sightings was more robust when the analysis was restricted to just the eleven April cruises ($r^2 = 0.781$, $p = 0.00031$); no trend was found in the three March sightings. Dall's porpoise scaled sightings were highest in 2011 with 25.13 animals seen per 1000 km. There were no on-effort, on-transect sightings of Dall's porpoise in 2016 or the incomplete survey years 2010, 2020, and 2021, all of which lack spring data. Note that the annual decline was determined using only data from years in which all four surveys were collected, in order to minimize the impact of differential seasonal effort.

3.3.4 Relationships to the NPGO

The NPGO is correlated with upwelling, nutrient concentration, and chlorophyll in the California Current, with the positive phase associated with more productivity (Chenillat et al., 2012; Lorenzo et al., 2008). The NPGO has been in a negative phase for most of our study period, with a notable positive phase from 2007-2013 (Figure 3.2a). The NPGO had the fewest number of statistically significant correlations with cetacean scaled sightings in our study (Figure 3.6) in comparison to other climate indices tested. Four species had at least one statistically significant negative correlation with the NPGO (humpback whales, short-beaked common dolphins, long-beaked common dolphins, and bottlenose dolphins), whereas three species had at least one positive correlation with the NPGO (short-beaked common dolphins, Pacific white-sided dolphins, and Dall's porpoise). There were three species that had no significant correlations with the NPGO: fin whales, blue whales, and Risso's dolphin.

Fall humpback whale scaled sightings were negatively correlated with the NPGO (same month: $r^2 = 0.218$, $p = 0.059$; 12-month average: $r^2 = 0.318$, $p = 0.018$). Short-beaked common dolphin scaled sightings were correlated with the NPGO in 3 of 4 seasons but not annually. The direction of correlation varied in each season: negative in winter (same month: $r^2 = 0.289$, $p = 0.032$), positive in the summer (12-month average: $r^2 = 0.201$, $p = 0.071$), and intermediate in the fall, when scaled sightings were lower during times of strongly positive and negative NPGO values than when NPGO values were intermediate (12-month average: $r^2 = 0.310$, $p = 0.075$). Long-beaked common dolphin scaled sightings were negatively correlated with the NPGO in summer (same month: $r^2 = 0.178$, $p = 0.091$; 12-month average: $r^2 = 0224$, $p =0.055$). Fall scaled sightings of Pacific white-sided dolphin were positively correlated with the 12-month average NPGO ($r^2 =$

0.222, p = 0.056). Bottlenose dolphin scaled sightings were negatively correlated with the NPGO during the winter (same month: $r^2 = 0.393$, p = 0.039; 12-month average: $r^2 = 0.366$, p = 0.052) while high bottlenose dolphin springtime scaled sightings were associated with both extremely positive and negative NPGO values ($r^2 = 0.375$, p = 0.075). Annual bottlenose dolphin scaled sightings were negatively correlated with the prior year's mean NPGO value ($r^2 = 0.454$, p = 0.036). Annual Dall's porpoise scaled sightings were positively correlated with the same-year ($r^2 = 0.426$, p =0.0034) and the prior-year's mean NPGO ($r^2 = 0.329$, p = 0.032). Seasonally, Dall's porpoise scaled sightings were positively correlated with the NPGO in the winter (12-month average: $r^2 = 0.366$, p =.0.059) and spring(same month: $r^2 = 0.329$, p = 0.032).

3.3.5 Relationships with the PDO

The PDO is the first mode of variability of sea surface temperature (SST) in the North Pacific and oscillates between warm (positive) and cool (negative) phases with wide-ranging ecosystem effects (Mantua et al., 1997). The PDO was predominantly in a cool phase from 2008-2014 and 2020 -2021 and in a warm phase from 2014-2020 (Figure 3.2b). Every species aside from bottlenose dolphins had at least one statistically significant correlation between scaled sightings and the PDO (Figure 3.7). Humpback whales, long-beaked common dolphins, and Risso's dolphins had positive correlations with the PDO, while fin whales and Dall's porpoise had negative correlations with the PDO. Short-beaked common dolphins and Pacific white-sided dolphins had both positive and negative correlations with the PDO. The same-year and same-month correlations between cetacean scaled sightings and the PDO were stronger on average (that is, explained more of the variability in cetacean scaled sightings) than the correlations with the prior-year and 12-month average PDO.

Fin whale spring scaled sightings were negatively correlated with the 12-month average PDO ($r^2 = 0.256$, $p = 0.065$). Humpback whale fall scaled sightings were positively correlated with the 12-month average PDO ($r^2 = 0.231$, $p = 0.051$). While springtime blue whale scaled sightings are strongly correlated with the PDO (same month, $r^2 = 0.726$, $p = 0.00081$), blue whales are highly seasonal in the CalCOFI region and were only seen in the spring during two years (2011 and 2016), thus this result should be taken with caution. Short-beaked common dolphin scaled sightings were positively correlated with the PDO in the winter (same month, $r^2 = 0.300$, $p = 0.028$) and negatively correlated in the summer (12-month average, $r^2 = 0.1774$, $p = 0.095$). Long-beaked common dolphin annual scaled sightings were strongly positively correlated with the same-year average PDO value as well as with the prior-year's average value. Seasonally, long-beaked common dolphin scaled sightings were strongly positively correlated with the PDO in the winter (same-month, $r^2 = 0.743$, $p = 0.00015$) and weakly in the fall (12-month average, $r^2 = 0.197$, $p = 0.074$). Pacific white-sided dolphin scaled sightings were positively correlated with the PDO in the spring (same month: $r^2 = 0.239$, $p = 0.076$) but negatively correlated with the PDO during the summer (same month: $r^2 = 0.170$), $p = 0.10$), albeit weakly. Risso's dolphin had a positive correlation between annual scaled sightings and the same-year average PDO value ($r^2 = 0.790$, $p = 0.00018$). Fall Risso's dolphin scaled sightings were greater during times with strongly negative and strongly positive PDO values (same month, $r^2 = 0.512$, $p = 0.0065$), while summer scaled sightings were positively correlated with the PDO (12-month average, $r^2 = 0.323$, $p = 0.065$). Dall's porpoise annual scaled sightings were negatively correlated with both the same-year average PDO ($r^2 = 0.555$, $p = 0.00223$) as well as the prior-year PDO ($r^2 = 0.334$, $p = 0.030$). Seasonally, both the winter (same month: $r^2 = 0.245$, $p = 0.051$; 12-month average $r^2 = 0.213$, $p = 0,072$) and spring (same month: $r^2 = 0.268$, $p = 0.058$) scaled sightings were negatively correlated with the PDO.

3.3.6 Relationships with the MEI

The MEI measures the El Niño Southern Oscillation; MEI values greater than 0.5 indicate El Niño events and values below -0.5 indicate La Niña events. Values above 1.5 or below -1.5 denote strong events. During our survey period, we had one strong El Niño (2015-2016) and three strong La Niña events (2008-2009; 2010-2012; 2020-2021; Figure 3.2c). A negative correlation between cetacean scaled sightings and the MEI indicates a preference for La Niña conditions in the CalCOFI region, while a positive correlation indicates a preference for El Niño conditions. Three species had at least one statistically significant negative correlation with the MEI: fin whales, blue whales, and Dall's porpoise. Four species had at least one statistically significant positive correlation with the MEI: Short-beaked common dolphins, long-beaked common dolphins, Pacific white-sided dolphins, and Risso's dolphins. There were no statistically significant correlations between humpback whales or bottlenose dolphins and the MEI.

Fin whale scaled sightings in the summer were negatively correlated with the MEI (same month: $r^2 = 0.329$, $p = 0.016$). Blue whales' summertime scaled sightings were also negatively correlated with the MEI (12-month average: $r^2 = 0.289$, $p = 0.092$). This correlation was driven by the extremely high number of blue whale scaled sightings during the two most extreme La Niña events (2011 and 2021); sightings during other summer cruises were fairly consistent regardless of MEI values. During our survey period, blue whales were only seen during the spring in two years: one was during a strong La Niña (2011) and the other during the strong El Niño (2016). Therefore, springtime blue whale scaled sightings are strongly correlated with the MEI (same month, $r^2 = 0.887$, $p = 6.3 \times 10^{-6}$; 12-month average: $r^2 = 0.970$, $p = 3.85 \times 10^{-9}$); this result should be taken with caution, given the few sightings contributing to the results. Short-beaked common

dolphin annual scaled sightings were weakly positively correlated with the same-year MEI (r^2 = 0.219, p = 0.091), but the only significant seasonal correlation was fall during which scaled sightings were lower in both strong La Niña and El Niño years (r^2 = 0.295, p = 0.087). Long-beaked common dolphin annual scaled sightings were strongly positively correlated with the same-year average MEI (r^2 = 0.869, p = 1.38 x 10^{-5}); seasonally only fall scaled sightings were significantly correlated with the MEI (12-month average r^2 = 0.295, p = 0.087). Pacific white-sided dolphin scaled sightings were positively correlated with MEI in the spring (same month r^2 = 0.352, p = 0.092; 12-month average r^2 =0.450, p = 0.037) and fall (same month: r^2 = 0.398, p = 0.029). Risso's dolphin annual scaled sightings were positively correlated with the average MEI value of the same (r^2 = 0.593, p = 0.0071) and prior year (r^2 = 0.351, p = 0.092); summer scaled sightings were strongly positively correlated with the MEI (12-month average, r^2 = 0.617 , p = 0.0012). Dall's porpoise annual scaled sightings were negatively correlated with both the same (r^2 = 0.322, p = 0.034) and prior year (r^2 = 0.275, p = 0.054) average MEI; winter scaled sightings were weakly negatively correlated with the MEI (12-month average: r^2 = 0.184, p =0.097).

3.3.7 Associations with Marine Heatwaves

A marine heatwave is defined as a period of at least five contiguous days during which the temperature exceeds 90% of the measured temperatures at a given location and Julian day (Hobday et al., 2016); the Marine Heatwave Tracker product used here has a reference period of 1984-2020. During our study period, the largest, most intense marine heatwave occurred from 2014-2016 but smaller, less-intense marine heatwaves occurred throughout the record (Figure 3.2d). We found more statistically significant correlations between cetacean scaled sightings and marine heatwave extent than with any other climate variable tested (Figure 3.9). Most of these correlations were

positive, indicating an increase in those species during a marine heatwave: short-beaked common dolphins, long-beaked common dolphins, Risso's dolphins, and in the fall, humpback whales. Several correlations indicated an intermediate response: an increase in sightings with increasing marine heatwave extent up to a point, after which sightings decreased again. This was generally detectable with the 12-month average marine heatwave extent. Dall's porpoise was the only species to have a statistically significant negative correlation with marine heatwave extent. No statistically significant correlations were seen with fin whales and Pacific white-sided dolphins.

Humpback whale fall scaled sightings were positively correlated with the same-month marine heatwave extent ($r^2 = 0.326$, $p = 0.021$), whereas they had an intermediate response to the 12-month average extent ($r^2 = 0.418$, $p = 0.030$). Spring blue whale scaled sightings had an intermediate response to marine heatwave extent (same month: $r^2 = 0.442$, $p = 0.041$; 12-month average: $r^2 = 0.363$, $p = 0.084$); however, there were only two years with spring blue whale sightings (2011 and 2016, the latter occurring during the largest marine heatwave) so these results should be interpreted with caution. Short-beaked common dolphin annual scaled sightings were positively correlated with average marine heatwave extent of the same year ($r^2 = 0.241$, $p = 0.074$) whereas there was an intermediate response with the average marine heatwave extent of the prior year ($r^2 = 0.502$, $p = 0.022$). This annual response was driven by the winter season; short-beaked common dolphin winter scaled sightings were positively correlated with marine heatwave extent in the same month ($r^2 = 0.520$, $p = 0.0016$) and had an intermediate response with the 12-month average marine heatwave extent ($r^2 = 0.514$, $p = 0.0091$). Long-beaked common dolphins had similar—but stronger—correlations with marine heatwave extent as short-beaked common dolphins. Long-beaked common dolphin annual scaled sightings were positively correlated with both the average of the same year ($r^2 = 0.708$, $p = 0.0011$) as well as the average of the prior year's

marine heatwave extent ($r^2 = 0.784$, $p = 0.00022$). Winter scaled sightings were strongly positively correlated with the same month marine heatwave extent ($r^2 = 0.944$, $p = 7.7 \times 10^{-9}$), whereas there was a weaker, intermediate response to the 12-month average marine heatwave extent ($r^2 = 0.465$, $p = 0.017$). Bottlenose dolphin annual scaled sightings were positively correlated with the average of the prior year's marine heatwave extent ($r^2 = 0.265$, $p = 0.060$) and summertime scaled sightings had an intermediate response to the 12-month average marine heatwave extent ($r^2 = 0.402$, $p = 0.035$). Annual scaled sightings of Risso's dolphins were correlated with the annual average marine heatwave extent of the same year ($r^2 = 0.410$, $p = 0.014$) as well as with the average of the prior year ($r^2 = 0.696$, $p = 0.00021$). Seasonally, Risso's dolphin scaled sightings had a strong positive correlation with marine heatwave extent in the spring (same month: $r^2 = 0.855$, $p = 2.4 \times 10^{-5}$; 12-month average: $r^2 = 0.801$, $p = 0.00014$) and an intermediate response in the summer (12-month average, $r^2 = 0.530$, $p = 0.0074$). Dall's porpoise annual scaled sightings had a negative correlation to both the average marine heatwave extent of the same year ($r^2 = 0.634$, $p = 0.0040$) as well as the prior year ($r^2 = 0.486$, $p = 0.026$); springtime scaled sightings showed an intermediate response correlation (same month: $r^2 = 0.354$, $p = 0.09$).

3.4 Discussion

The past several years have been unusual in the Southern California Bight and the California Current more broadly. A marine heatwave, unprecedented in spatial extent, intensity, and duration, started in the winter of 2013-2014 in the north Pacific and continued through 2016, exacerbated by the strong 2015-2016 El Niño (Jacox et al., 2018). Sea-surface temperatures have remained above average in the southern CalCOFI region since 2014, despite La Niña conditions in 2020-2021 (Weber et al., 2021). This marine heatwave impacted North Pacific ecosystems in many ways, including shifting the distributions of animals throughout the California Current, with

many species moving northward (Cavole et al., 2016) or inshore (Santora et al., 2020). We would expect such changes in the ecosystem to be reflected in changes in the cetacean distributions. Indeed, we found that the marine heatwave was the most important correlate of marine mammal presence in the CalCOFI region (Figure 3.9). These correlations were particularly strong with the delphinids and porpoise species.

3.4.1 Overall Temporal Trends

The most dramatic change during our survey was the overall decrease of Dall's porpoise presence in the study region starting in 2014 (Figures 3.4k-l and 3.5). This relatively recent development was not captured in a previous study by Campbell et al. (2015) which analyzed the CalCOFI visual cetacean surveys from 2004-2013, during which Dall's porpoise density was steady. Dall's porpoises are known to be associated with cooler waters (Becker et al., 2017; Fleming et al., 2018; Jefferson, 2018). It is therefore unsurprising that Dall's porpoise scaled sightings declined after 2013, with the onset of the large marine heatwave and the persistently above-average temperatures in the CalCOFI region that followed. A recent review found that Dall's porpoises were experiencing a northward contraction in their range, consistent with their decreased presence in the southern California Current (Weelden et al., 2021). However, increased mortality cannot be ruled out: Dall's porpoise strandings are positively correlated with SST and have a lagged correlation with the PDO, at least in the northern California Current (Warlick et al., 2022); further research will be needed to determine if this relationship holds in the southern California Current as well. Whether the decrease in Dall's porpoise scaled sightings in this survey is due solely to a northward distribution shift or whether mortality has contributed to the reduction is unknown.

The trajectory of Dall's porpoise in the region may be following that of the short-finned pilot whale. This squid-eating delphinid was once abundant in the Southern California Bight, but their populations decreased following the 1982-1983 El Niño (Shane, 1995). By the 1990s, they were absent from the region (Smultea & Jefferson, 2014). The loss of short-finned pilot whales from the region presumably opened up a niche to be filled by another squid-eating delphinid, Risso's dolphin, now the fifth-most abundant delphinid species in the region. It is unclear at this time whether a similar species replacement will occur following the reduction of Dall's porpoise in the region, opening up the niche previously occupied by the porpoise. Dall's porpoises forage on small squid and mesopelagic fishes (Ohizumi et al., 2003; Pauly et al., 1998). Similar prey is exploited by short-beaked common dolphins, long-beaked common dolphins, and Risso's dolphins (Pauly et al., 1998) – all animals that had a positive relationship with the marine heatwave in our study. We may see more permanent increases in the population of these species if marine heatwaves become more frequent under climate change.

Scaled sightings of Pacific white-sided dolphin showed a weak decreasing trend over the study period, driven by decreases in scaled sightings during the winter season (Figures 3.4e-f and 3.5). Interestingly, their wintertime scaled sightings were not correlated with any of the climate variables tested in the study. The observed decline may be caused by changes in the underlying ecosystem during the winter that are not reflected in the climate variables used in this study. The decline may also be due to increased interspecific competition: winter sightings of both offshore bottlenose dolphins and short-beaked common dolphins have increased over the study period.

Similarly, species competition may be the driver of the simultaneous summertime decrease in short-beaked common dolphin scaled sightings and increase in long-beaked common dolphin

scaled sightings. These two delphinids exhibit some geographic and habitat niche partitioning: short-beaked common dolphins are typically found farther offshore than long-beaked common dolphins, which are found within 100 nautical miles of the coast in the Eastern Pacific (Heyning & Perrin, 1994). Historically, short-beaked common dolphins moved into the Southern California Bight from offshore during periods when long-beaked common dolphins retreated farther south into the waters off Baja (Banks & Brownell, 1969). We may be seeing the reverse: with warmer-than-average temperatures in the CalCOFI region since 2014, long-beaked common dolphins may be increasing at the expense of short-beaked common dolphins, at least in the summer.

3.4.2 Marine Heatwaves

In our study, two species were found to have particularly strong correlations with marine heatwave extent: long-beaked common dolphins and Risso's dolphins. The distributions of both animals are known to have shifted historically in response to changes in oceanographic conditions. In the mid-1800s, warm-water conditions in the central California Current resulted in many tropical fish species moving northward (Hubbs, 1948); stranded cetacean specimens indicated that long-beaked common dolphins were common as far north as Monterey Bay during this time period. But by the turn of the 20th century, cooler oceanographic conditions prevailed, and the dolphins retreated south into the waters off Baja California and the Gulf of California (Banks & Brownell, 1969). Stranding data suggests that long-beaked common dolphins became more abundant in the Southern California Bight during and after the 1982-1983 El Niño (Heyning & Perrin, 1994). Risso's dolphins have been sighted in the Southern California Bight intermittently during periods of warm water. For example, Risso's dolphins were not seen in surveys during the 1950s and 1960s (Smultea & Jefferson, 2014), however they were abundant during 1974 when sea-surface

temperatures in the region were “unusually high” (Leatherwood et al., 1980). The population of Risso’s dolphins in the southern California Bight increased during the 1980s and 1990s, coinciding with the decline of another squid-eating cetacean, the short-finned pilot whale, following the strong 1982-1983 El Niño (Shane, 1995; Smultea & Jefferson, 2014). These historical accounts support the hypothesis of movement of both long-beaked common dolphins and Risso’s dolphins into the Southern California Bight in response to warm oceanographic conditions.

Recent habitat modeling suggests that long-beaked common dolphins moved north from Mexican waters into the US portion of the California Current – including the southern CalCOFI region – in 2014 in response to the marine heatwave, and earlier in 2008 in response to warm ocean conditions (Becker et al., 2022). We did not find such an increase in 2008 or in 2014, when sightings were lower than average. We did, however, find a dramatic increase in animals seen in 2015 and 2016 during the latter portion of the marine heatwave. The increase in 2015 was primarily due to the large number of sightings of long-beaked common dolphins during the winter cruise, when an average of 90% of the southern California region was experiencing marine heatwave conditions. This is consistent with the distribution shifts proposed by Becker et al. (2022), but a year later than predicted; the reason for this delay is unknown. This illustrates the strength of our dataset and the importance of frequent sampling in order to diagnose fine-scale temporal patterns.

Short-beaked common dolphins, like their close relatives the long-beaked common dolphins, showed a correlation with marine heatwave extent, driven by changes during the winter season. Habitat modelling predicted greater abundances of short-beaked common dolphins in the Southern California Bight in 2014 due to marine heatwave conditions, reflecting a northward shift of dolphins residing in Mexican waters off Baja (Becker et al., 2022). We found an increase in

short-beaked common dolphin scaled sightings a year later than predicted, as scaled sightings were average in 2014 but extremely high in 2015. However, in 2016 annual scaled sightings had sunk to their second-lowest in the study period (considering years with complete seasonal survey effort only). Although the marine heatwave was still ongoing, other changes to the environment or prey distribution may have reduced the favorability of the conditions in 2016 relative to 2015 in the CalCOFI region.

For several dolphin species (long-beaked and short-beaked common dolphin and Risso's dolphin), the animals that were seen during the winter and spring of 2015 were congregated in very large groups. Common dolphins of both subspecies exhibit fission-fusion behavior, when small groups of individuals (fewer than 30 individuals) come together to form super groups of hundreds to thousands of dolphins (Perrin, 2018). Likewise, Risso's dolphins are known to spend most of their time in smaller groups of approximately 10-30 individuals; however, large assemblages of over 1000 individuals have been observed (Hartman, 2018). During the winter 2015 cruise, the largest groups of the 18 years of CalCOFI visual surveys were observed for both long-beaked (~3300 individuals) and short-beaked common dolphins (~4600 individuals). During the spring 2015 cruise, the largest group of Risso's dolphin was encountered (~370 individuals), although this group was diffuse. Dolphin school size can be a function of prey type and availability, with trade-offs between cooperation and competition among dolphins. While research is limited regarding the roles of climate on group size of dolphin species, SST has been found to have a non-linear correlation with group size in common and Risso's dolphin, with warmer temperatures favoring larger groups (Gygax, 2002). There is evidence that group size can vary with large-scale climate indices in Pacific killer whales and bottlenose dolphins, due to environmentally forced

changes in the dolphins' prey; increased prey abundance was correlated with larger group sizes (Lusseau et al., 2004).

The increase in delphinid sightings in the CalCOFI region during the 2014-2016 marine heatwave presumably reflected favorable prey conditions within the region. During the heatwave, many animals exhibited unusual distribution patterns, including zooplankton, fish, squid, and crustaceans (Cavole et al., 2016). While many important prey species such as krill, sardine, and anchovy were negatively impacted by the marine heatwave (Cimino et al., 2020; Killeen et al., 2021; McClatchie et al., 2016), other potential prey species increased in the CalCOFI region. Large numbers of tropical fish were seen in the southern California Bight during the 2014-2016 marine heatwave and El Niño (Walker et al., 2020). Ichthyoplankton species richness increased in the southern California Current, driven primarily by an increase in warm water species, although cold-water associated ichthyoplankton also increased in abundance in a narrow region close to the shore where cooler waters acted as a refuge (Nielsen et al., 2021). Changes in larval fish species abundance can reflect both a change in the survival rate of larval fishes as well as a change in the distribution and spawning behavior of the adult fish (Nielsen et al., 2021) and thus may be indicative of prey availability for piscivore cetaceans.

While our study focuses on changes in animal sightings within the southern CalCOFI region, reflecting movements of the animals into and out of the region, it is possible that cetaceans may have altered their distributions within the region. For example, marine heatwaves may compress whale habitat inshore where upwelling leads to cooler waters and refugia for prey species (Santora et al., 2020). This habitat compression can lead to increased overlap between cetacean species and coastal fisheries, increasing entanglement risk (Santora et al., 2020). Such habitat

compression occurred in the fall of 2015, with species typically found farther offshore, such as baleen whales and short-beaked common dolphins moving inshore (McClatchie et al., 2016). However, a more in-depth analysis of marine mammal spatial distributions within the CalCOFI region is needed to fully understand if and when cetaceans show within-region distribution shifts in response to climate variability such as marine heatwave events.

3.4.3 El Niño / La Niña

El Niño and La Niña events can have profound impacts on the ecosystem of the California Current. During our survey period of 2004-2021, we had one strong El Niño (2015-2016) and three strong La Niña periods (2008-2009; 2010-2012; 2020-2021). La Niña conditions are associated with cooler temperatures, increased productivity, and increased abundance of krill (Checkley & Barth, 2009; Cimino et al., 2020). While El Niño conditions are warmer and less productive (Checkley & Barth, 2009), they are associated with an increase in fish species richness in the CalCOFI region, (Koslow et al., 2017) providing potential prey for piscivore cetaceans. We found that delphinids (except for bottlenose dolphin) were positively correlated with the MEI, indicating a preference for El Niño conditions. Blue whales, fin whales, and Dall's porpoise, on the other hand, were negatively correlated with the MEI, indicating a preference for La Niña conditions.

Krill abundance increases during La Niña conditions in the California Current (Cimino et al., 2020). The three baleen whales in our study forage on krill: blue whales are obligate krill foragers, but fin and humpback whales are both generalists that can forage on zooplankton or fish (Pauly et al., 1998). While we found correlations between blue whale and fin whale sightings and the MEI during the summer, we found no correlation between humpback whale sightings and the MEI. Summer is considered to be the prime foraging season for baleen whales, and both blue and

fin whales are most abundant in the CalCOFI region during the summer (Table 2). In contrast, summer is the season with the lowest humpback whale abundance in our study area, indicating that the CalCOFI region is a less important foraging ground for humpback whales in the summer than for blue or fin whales (Table 2). Further research is needed to test for relationships between humpback whale abundance and the MEI at their prime summertime foraging grounds.

During the summer of 2021, blue whale scaled sightings in the CalCOFI region were more than double those of the next-highest cruise. During this time there was a strong La Niña which started in September 2020 and continued throughout 2021. Three of the years with the highest summertime blue whale scaled sightings occurred during La Niña years: 2011, 2017, 2021. However, other La Niña years did not have high blue whale scaled sightings. Consequently, we found only a weak relationship between summertime blue whale scaled sightings and the MEI; it was almost entirely driven by the 2011 and 2021 cruises, which had both the most negative MEI values in our survey period and much higher scaled sightings than any other cruises (Figures 3.3e and 3.8). This may indicate that there is a threshold effect whereby only sufficiently strong La Niña events provoke a large increase in blue whale presence in the CalCOFI region. There may also be a more complicated temporal lag between the onset of La Niña events and when blue whales respond. Blue whales modulate the timing of their foraging due to the prior year's sea-surface temperature (Szesciorka et al., 2020); it is possible that a change in their migration timing relative to the timing of our surveys might complicate our ability to detect a response.

Both long-beaked common dolphins and Risso's dolphins were strongly correlated with the MEI on an annual basis. However, a closer look at the seasonal data complicates this association. A large El Niño event began in the summer of 2015, whereas larger-than-average

schools of long-beaked common dolphins and Risso's dolphin were seen in the winter and spring of 2015, respectively, *before* the onset of the El Niño. While scaled sightings were high for both species in 2015, it was not due to the El Niño event; rather, the marine heatwave was the apparent driver of the elevated 2015 scaled sightings. However, Risso's dolphin scaled sightings remained elevated in 2016, particularly in the summer, which drove the strong seasonal correlation between summertime scaled sightings and the 12-month average MEI. Long-beaked common dolphins had a weak correlation of the 12-month average MEI and fall sightings; 2016 had the highest number of Risso's dolphin scaled sightings during the fall and the second highest scaled sightings of Risso's dolphins overall. These nuanced relationships between marine mammal presence and climate variables are only possible to detect when using seasonally resolved data.

3.4.4 PDO

With the exception of bottlenose dolphins, every cetacean species in our survey had at least one statistically significant correlation between scaled sightings and the PDO (Figure 3.7). The PDO is defined as the leading principal component of North Pacific SST variability, reflecting warm and cool multidecadal phases (Mantua et al., 1997). Both the PDO and marine heatwave extent were non-linearly correlated (r^2 = 0.413, p= 2.24 x10^{-25}) during our study period. It is therefore not surprising that many species with strong responses to the marine heatwave also had a strong response to the PDO. However, there were notable differences in correlations between the marine heatwave extent and the PDO for several species. For example, both fin whales and Pacific white-sided dolphins had statistically significant correlations with the PDO but not with marine heatwave extent, while the opposite was true for bottlenose dolphins.

3.4.5 NPGO

A positive NPGO is associated with upwelling-favorable conditions in the southern California Current, when early onset of upwelling-favorable winds results in a more productive ecosystem (Chenillat et al., 2012; Lorenzo et al., 2008). Counterintuitively, most of the correlations we found between cetacean scaled sightings and the NPGO were negative, indicating that fewer cetaceans were seen during the "productive phase" of the NPGO. This may be due to regional variation of the NPGO response within the California Current: upwelling has a stronger response to the NPGO in the central California Current relative to the southern California Current (Chenillat et al., 2012). Cetaceans may move north into the central California Current to take advantage of the greater upwelling-driven productivity in this region, thus driving a negative correlation with the NPGO inside the CalCOFI study region.

The NPGO is positively correlated with krill abundance in the California Current (Sydeman et al., 2013). Humpback whales forage on both krill and pelagic fishes (Pauly et al., 1998). Stable isotope analyses have shown that humpback whale diet is correlated with the NPGO in the California Current: during the positive NPGO phase their diet is dominated by krill, while during the negative, less-productive phase, humpback whale diet was dominated by schooling fish (Fleming et al., 2015). In our study, humpback whale sightings in the fall were negatively correlated with the NPGO (Figure 3.6). Humpback whale abundance was quite low during the fall when the NPGO was positive, but more variable when the NPGO was neutral or negative. These results suggest that humpback whale abundance in the fall is low during years when humpbacks forage primarily on krill, but not during years when pelagic fish dominate their diet. This relationship between the NPGO and humpback abundance is likely the driver of fluctuations in

fall humpback whale sightings: no on-effort, on-transect humpback whale sightings occurred between 2007-2011 or in 2013 – times when the NPGO was negative (Figure 3.2a). It is not surprising that the correlation between humpback whales was stronger with the 12-month average NPGO value than same month NPGO value: the NPGO impacts the California Current through the timing of the onset of upwelling (Chenillat et al., 2012), and it takes time for changes in upwelling-driven productivity to influence the prey of humpback whales, zooplankton and small pelagic fish.

3.4.6 Survey limitations

Group size estimates can vary widely among species and observers and thus represent a source of bias in visual observations, particularly for dolphins in group sizes larger than 25 where group sizes are frequently underestimated (Gerrodette et al., 2019). This will result in a negative bias in density estimation for species that regularly form large groups, such as the common dolphins, and also for species such as Risso's dolphins that periodically form large groups. The large scaled sightings of Risso's dolphins, long-beaked common dolphins, and short-beaked common dolphins in 2015 were driven by such large-group encounters; it is possible that the true number of animals seen for that year may be even greater than our estimates. If so, the impact of the marine heatwave on the delphinid populations in the CalCOFI region would be even larger than our analyses indicate.

Another difficulty with visual surveys is the inability to differentiate among multiple populations of the same species. This may complicate our ability to detect the impact of climate variability on a species if different populations overlap or replace one another in a given region. For example, there are two genetically distinct populations of Pacific white-sided dolphins in the

California Current: a northern population that is found from central California north to Washington, and a southern population that primarily occurs off Baja California (Lux, 1997, as cited in Soldevilla et al., 2010). Habitat modeling and acoustic evidence suggest that both populations are found in the southern CalCOFI region (Becker et al., 2022; Soldevilla et al., 2010). Because these two populations cannot be distinguished visually, we cannot determine which group of Pacific white-sided dolphins was seen during visual surveys. Thus, any changes between the populations will not be detectable in our data. This may obscure our ability to detect the responses of Pacific white-sided dolphins to climate variability if, for example, both populations respond to a marine heatwave by moving north. In this case, the northern population of Pacific white-sided dolphins would leave the southern CalCOFI region to be replaced by the southern population moving north from Mexican waters into the Southern California Bight, obscuring the actual response of the species to the marine heatwave. To test this replacement hypothesis, additional techniques such as genetic sampling or acoustic recordings are necessary.

This issue may also affect Risso's dolphins. Habitat models have suggested that Risso's dolphins have distinct populations within the California Current: an inshore population and an offshore population (Becker et al., 2016). The majority of the Risso's dolphins in our study were found inshore, presumably associated with the inshore population. Habitat models in the California Current have difficulty modeling the distributions of Risso's dolphin; this is thought to arise from either different responses of these two populations to oceanographic conditions, or difficulty modelling the environmental drivers of their large and small mesopelagic squid prey (Becker et al., 2016, 2020; Pauly et al., 1998). While we found several correlations between Risso's dolphins and climate variability, it is possible that these results were distorted in some way by our inability to visually separate the two populations.

3.5 Conclusions and future outlook

Cetaceans are important top predators in the California Current Ecosystem. Our study has investigated the relationship between cetaceans in the CalCOFI region and climate variability, including marine heatwaves. Since 2014, the southern California Current has had warmer than average SST (Weber et al., 2021) —driven, in particular, by an intense, long-lasting marine heatwave from 2014-2016 as well as several subsequent heatwaves (Figure 3.2d). Marine heatwaves are forecasted to increase under climate change (Frölicher et al., 2018) and therefore it is important to understand how marine heatwaves impact ecosystems such as the California Current. We found more statistically significant correlations between cetacean scaled sightings and marine heatwave extent than with any other climate variable tested. During the 2014-2016 marine heatwave, scaled sightings of three delphinids (short-beaked and long-beaked common dolphins, and Risso's dolphins) increased dramatically; increases in scaled sightings coincided with the formation of large groups in these species. If marine heatwaves increase in frequency, we may expect to see these species more frequently in the CalCOFI region. Although annual scaled sightings for most species showed no statistically significant trend over time, annual scaled sightings of Dall's porpoise and Pacific-white sided dolphins decreased over the study period. The decline in Dall's porpoise scaled sightings has occurred since 2014 and the onset of warmer-than-usual SST and increased marine heatwave extent. If warm conditions persist, it is possible that Dall's porpoise may shift their range to the north, resulting in a continued decline in sightings within the CalCOFI region.

Our study also showed the importance of seasonally resolved data in understanding complex relationships between cetaceans and climate variability. For example, we found that blue and fin whale scaled sightings were greater during La Niña conditions, but only during the summer

season; no relationship was found on annual timescales. We also found that long-beaked common and Risso's dolphin scaled sightings were higher during El Niño events when aggregated on an annual basis, in large part due to increased scaled sightings in 2015. Looking at the data seasonally shows that the increase in scaled sightings in 2015 occurred before the onset of the 2015-2016 El Niño and is thus attributed to the 2014-2016 marine heatwave and not the ENSO event. Frequent data collection improves our understanding of how ecosystems respond to changes in climate forcing, which will become even more important as climate change continues.

Chapter 3, in part, is currently being prepared for submission for publication of the material. Giddings, A., Franks, P. J. S. & Baumann-Pickering, S. The dissertation author was the primary investigator and author of this paper.

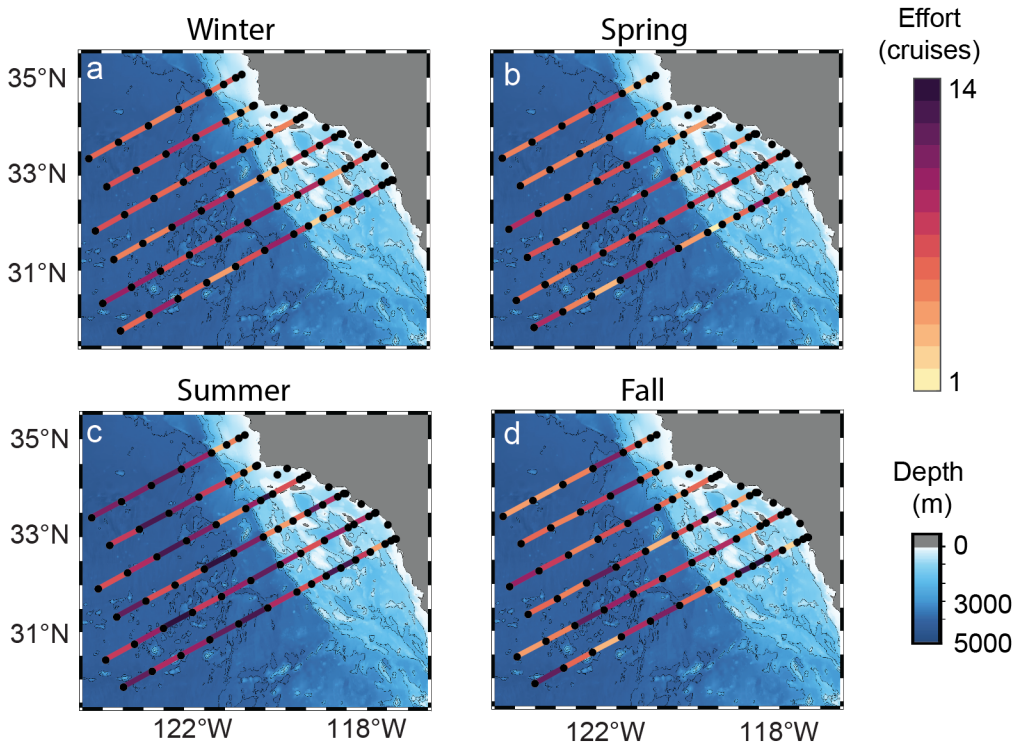

Figure 3.1: Marine mammal visual survey effort, 2004-2021, during a) winter (b) spring (c) summer and (d) fall. Survey effort is depicted with a colored line showing the number of cruises during which on-effort marine mammal visual surveys occurred along a given transect between CalCOFI stations (black dots).

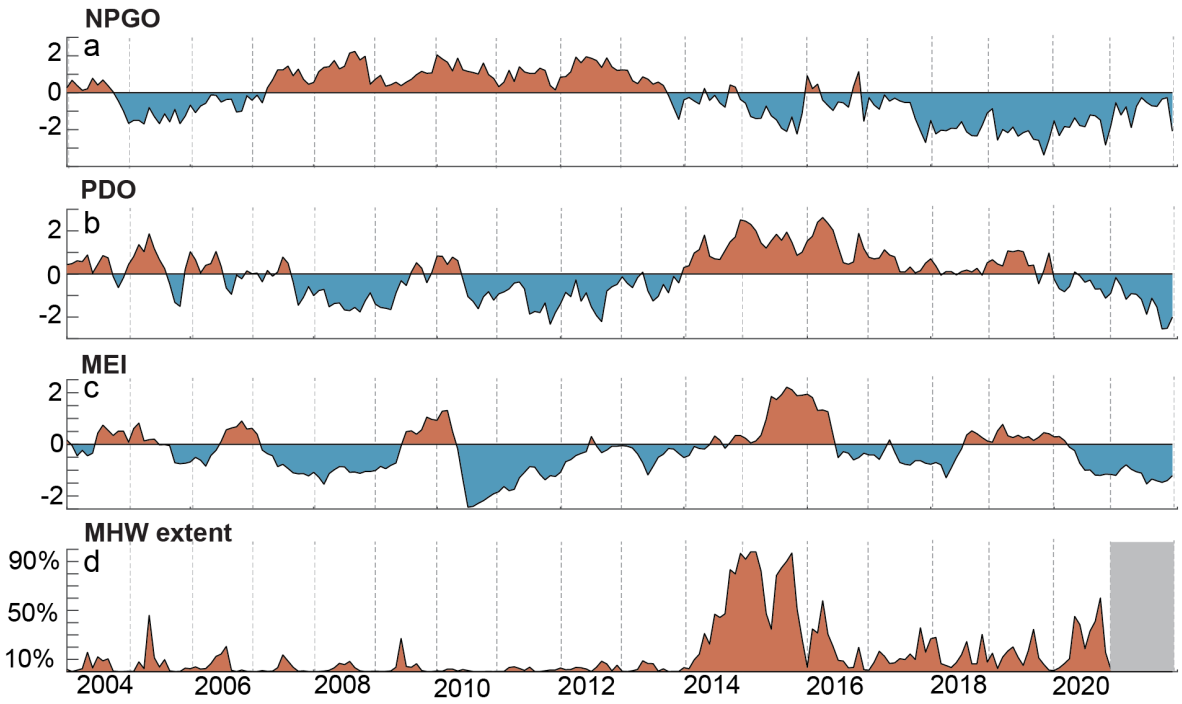

Figure 3.2: Time series of climate indices and marine heatwave extent, 2004-2021. (a) North Pacific Gyre Oscillation (NPGO) (b) Pacific Decadal Oscillation (PDO) (c) Multivariate ENSO Index Version 2 (MEI) (d) monthly average Marine heatwave spatial extent (MHW). Note that the MHW data was not available for 2021 (grey box).

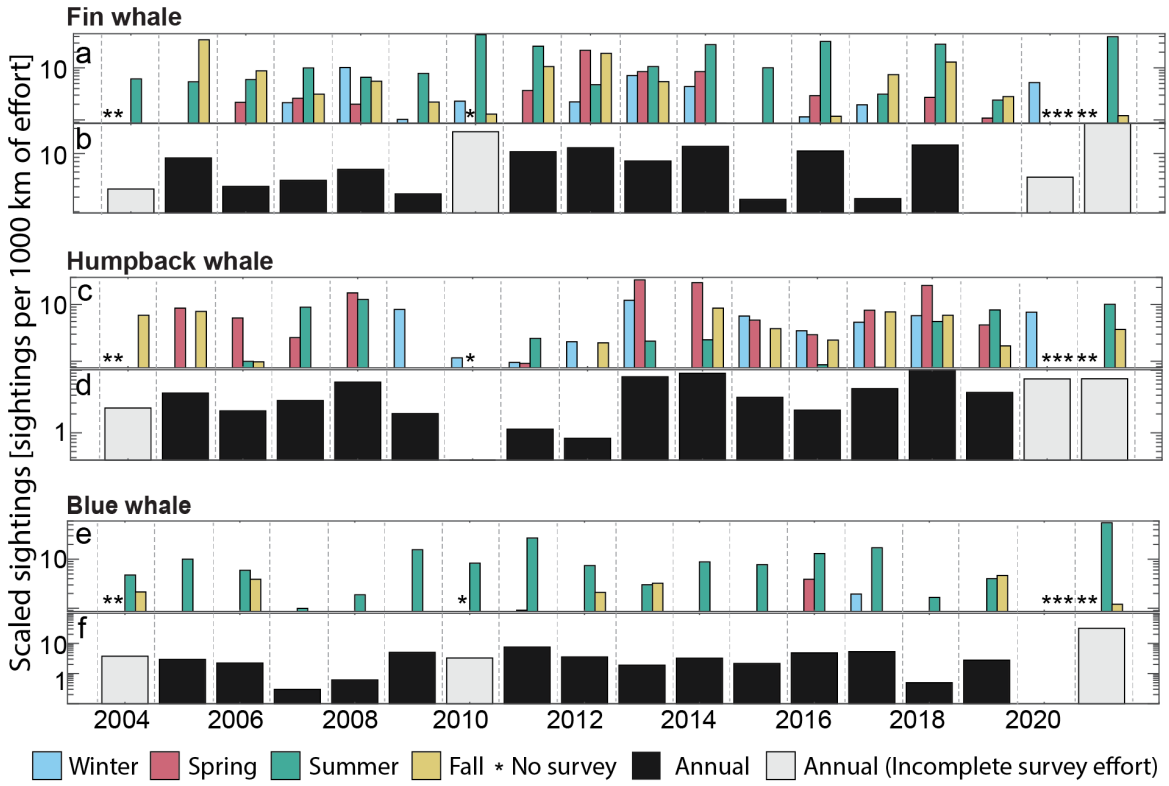

Figure 3.3: Baleen whale scaled sightings (defined as sightings per 1000 km of on-effort, on-transect survey effort). Seasonal (a, c, e) and annual (b, d, f) sightings, scaled per 1000 km of effort for (a, b) fin whales, (c, d) humpback whales, and (e, f) blue whales. Note that the y-axis is a log scale. Seasonal scaled sightings are colored by season: winter = blue, spring = magenta, summer = green, fall = yellow. Annual scaled sightings from years in which one or more seasons were not sampled are shown in light grey. Asterisks indicate seasons in which no visual surveys were conducted: the winter and spring of 2004, the spring of 2010, the spring, summer, and fall of 2020, and the winter and spring of 2021.

Figure 3.4: Toothed whale scaled sightings (defined as sightings per 1000 km of on-effort, on-transect survey effort). Seasonal (a, c, e, g, i, k) and annual (b, d, f, h, j, l) sightings, scaled per 1000 km of effort for (a, b) short-beaked common dolphins, (c, d) long-beaked common dolphins, (e, f) Pacific white-sided dolphins, (g, h) bottlenose dolphins, (i, j) Risso's dolphins, and (k, l) Dall's porposes. Note that the y-axis is a log scale. Seasonal scaled sightings are colored by season: winter = blue, spring = magenta, summer = green, fall = yellow. Annual scaled sightings from years in which one or more seasons were not sampled are shown in light grey. Asterisks indicate seasons in which no visual surveys were conducted: the winter and spring of 2004, the spring of 2010, the spring, summer, and fall of 2020, and the winter and spring of 2021.

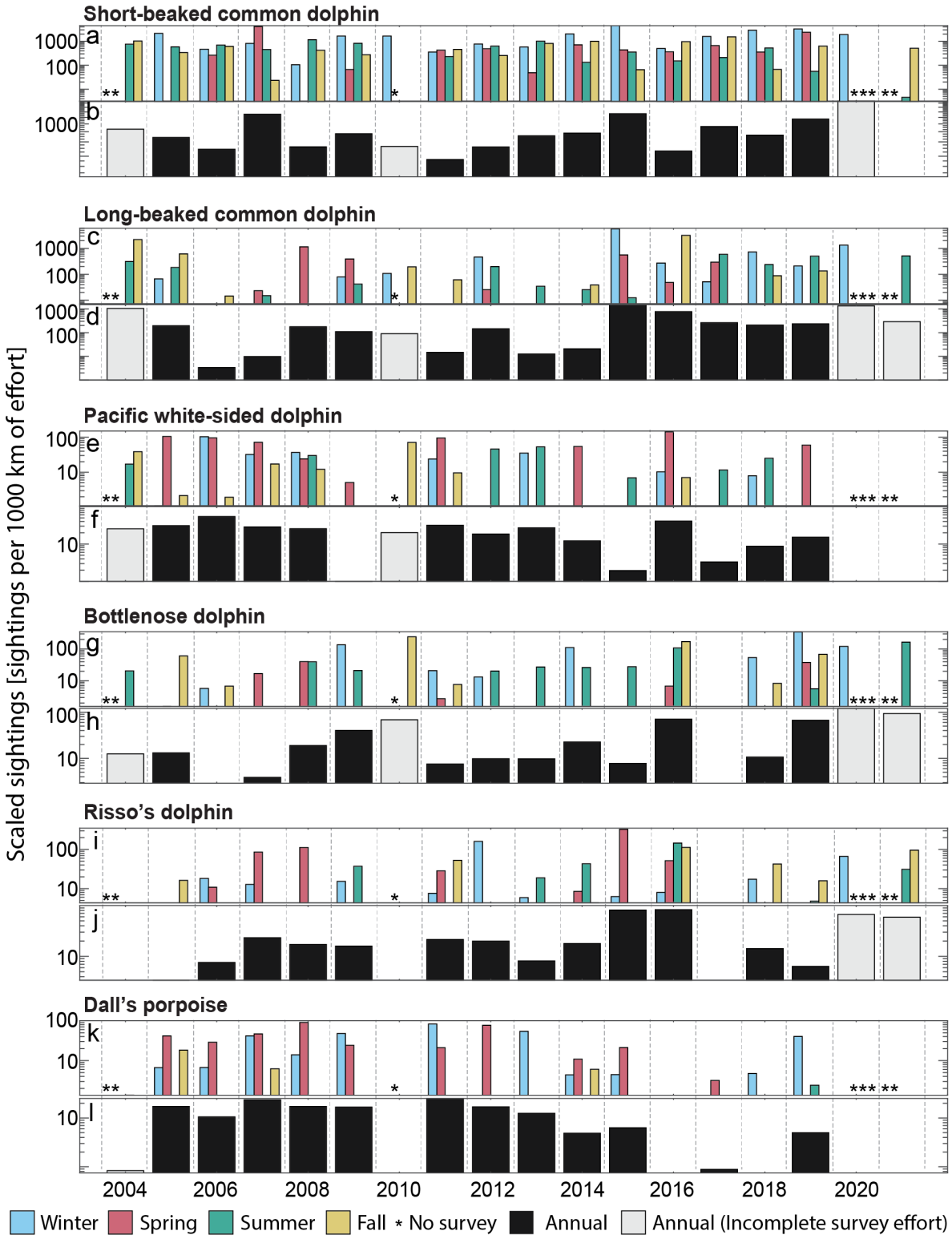
Short-beaked common dolphin
Long-beaked common dolphin
Pacific white-sided dolphin
Bottlenose dolphin
Risso's dolphin
Dall's porpoise
Scaled sightings [sightings per 1000 km of effort]
2004
2006
2008
2010
2012
2014
2016
2018
2020
Winter
Spring
Summer
Fall
* No survey
Annual
Annual (Incomplete survey effort)

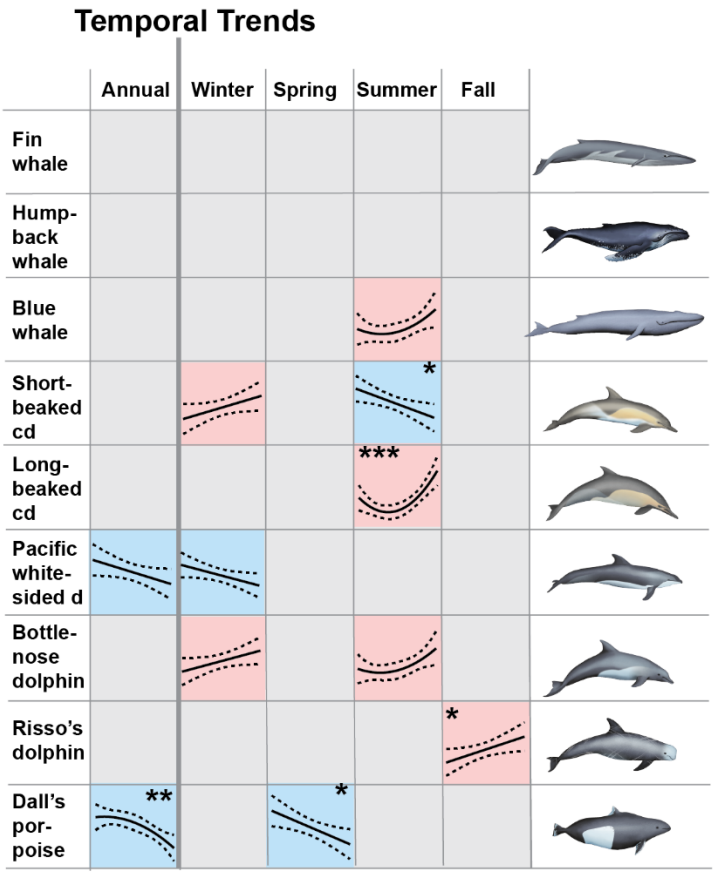

Figure 3.5: Annual and seasonal trends in scaled sightings (y-axis) over time (x-axis). Linear or quadratic models and 95% confidence intervals are shown for trends that were statistically significant at the p=0.1 level. Asterisks indicate statistical significance: no asterisk ($0.05 < p < 0.1$), one asterisk ($0.01 < p < 0.05$), two asterisks ($0.001 < p < 0.01$) , or three asterisks ($p < 0.001$) Grey boxes indicate there was no statistically significant trend. Blue indicates a decreasing trend and pink indicates an increasing trend. Cetacean illustrations by Freya Hammar.

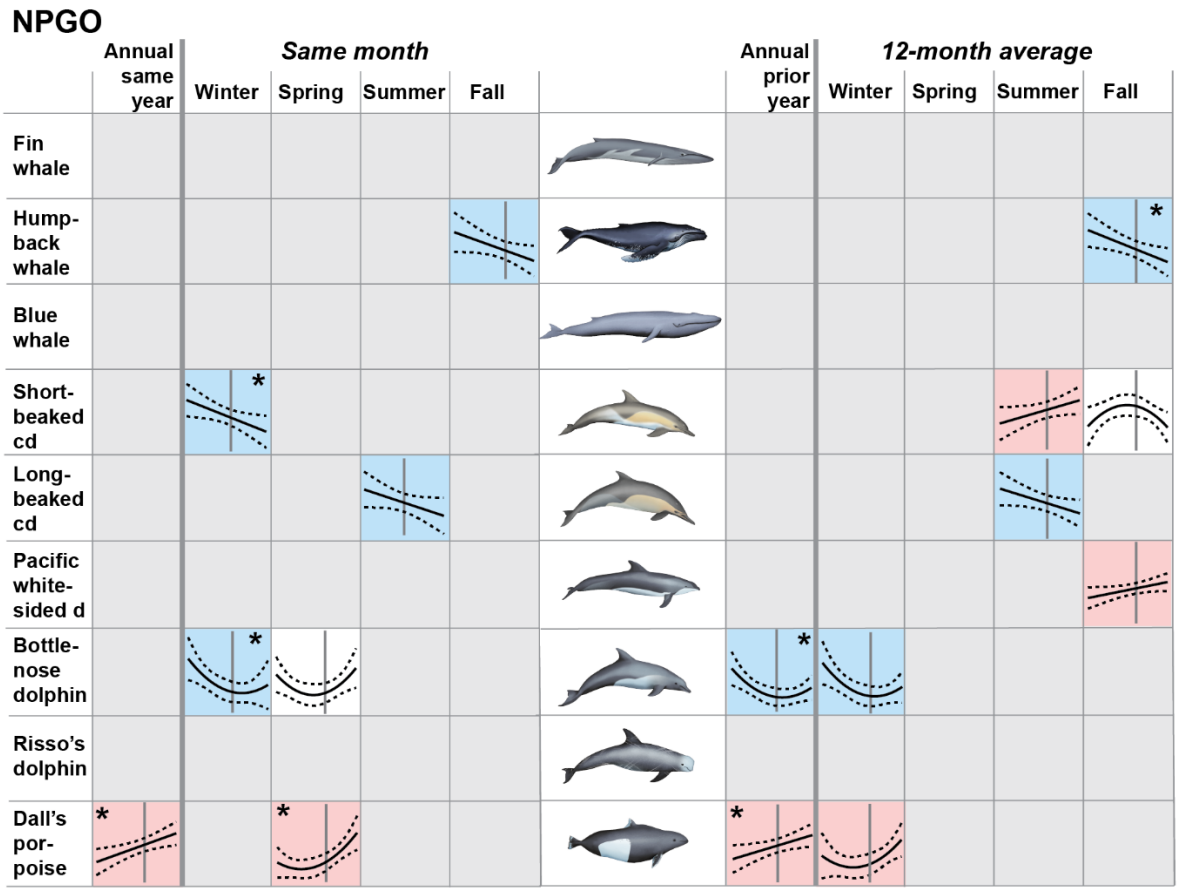

Figure 3.6: Correlations between the NPGO (x-axis) and annual and seasonal scaled sightings (y-axis). Linear or quadratic models and 95% confidence intervals are shown for correlations that were statistically significant at the p=0.1 level. Asterisks indicate statistical significance: no asterisk ($0.05 < p < 0.1$), one asterisk ($0.01 < p < 0.05$), two asterisks ($0.001 < p < 0.01$) , or three asterisks ($p < 0.001$) Grey boxes indicate there was no statistically significant correlation. Blue indicates a negative correlation, pink indicates a positive correlation, and white indicates an intermediate response. A grey line is placed at the 0 value of the NPGO, with negative values to the left and positive values to the right. Cetacean illustrations by Freya Hammar.

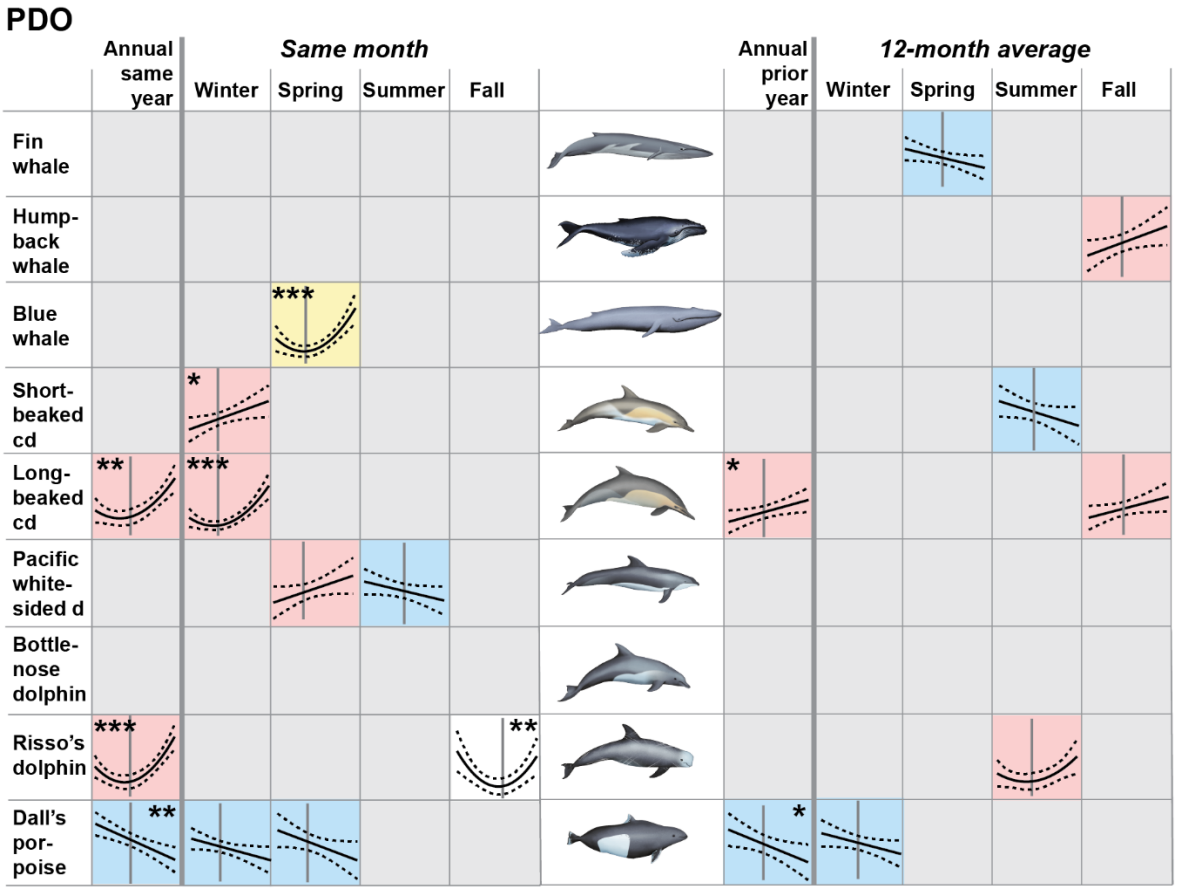

Figure 3.7: Correlations between the PDO (x-axis) and annual and seasonal scaled sightings (y-axis). Linear or quadratic models and 95% confidence intervals are shown for correlations that were statistically significant at the p=0.1 level. Asterisks indicate statistical significance: no asterisk ($0.05 < p < 0.1$), one asterisk ($0.01 < p < 0.05$), two asterisks ($0.001 < p < 0.01$) , or three asterisks ($p < 0.001$) Grey boxes indicate there was no statistically significant correlation. Blue indicates a negative correlation, pink indicates a positive correlation, and white indicates an intermediate response. Yellow indicates that the correlation is based on extremely limited data and thus should be interpreted with caution. A grey line is placed at the 0 value of the PDO, with negative values to the left and positive values to the right. Cetacean illustrations by Freya Hammar.

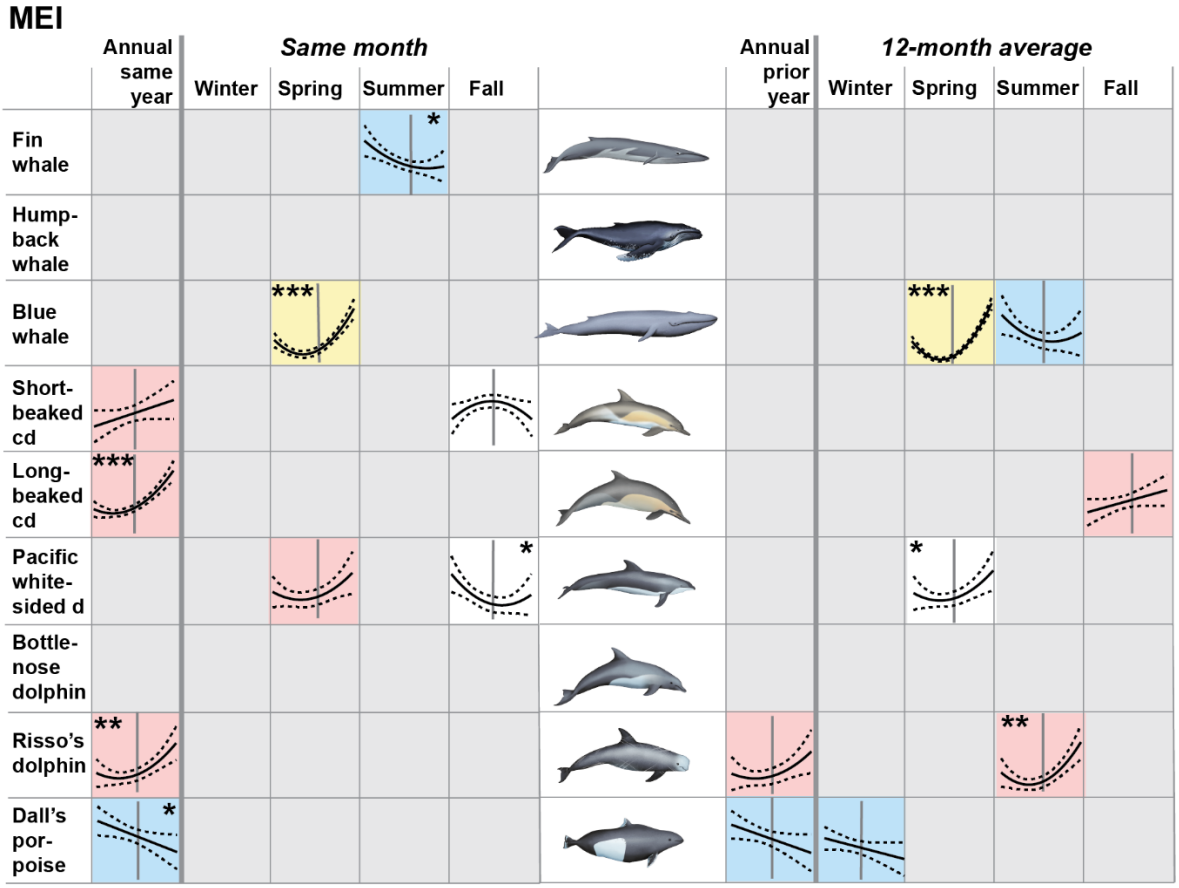

Figure 3.8: Correlations between the MEI (x-axis) and annual and seasonal scaled sightings (y-axis). Linear or quadratic models and 95% confidence intervals are shown for correlations that were statistically significant at the p=0.1 level. Asterisks indicate statistical significance: no asterisk ($0.05 < p < 0.1$), one asterisk ($0.01 < p < 0.05$), two asterisks ($0.001 < p < 0.01$) , or three asterisks ($p < 0.001$) Grey boxes indicate there was no statistically significant correlation. Blue indicates a negative correlation, pink indicates a positive correlation, and white indicates an intermediate response. Yellow indicates that the correlation is based on extremely limited data and thus should be interpreted with caution. A grey line is placed at the 0 value of the MEI, with negative values to the left and positive values to the right. Cetacean illustrations by Freya Hammar.

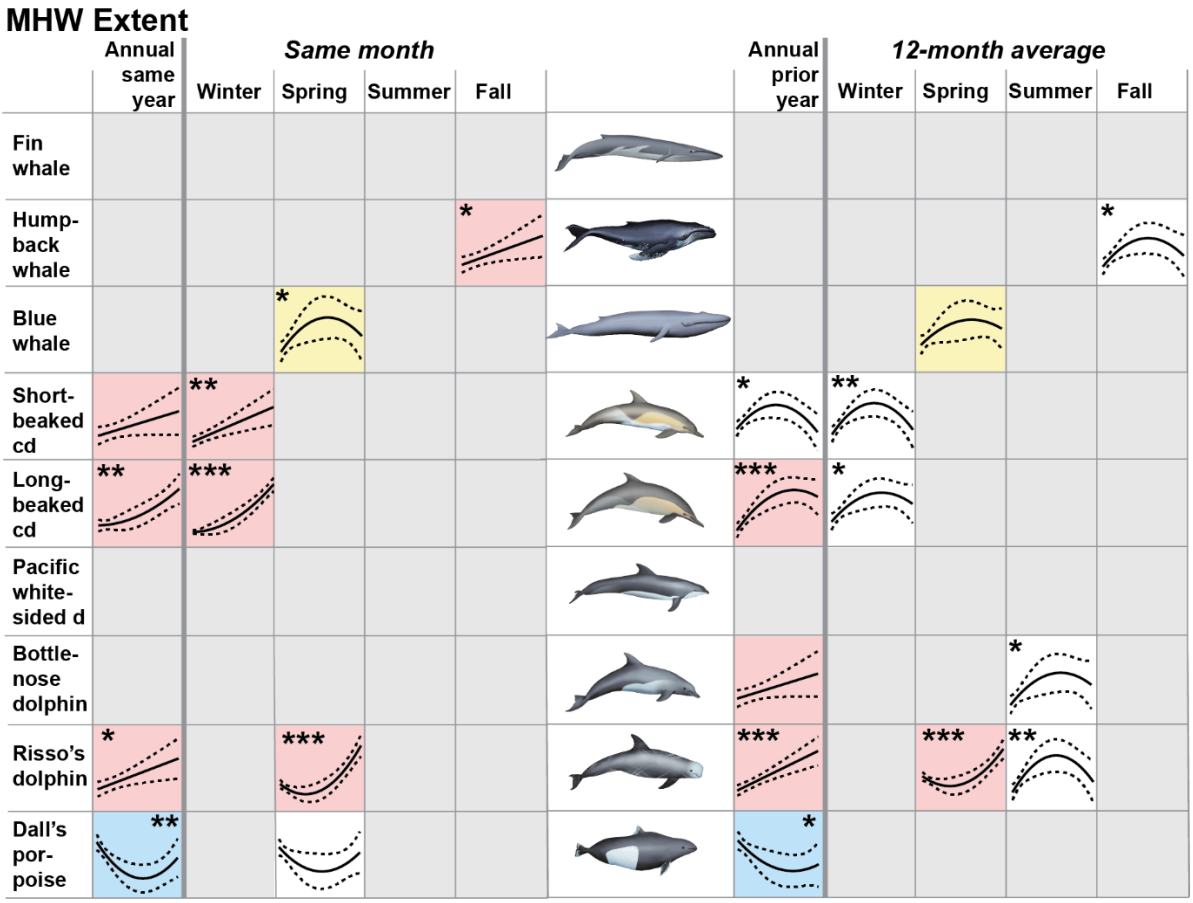

Figure 3.9: Correlations between MHW extent (x-axis) and annual and seasonal scaled sightings (y-axis). Linear or quadratic models and 95% confidence intervals are shown for correlations that were statistically significant at the p=0.1 level. Asterisks indicate statistical significance: no asterisk ($0.05 < p < 0.1$), one asterisk ($0.01 < p < 0.05$), two asterisks ($0.001 < p < 0.01$) , or three asterisks ($p < 0.001$) Grey boxes indicate there was no statistically significant correlation. Blue indicates a negative correlation, pink indicates a positive correlation, and white indicates an intermediate response. Yellow indicates that the correlation is based on extremely limited data and thus should be interpreted with caution. Cetacean illustrations by Freya Hammar.

Table 3.1: Number of sightings and average group size, 2004-2021. Analysis in this study was limited to t on-effort, on-transect sightings.

Common name	**Scientific name**	**On-effort and On-transect encounters**	**Average group size, on-effort on-transect**	**Off-effort / Off-transect encounters**	**Average group size, off-effort, off-transect**
Fin whale	*Balaenoptera physalus*	260	1.94	150	2.18
Humpback whale	*Megaptera novaeangliae*	158	1.73	451	2.44
Blue whale	*Balaenoptera musculus*	158	1.61	104	1.66
Short-beaked common dolphin	*Delphinus delphis delphis*	535	90.13	273	90.04
Long-beaked common dolphin	*Delphinus delphis bairdii*	77	261.52	260	265.08
Pacific white-sided dolphin	*Lagenorhynchus obliquidens*	77	16.96	101	40.73
Bottlenose dolphin	*Tursiops truncatus*	59	27.32	98	24.14
Risso's dolphin	*Grampus griseus*	66	22.23	97	22.03
Dall's porpoise	*Phocoenoides dalli*	91	6.71	131	6.07

Table 3.2: Abundance and density estimates, 2004-2021. The table also includes the coefficient of variation as well as the unidentified individual correction factor, used for fin, humpback, and blue whales as well as for short- and long-beaked common dolphins.

	Season				
	Winter	**Spring**	**Summer**	**Fall**	**Overall**
Fin whale					
Abundance	543	684	2650	1251	1467
Lower 95% Confidence Interval	317	391	1712	783	655
Upper 95% Confidence Interval	930	1199	4102	2000	3284
Density (animals per 1000 km^2)	2.28	2.87	11.11	5.25	6.15
Coefficient of Variation (cv)	0.28	0.29	0.23	0.24	0.43
Unidentified individual correction factor (c)	2.58	1.75	1.54	1.81	1.70
Humpback whale					
Abundance	886	1347	469	494	686
Lower 95% Confidence Interval	545	859	191	302	390
Upper 95% Confidence Interval	1440	2113	1149	806	1207
Density (animals per 1000 km^2)	3.71	5.65	1.96	2.07	2.87
Coefficient of Variation (cv)	0.25	0.23	0.48	0.25	0.29
Unidentified individual correction factor (c)	2.58	1.75	1.54	1.81	1.70
Blue whale					
Abundance	39	65	1549	201	623
Lower 95% Confidence Interval	5	31	1129	111	179
Upper 95% Confidence Interval	316	136	2127	363	2163
Density (animals per 1000 km^2)	0.16	0.27	6.50	0.84	2.61
Coefficient of Variation (cv)	1.47	0.39	0.16	0.31	0.71
Unidentified individual correction factor (c)	2.58	1.75	1.54	1.81	1.70
Short-beaked common dolphin, <= 20 per group					
Abundance	41444	30545	40684	25462	33404
Lower 95% Confidence Interval	30151	20936	30062	17503	23634
Upper 95% Confidence Interval	56967	44563	55060	37039	47211
Density (animals per 1000 km^2)	173.77	128.07	170.59	106.76	140.06
Coefficient of Variation (cv)	0.16	0.19	0.16	0.19	0.18
Unidentified individual correction factor (c)	1.08	1.34	1.53	1.41	1.28

Table 3.2: Abundance and density estimates, 2004-2021, Continued

Short-beaked common dolphin, >20 per group					
Abundance	596618	292289	227259	287232	334868
Lower 95% Confidence Interval	323442	176660	140046	189688	173931
Upper 95% Confidence Interval	1100515	483601	368782	434936	644719
Density (animals per 1000 km^2)	2501.60	1225.56	952.89	1204.36	1404.10
Coefficient of Variation (cv)	0.32	0.26	0.25	0.21	0.34
Unidentified individual correction factor (c)	1.08	1.34	1.53	1.41	1.28
Long-beaked common dolphin					
Abundance	194024	17182	51608	108529	90552
Lower 95% Confidence Interval	58568	7178	25610	25883	35716
Upper 95% Confidence Interval	642767	41127	103998	455073	229578
Density (animals per 1000 km^2)	813.54	72.04	216.39	455.06	379.68
Coefficient of Variation (cv)	0.67	0.47	0.37	0.84	0.50
Unidentified individual correction factor (c)	1.08	1.34	1.53	1.41	1.28
Pacific white-sided dolphin					
Abundance	7152	14312	7221	2371	7484
Lower 95% Confidence Interval	2696	8127	2810	664	4014
Upper 95% Confidence Interval	18973	25202	18555	8464	13954
Density (animals per 1000 km^2)	29.99	60.01	30.28	9.94	31.38
Coefficient of Variation (cv)	0.53	0.29	0.51	0.72	0.33
Unidentified individual correction factor (c)	-	-	-	-	-
Bottlenose dolphin					
Abundance	11704	2136	5254	9995	7143
Lower 95% Confidence Interval	5686	643	2659	4020	3883
Upper 95% Confidence Interval	24095	7102	10379	24851	13140
Density (animals per 1000 km^2)	49.08	8.96	22.03	41.91	29.95
Coefficient of Variation (cv)	0.38	0.68	0.36	0.49	0.32
Unidentified individual correction factor (c)	-	-	-	-	-
Risso's dolphin					
Abundance	2263	6552	2359	3429	3497
Lower 95% Confidence Interval	1197	1949	1109	1741	1971
Upper 95% Confidence Interval	4281	22025	5018	6752	6203
Density (animals per 1000 km^2)	9.49	27.47	9.89	14.38	14.66
Coefficient of Variation (cv)	0.33	0.68	0.40	0.36	0.30
Unidentified individual correction factor (c)	-	-	-	-	-

Table 3.2: Abundance and density estimates, 2004-2021, Continued

Dall's porpoise					
Abundance	4929	9492	153	791	3293
Lower 95% Confidence Interval	2841	5758	75	215	1016
Upper 95% Confidence Interval	8551	15646	312	2912	10671
Density (animals per 1000 km^2)	20.67	39.80	0.64	3.32	13.81
Coefficient of Variation (cv)	0.29	0.26	0.38	0.75	0.66
Unidentified individual correction factor (c)	-	-	-	-	-

Supplemental Figure 3.1: Estimated detection functions and scaled histograms of perpendicular distance used for density estimation. Black circles represent the probability of detection based on perpendicular distances; for fin whales, Pacific white-sided dolphins, and Risso's dolphins the black circles represent the probability of detection based on perpendicular distance and Beaufort sea state. The detection functions for short-beaked common dolphins were estimated separately for small (≤20 dolphins) or large (>20 dolphins) group sizes

Detection Functions

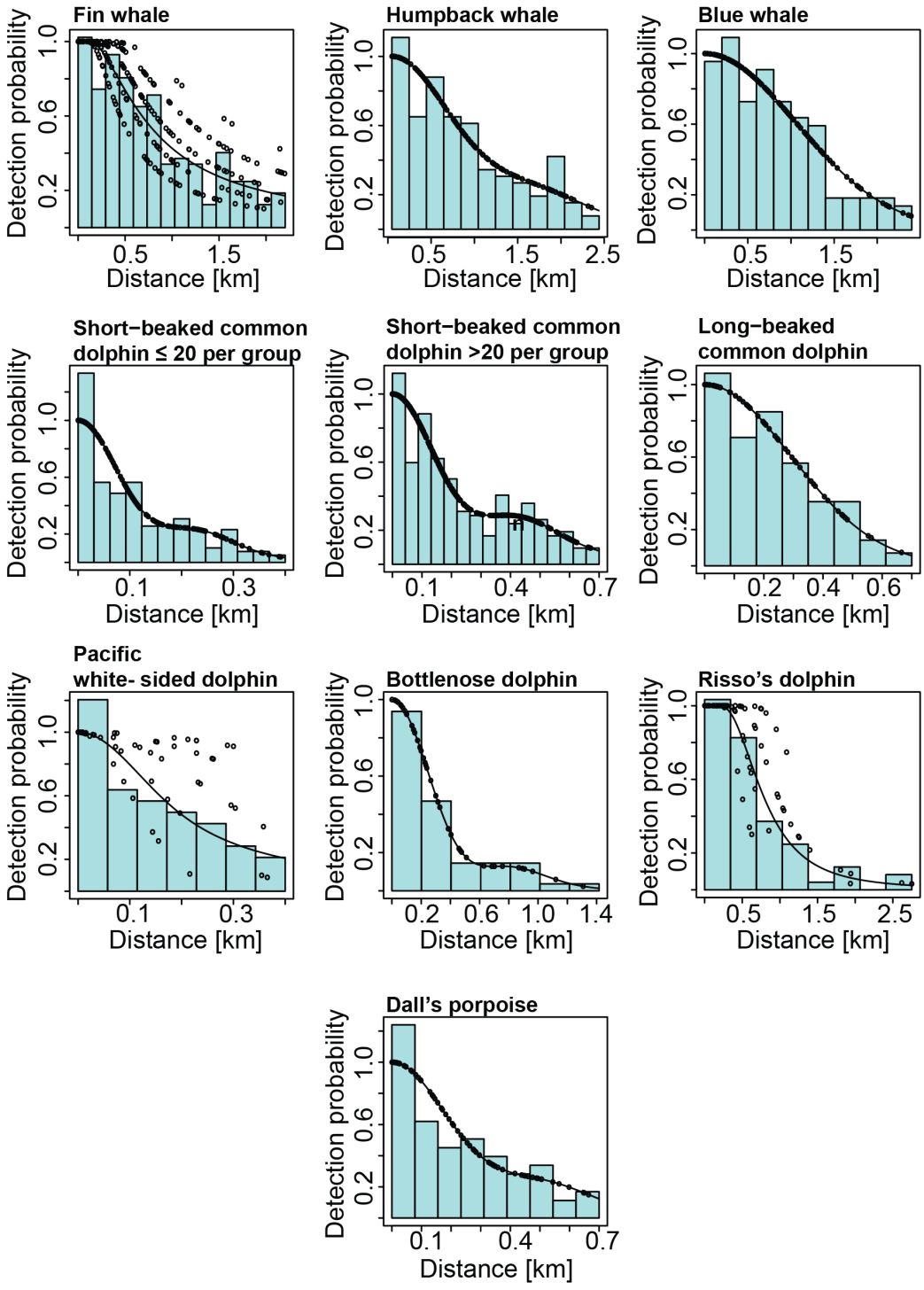

Supplemental Table 3.1: Detection function summary.

Species	Truncation	Model	Covariates	Trackline Detection Probability	Cramer-von Mises p-value
Fin whale	10%	Hazard-rate	sea state	0.921	0.90
Humpback whale	2700 m	Half-normal with cosine adjustment term of order 2	-	0.921	0.72
Blue whale	2400 m	Half-normal	-	0.921	0.96
SB common dolphin group size <= 20	400 m	Half-normal with cosine adjustment term of order 2,3	-	0.856	0.12
SB common dolphin group size > 20	700 m	Half-normal with cosine adjustment terms of order 2,3	-	0.97	0.57
LB common dolphin	700 m	Half-normal	-	0.97	0.90
Pacific white-sided dolphin	400 m	Half-normal	sea state	0.856	0.18
Bottlenose dolphin	10%	Half-normal with cosine adjustment terms of order 2,3	-	0.856	0.88
Risso's dolphin	-	Hazard-rate	sea state	0.856	0.98
Dall's porpoise	700 m	Half-normal with cosine adjustment term of order 2	-	0.822	0.22

Chapter 4

Where there's a whirl there's a whale: habitat partitioning in mesoscale features

Niche partitioning reduces competition among species and facilitates their coexistence. In the ocean, mesoscale features such as fronts and eddies represent rich foraging hotspots; differential use of types of mesoscale features may be a mechanism for niche partitioning for species with similar foraging ecologies. Here, we combine satellite-altimetry-derived finite-size Lyapunov exponents (FSLEs) and eddy positions with visual marine mammal surveys to investigate the relationships of six cetacean species with mesoscale features in the Southern California Bight from 2004-2021. We found that blue, fin, and humpback whales showed habitat partitioning through a combination of geographic separation and species-specific preferences for certain mesoscale features. Blue whales showed a preference for FSLEs but no selection for or against eddies; fin whales showed a preference for FSLEs and a preference for cyclonic eddies; for humpback whales we found weak evidence of a preference for FSLEs and a strong preference for areas without eddies. Pacific white-sided dolphins also showed a preference for areas without eddies. Short-beaked common dolphins showed a slight preference for cyclonic eddies in the summer and a weak preference for FSLEs in the fall. Dall's porpoises had a strong association with rare, intense FSLE ridges $\leq$ -0.2 day^{-1}. These results show that mesoscale features are targeted by several cetacean species in the Southern California Current. Additionally, mesoscale features seem to provide physical structures for habitat partitioning among closely related baleen whales.

4.1 Introduction

Habitat partitioning is a strategy used by sympatric organisms to reduce interspecific competition. Competitive exclusion theory posits that species occupying the same niche (that is, perfect competitors) cannot coexist because one species will outcompete the others for limited resources, driving the weaker competitors to extinction (Gause, 1934; Hardin, 1960). Under this theory, the coexistence of closely-related species occurs when competitors modify their niches to avoid direct competition. One mechanism for niche separation is habitat partitioning, in which species exploit heterogeneity in their environment to reduce competition (Wisheu, 1998). In the ocean environment, dynamic fluid flows create features such as eddies, fronts, and filaments. Differential exploitation of these features may represent an avenue of niche partitioning, resulting in reduced competition among closely related sympatric species.

Fronts, eddies, and filaments that exist on spatial scales from tens to hundreds of kilometers and on temporal scales on the order of weeks to months are known as mesoscale features (Jr., 2014). Biophysical coupling at fronts and eddies often results in locally enhanced phytoplankton growth which attracts higher tropic levels; mesoscale features therefore function as important pelagic foraging habitats for many species, including mobile vertebrates such as fish, seabirds, and cetaceans (Lehahn et al., 2017; McGillicuddy Jr., 2014; Scales et al., 2014). Mesoscale features can be studied using Lagrangian coherent structures (LCSs), which show areas of convergence such as fronts and the edges of eddies (Beron-Vera et al., 2008; d'Ovidio et al., 2004; Lehahn et al., 2017). LCSs are known to aggregate prey such as krill (Maps et al., 2015); vertebrate predators such as penguins (Lowther et al., 2014; Oliver et al., 2019), great frigatebirds (Kai et al., 2009), and southern elephant seals (Penna et al., 2015) have been shown to forage at LCSs. Bycatch of marine tetrapods is also greater at LCSs in at least one fishery (Scales et al., 2018).

Some studies have shown relationships between cetaceans – highly mobile marine predators of mid- to upper-trophic level organisms – and mesoscale features. For example, fin whales have been associated with LCSs in the Mediterranean Sea and California Current (Cotte et al., 2011; Scales et al., 2017), as have humpback whales near the Antarctic Penninsula (Johannessen et al., 2022). However, these studies frequently focus on one species in isolation. A notable exception is a study by (Doniol-Valcroze et al., 2007) of baleen whales in the Gulf of St. Lawrence, which showed not only that the whales were associated with thermal fronts, but that the average distance between the whales and the fronts varied by species, indicative of habitat partitioning (Doniol-Valcroze et al., 2007). Investigating the relationships of sympatric cetacean species with mesoscale features will enable us to test the hypothesis that mesoscale features are used as a method of habitat partitioning.

In this study, we identify relationships between mesoscale features and six sympatric species of cetacean in the southern California Current. We use line-transect survey data taken from 64 quarterly California Cooperative Fisheries Investigations (CalCOFI) cruises from 2004-2021, which enables us to test these associations on a seasonal level. We also compare the mesoscale environment between years with encounters of a given species and years without encounters.

4.2 Methods

4.2.1 Visual surveys

Visual surveys of marine mammals were conducted on quarterly CalCOFI cruises covering each season: winter (January or February), spring (March or April), summer (June, July, or August), and fall (October or November). We limited our analysis to the southern CalCOFI region (lines 76.7-93.3, Figure 4.1a), because this region is sampled each quarter; additional CalCOFI

lines are typically sampled only once or twice per year. Inshore stations are 20 nautical miles apart along-track, while offshore stations are 40 nautical miles apart.

Visual observations were conducted on each quarterly CalCOFI cruise from the summer of 2007 to fall of 2021, with the exceptions of the spring 2010 cruise, and spring 2020 through spring 2021 due to COVID-related restrictions. Visual surveys were conducted according to the protocols outlined in Campbell et al. 2015 (2015). Briefly, visual surveys were conducted by two observers (except for the fall 2019 cruise, when only one observer was present) using 7x50 Fuijinon binoculars during daylight transits between CalCOFI oceanographic stations. Sightings were logged systematically including supporting information such as Beaufort sea state. For our analyses, we included only sightings that were "on-effort" as well as "on-transect" as per the criteria in Campbell et al. 2015 (2015). Transects were defined as segments between CalCOFI oceanographic stations on the lines perpendicular to the coast.

4.2.2 LCS and eddy data

We quantify LCS using finite size Lyapunov exponents (FSLEs). We obtained backwards-in-time FSLEs from Archiving, Validation, and Interpretation of Satellite Oceanography (AVISO) (https://www.aviso.altimetry.fr/). FSLEs were calculated using geostrophic velocity fields derived from satellite altimetry based on the methodology of d'Ovidio et al. (d'Ovidio et al., 2004). Backwards-in-time FSLEs show regions of convergence in forward time. FSLEs (λ, equation 1) are given by the times □ required for particles at position x, initially separated by finite distance δ_0 at time t, to separate to a final finite distance δ_f:

(1) $\lambda(\mathbf{x},t,\delta_0,\delta_f) \equiv \frac{1}{\tau}\log\frac{\delta_f}{\delta_0}$

Rapid separations yield large negative values of the FSLE (λ), while slower separations generate FSLEs closer to 0. The initial separation δ_0 in the FSLE dataset is 0.02° and the final separation distance δ_f is 0.6°. A maximum integration window of 200 days is used; if separation time exceeds this window, a value of 0 is given. The FSLE dataset has a temporal resolution of 1 day and a spatial resolution of 0.04° (Figure 4.1b and d).

The altimetric Mesoscale Eddy Trajectory Atlas product (META3.2 DT allsat, DOI:10.24400/527896/a01-2022.005.210802; (Pegliasco et al., 2022)) was produced by SSALTO/DUACS and distributed by AVISO+ (https://www.aviso.altimetry.fr/) with support from CNES, in collaboration with IMEDEA. This atlas was downloaded on 2022-04-12 and covers the period from January 1993 to August 2021. Maps of the eddy field were created using the "effective_contour_latitude" and "effective_contour_longitude" variables which represent twenty latitude and longitude pairs describing largest contour of each detected eddy (Figure 4.1c and d). Eddies were flagged as "cyclonic" or "anticyclonic" as per the Mesoscale Eddy Trajectory Atlas. The spatial resolution of the maps is 0.01°.

4.2.3 Data processing

At each cetacean encounter location, we selected the minimum (i.e., most intense) FSLEs within a 3x3 pixel (0.12° x 0.12°) box centered on the ship's position. We noted whether the ship was outside of an eddy or within, and if within an eddy, which type (cyclonic or anticyclonic).

We defined a seasonal species domain by enclosing the area in which all of our on-effort, on-transect encounters for that species occurred during that season over the entire study period (see maps in Figures 4.2-5).

Within a seasonal species domain, we defined cruise tracks as periods when marine mammal observers were both on-effort and on-transect. In order to compare the FSLE and eddy values of each encounter with the general conditions available during the survey effort, we examined the FSLE and eddy conditions along the cruise tracks for each cruise within the seasonal species domain. For FSLE data, we selected the minimum FSLEs within a 3x3 pixel (0.12° x 0.12°) box centered on the ship's position every 0.4° while the observers were on-effort and on-transect. For the eddy data, we collected information every 0.1° about whether the ship was outside or within an eddy, and if within, whether the eddy was cyclonic or anticyclonic. The 0.1° steps were chosen based on the spatial resolution of our data.

4.2.4 Statistical analysis

We conducted our analyses at the level of species and season. We limited our analysis to encounters with a positive identification at the species level, or, in the case of short-beaked common dolphin, to the subspecies level. In order to improve our ability to detect statistically significant trends, we limited our analyses to species/season pairs that had at least 30 on-effort, on-transect sightings over the course of our study period (2004-2021). We pooled all encounters from a given species in a given season and compared it to environmental data from all the cruise tracks within the appropriate seasonal species domain where at least one encounter of that species occurred.

All statistical work was conducted within R. We used bootstrapping with 10,000 iterations to obtain 95% confidence intervals on the mean FSLE intensities for each species/season pair; means were considered significantly different if the 95% confidence intervals did not overlap. We used kernel density estimation to plot probability density functions (PDFs) for FSLE intensities.

We then assessed differences between the PDFs of FSLE intensities found at cetacean encounters and those measured along cruise tracks using two-sample Kolmogorov-Smirnov tests. We used the binomial proportion test to check for statistically significant differences between the proportion of encounters or cruise tracks within and outside of eddies as well as between the proportion of cyclonic and anticyclonic eddies in both encounters and cruise tracks.

For species that did not have at least one encounter in every cruise in a given season, we performed the same analysis as above, comparing cruise tracks from years in which there was an encounter of a species in that season to cruise tracks from years in which there were no encounters of a species in that season.

4.3 Results

4.3.1 Cetacean encounters

4.3.1.1 Spring

Four species were encountered at least 30 times during the spring season: humpback whale, Pacific white-sided dolphin, short-beaked common dolphin, and Dall's porpoise (Figure 4.2).

The vast majority of humpback whale encounters occurred inshore; only six encounters occurred offshore (Figure 4.2a). The humpback and cruise FSLE intensity PDFs were not found to be significantly different ($p=0.56$, Figure 4.2b). There was no evidence of a preference of humpback whales for or against eddies when compared with the proportion of the cruise tracks found within and outside of eddies ($p=0.47$, Figure 4.2c). Furthermore, the relative proportions of cyclonic to anticyclonic eddies were similar between the whale encounters and the cruise tracks ($p=1$, Figure 4.2c).

Pacific white-sided dolphin encounters primarily occurred inshore on the northernmost line (line 76.7), although the line with the second-highest number of encounters was the second-most southern line (line 90; Figure 4.2d). Only one encounter occurred in the far south at line 93.3. There was no significant difference between the PDF of FSLE intensities at the Pacific white-sided dolphin encounter locations compared to those found more broadly in the dolphin's springtime domain (Figure 4.2e). Pacific white-sided dolphin encounters were significantly less likely to be in an eddy than expected when compared with the probability of encountering eddies along the cruise tracks within the Pacific white-sided dolphin springtime domain ($p = 0.022$, Figure 4.2f). While Pacific white-sided dolphin encounters were more likely to occur in cyclonic eddies relative to anticyclonic eddies, this relationship was not significantly different from the proportion of cyclonic to anticyclonic eddies in the cruise tracks ($p=0.99$, Figure 4.2f).

Short-beaked common dolphins encounters were widespread, encompassing both the offshore and inshore regions in the southern half of the CalCOFI region(Figure 4.2g). However, north of line 86.7, short-beaked common dolphins were found almost exclusively offshore. While the FSLE intensities at short-beaked common dolphin locations were slightly stronger than those values at the cruise tracks, this difference was not statistically significant ($p=0.14$, Figure 4.2h). The percentage of short-beaked common dolphin encounters that occurred within an eddy was similar to the percentage of cruise track locations within eddies ($p=0.41$, Figure 4.2i). While short-beaked common dolphin encounters that were within eddies were more likely to be within cyclonic eddies, this was not statistically significantly different from the proportion of cyclonic eddies at cruise track locations ($p=0.41$, Figure 4.2i).

Dall's porpoise encounters occurred primarily offshore, near the shelf-break (Figure 4.2j). Dall's porpoise encounters were more likely to occur at stronger FSLE intensities (p=0.056, Figure 4.2k). We did not find strong evidence of a difference in encounters within eddies compared to the cruise tracks (p=0.15, Figure 4.2l), and the proportion of encounters within cyclonic eddies relative to anticyclonic eddies were almost identical to the proportion found along the cruise tracks (p=1, Figure 4.2l).

4.3.1.2 Summer

Four species were encountered 30 or more times in the summer during our study period: blue whale, fin whale, humpback whale, and short-beaked common dolphin (Figure 4.3).

Blue whales were encountered both inshore and offshore, although they were found mostly in the eastern half of the offshore area (Figure 4.3a). The greatest number of blue whale encounters occurred on the southernmost line (93.3). Blue whale encounters were also notably absent north of Point Conception on the inshore portion of line 76.7. The mean FSLE intensity at blue whale encounter locations was significantly stronger (more negative) than the mean FSLE intensity at the cruise track locations (Table 1). The PDF of FSLE intensities at blue whale locations was accordingly significantly shifted towards stronger intensities compared with the PDF of FSLE intensities at cruise track locations ($p=1.8x10^{-5}$, Figure 4.3b). The percentage of blue whale encounters that occurred within an eddy was almost the same as the percentage of locations along the cruise tracks that occurred within eddies (p=0.59, Figure 4.3c). Blue whale encounters that occurred within eddies were in cyclonic eddies 74% of the time, while the cruise track locations within eddies were in cyclonic eddies 55% of the time; however, this difference was not statistically significant (p=0.12, Figure 4.3c).

Fin whales were also encountered both inshore and offshore, and as with blue whales the offshore encounters were restricted to the eastern half of the area (Figure 4.3d). Although fin whale encounters occurred on all CalCOFI lines, the greatest number of encounters (53, 34% of total encounters) occurred on the northernmost line (76.7). As with blue whales, the mean FSLE intensity at fin whale encounter locations was significantly stronger (more negative) than the mean FSLE intensity at the cruise track locations (Table 1), and the PDF of FSLE intensities at fin whale encounter locations was shifted to significantly stronger FSLE intensities ($p=7.5x10^{-7}$, Figure 4.3e). Fin whale encounters occurred within eddies 29% of the time, while cruise track locations occurred within eddies only 20% of the time, a statistically significant difference ($p=0.0030$, Figure 4.3f). The fin whale encounters that occurred within eddies were almost exclusively within cyclonic eddies, whereas eddies at cruise track locations were more balanced between cyclonic and anticyclonic ($p=1.1x10^{-5}$, Figure 4.3f).

Humpback whale encounters were primarily confined to the northern inshore region, with the majority occurring on line 76.7 (26 encounters, 72%, Figure 4.3g). While the peak of the FSLE intensity PDF at humpback whale encounter locations occurred at a stronger FSLE intensity than the peak of the FSLE PDF for cruise track locations, stronger FSLE intensities (less than -0.15 day^{-1}) were notably absent from the humpback whale encounter PDF, resulting in a narrower distribution of FSLE intensities for humpback whale encounters ($p=0.069$, Figure 4.3h). No humpback whale encounters occurred within eddies, while 16% of the cruise track locations occurred within eddies; this result was statistically significant ($p=0.016$, Figure 4.3i).

Short-beaked common dolphin encounters occurred both inshore and offshore, although the farthest offshore portions of most CalCOFI lines lacked encounters (Figure 4.3j). Short-beaked

common dolphin encounters were also absent from the northern inshore area around Point Conception (lines 76.7 and 80). The PDF of FSLE intensities at short-beaked common dolphin encounter locations was not significantly different from the PDF of FSLE intensities at the cruise track locations (p=0.80, Figure 4.3k). Three short-beaked common dolphin encounters occurred nearshore where eddy data was unavailable; of the remaining encounters, 30% occurred within eddies, while only 22% of the cruise track locations were located within eddies (p=0.021, Figure 4.3l). The ratio of cyclonic eddies to anticyclonic eddies was significantly different between the short-beaked common dolphin encounter locations and the cruise track locations (p=0.058, Figure 4.3l).

4.3.1.3 Fall

Three species had at least 30 encounters during fall cruises: fin whale, humpback whale, and short-beaked common dolphin (Figure 4.4).

Fin whale encounters occurred offshore and along the inshore/offshore transition, the shelf break (Figure 4.4a). Most of these encounters occurred along the central and north CalCOFI sampling lines, with only three encounters occurring on lines 90 and 93.3. The PDF of FSLE intensities at fin whale encounter locations was shifted towards stronger FSLE intensities relative to the PDF of FSLE intensities on cruise track locations, but this was only statistically significant at the $p \leq 0.1$ level (p=0.096, Figure 4.4b). Almost the exact proportion of fin whale encounters occurred within eddies as the proportion of cruise track locations found within eddies (p=0.88, Figure 4.3c). However, fin whale encounters that occurred within eddies were significantly more likely to be in cyclonic eddies relative to the cruise track locations within eddies (p=0.026, Figure 4.4c).

Humpback whale encounters occurred exclusively within the inshore region (Figure 4.4d). The PDF of FSLE intensities at fall humpback whale encounter locations was shifted towards stronger FSLE intensities relative to the PDF of FSLE intensities on cruise track locations; as with fin whales, this was only statistically significant at the $p \leq 0.1$ level ($p=0.085$, Figure 4..4e). Humpback whale encounters rarely occurred within eddies, but this was not significantly different from the proportion of cruise track locations within eddies ($p=0.22$, Figure 4.4f). The humpback whale encounters that occurred within eddies were exclusively within cyclonic eddies; however, this was not significantly different from the proportion of cyclonic and anticyclonic eddies along the cruise tracks ($p=0.82$, Figure 4.4f).

Short-beaked common dolphins were spread throughout the CalCOFI region, with the occasional pocket without sightings (e.g., the inshore-offshore transition region of line 76.7 and the far offshore end of line 90; Figure 4.4g). The PDF of FSLE intensities at short-beaked common dolphin sighting locations was shifted towards stronger FSLE intensities than the PDF of the FSLE intensities at cruise track locations ($p=0.014$, Figure 4.4h). Two short-beaked common dolphin encounters occurred within the nearshore region where eddy data was not available; of the remaining encounters, 31% of them occurred within eddies, which is almost identical to the percentage of cruise track locations within eddies ($p=0.87$; Figure 4.4i). Short-beaked common dolphin encounters that were within eddies were more likely to be in cyclonic eddies, but there is not strong statistical support for this being different from the cruise track locations ($p=0.14$; Figure 4.4i).

4.3.1.4 Winter

Three species had at least 30 encounters during the winter season: humpback whale, short-beaked common dolphin, and Dall's porpoise (Figure 4.5).

Humpback whale encounters occurred primarily inshore and along the shelf break at the inshore/offshore transition (Figure 4.5a). The northernmost line, 76.7, had the fewest humpback whale encounters. While the PDF of FSLE intensities at humpback whale encounter locations was shifted toward stronger values than the PDF of FSLE intensities at cruise track locations overall, the peak in the PDFs for the two distributions was the same ($p=0.078$, Figure 4.5b). Humpback whale encounters were no more or less likely to occur in eddies relative to the cruise track locations ($p=0.72$, Figure 4.5c), and the proportion within cyclonic versus anticyclonic eddies was not statistically different between whale encounters and cruise track locations ($p=0.72$; Figure 4.5c).

Short-beaked common dolphin encounters were distributed throughout the offshore area; they were only found inshore in the southern portions of the region (Figure 4.5d). The PDF of FSLE intensities for short-beaked common dolphin in the winter was significantly narrower than the PDF of FSLE intensities at the cruise track locations, having fewer low and high FSLE intensities than the cruise tracks ($p=0.015$, Figure 4.5e). Two short-beaked common dolphin encounters occurred nearshore where eddy data was not available; of the remaining encounters, almost the same as the percentage as the cruise track locations occurred within eddies ($p=0.69$, Figure 4.5f). However, short-beaked common dolphin encounters that occurred within eddies were significantly more likely to be in cyclonic eddies compared to the percentage of cruise locations ($p=0.047$, Figure 4.5f).

Dall's porpoise encounters occurred primarily inshore and in the mid-offshore area (Figure 4.5g). Encounters occurred most frequently on line 83.3; only sporadic encounters occurred on lines to the south. The PDF of FSLE intensities at Dall's porpoise encounter locations was significantly shifted toward stronger values than the PDF of FSLE intensities at cruise track locations ($p=0.042$, Figure 4.5h). Dall's porpoise encounters occurred within eddies 36% of the time, although this was not statistically significantly different from the percentage of cruise tracks locations with eddies ($p=0.30$, Figure 4.5i). However, the Dall's porpoise encounters that occurred within eddies were significantly more likely to be in cyclonic eddies relative to the percentage of cyclonic eddies along the cruise tracks ($p=0.0085$, Figure 4.5i).

4.3.2 Environmental comparison

Although we restricted our analysis to species with at least 30 encounters during a given season, not every species was encountered in each year. To test whether there was a difference in FSLE intensity or eddy activity between years when we encountered a given species versus years when we did not, we compared the on-effort, on-transect cruise tracks within the seasonal species domain for years with encounters of that species versus years without encounters for that species. Three species were encountered every year during at least one season and are thus not included in this analysis: blue whales and fin whales were encountered every summer, and short-beaked common dolphin were encountered every winter.

4.3.2.1 Spring

Spring cruises occurred from 2005 – 2019 with the exception of 2010, when no spring cruise occurred.

Spring humpback whale encounters occurred in 12 years, with two years having no humpback whale encounters: 2009 and 2012. The PDFs of FSLE intensities at cruise track locations were not significantly different in years with humpback whale encounters versus years without encounters ($p=0.17$, Figure 4.6a). A significantly larger proportion of cruise track locations were within eddies during years when no humpback whales were encountered versus years with encounters ($p=1.1\text{x}10^{-7}$, Figure 4.6b). For years without humpback whale encounters, exactly half of the locations that were within eddies were within cyclonic eddies and the other half anticyclonic eddies, whereas during years with humpback whale encounters, 59% of the locations within eddies occurred in cyclonic eddies ($p=0.059$, Figure 4.6b).

Pacific white-sided dolphin encounters occurred during spring cruises in nine years, while no encounters were recorded during the spring cruises in five years: 2012, 2013, 2015, 2017, and 2018. The PDF of FSLE intensities for years without Pacific white-sided dolphin encounters was significantly shifted towards weaker FSLE intensities compared with the PDF of FSLE intensities during years with encounters ($p=4.4\text{x}10^{-5}$, Figure 4.6c). The proportions of cruise track locations within eddies were similar for both years with encounters and without ($p=0.12$, Figure 4.6d), as were the proportions of cyclonic to anticyclonic eddies ($p=0.49$, Figure 4.6d).

Short-beaked common dolphins were seen every spring aside from 2008; in this year, common dolphins were encountered but they could not be identified as either short- or long-beaked. The FSLE PDFs were not significantly different for the year without encounters than for the years with encounters ($p=0.20$, Figure 4.6e). However, the year without confirmed short-beaked common dolphin encounters had fewer cruise track locations with eddies ($p=2.5\text{x}10^{-8}$,

Figure 4.6f), and the eddies were 100% anticyclonic (compared with 55% cyclonic eddies for years with encounters, $p=5.1x10^{-6}$, Figure 4.6f).

Dall's porpoise encounters occurred during spring cruises in 10 years, while no encounters occurred during four years: 2013, 2016, 2018, and 2019. The PDF of FSLE intensities was very similar between years with encounters and years without (p=0.56, Figure 4.6g). Years with Dall's porpoise encounters had a significantly larger percentage of cruise track locations within eddies than years without sightings ($p=2.3x10^{-8}$, Figure 4.6h). However, the proportion of cyclonic to anticyclonic eddies was similar between years with encounters and without (p=0.33, Figure 4.6h).

4.3.2.2 Summer

Summer cruises occurred from 2004-2021, aside from 2020. Blue whales and fin whales were encountered every summer.

Humpback whales were encountered in twelve years but not in five: 2004, 2009, 2010, 2012, and 2015. The PDF of FSLE intensities for years without humpback whale encounters was shifted towards weaker FSLE intensities relative to the PDF of years that did have humpback whale encounters (p=0.0040, Figure 4.6i). Years without encounters also had significantly fewer cruise track locations within eddies than years with encounters ($p=9.6x10^{-10}$, Figure 4.6j). All of the eddies along cruise tracks in years without encounters were cyclonic, while in years with humpback whale encounters, 57% of the locations within eddies were in cyclonic eddies ($p=7.1x10^{-9}$, Figure 4.6j).

Short-beaked common dolphins were encountered every year aside from 2010; during this year common dolphins were encountered but they could not be identified as either short- or long-

beaked. The PDF of FSLE intensities was not different between the year without encounters and the years with encounters ($p=0.94$; Figure 4.6k). During the year without short-beaked common dolphin encounters, 7% of the cruise track locations occurred within eddies, which were 29% cyclonic. These were both significantly different than in years with encounters, when 22% of the cruise track locations were within eddies ($p=5.2\text{x}10^{-10}$, Figure 4.6l), and these were 59% cyclonic ($p=0.0068$, Figure 4.6l).

4.3.2.3 Fall

Fall cruises during our study period occurred from 2004-2019.

Fin whales were encountered during fourteen years but were not encountered during two years: 2004 and 2015. The PDF of FSLE intensities at cruise track locations during years without fin whale encounters is narrower than the PDF of FSLE intensities during years with encounters; years without fin whale encounters had fewer weak and strong FSLE intensities, with the exception of intense FSLE intensities less than -0.25 ($p=0.0054$, Figure 4.7a). Years without fin whale sightings had fewer cruise track locations within eddies than years with sightings ($p=1.8\text{x}10^{-10}$, Figure 4.7b). Almost all of the cruise track locations within eddies during years without fin whale encounters were in cyclonic eddies, while during years with fin whale encounters the ratio of cyclonic to anticyclonic eddies at cruise track locations was closer to even ($p<2.2\text{x}10^{-16}$, Figure 4.7b).

Humpback whales were encountered in ten years but not during six: 2007, 2008, 2009, 2010, 2011, and 2013. The FSLE intensities for years without humpback whale encounters showed a similar peak in the PDF as years with humpback whale encounters but had fewer FSLE intensities

stronger than -0.1 ($p=0.05$, Figure 4.7c). Cruise tracks during years with humpback whale encounters had a smaller proportion of locations within eddies compared to those without encounters ($p=1.8x10^{-10}$, Figure 4.7d); however, the ratio of cruise track locations within cyclonic eddies to anticyclonic eddies was similar ($p=0.27$, Figure 4.7d).

Short-beaked common dolphins were encountered every year aside from 2010; during this year common dolphins were encountered but they could not be identified as short- or long-beaked. The PDF of FSLE intensities during the year without short-beaked common dolphin encounters was slightly shifted towards weaker FSLE intensities ($p=0.0072$, Figure 4.7e). The proportion of cruise track locations within eddies was similar in the year without confirmed short-beaked common dolphin encounters compared to the years with encounters ($p=0.10$, Figure 4.7f); however, the year without encounters had significantly fewer cyclonic eddies along the cruise tracks ($p<2.2x10^{-16}$, Figure 4.7f).

4.3.2.4 Winter

Winter cruises were conducted from 2005-2020. Short-beaked common dolphins were encountered every year during the winter.

Humpback whales were also encountered during 10 years but not during six: 2005, 2006, 2007, 2008, 2014, and 2019. The FSLE PDF for years without humpback whale encounters was significantly shifted towards stronger FSLE intensities compared to years with encounters ($p=0.00019$, Figure 4.7g). Cruise tracks during years without humpback whale encounters had a higher percentage of sightings within eddies compared to years with humpback whale encounters

($p=6.2x10^{-13}$, Figure 4.7h). However, the proportion of cyclonic eddies to anticyclonic eddies was similar between years with encounters and without ($p=0.14$, Figure 4.7h).

Dall's porpoises were encountered during 10 years but not during six: 2010, 2012, 2015, 2016, 2017, and 2020. The PDFs of FSLE intensities were not significantly different between years with encounters and those without ($p=0.30$, Figure 4.7i). Years without Dall's porpoise encounters had fewer cruise track locations within eddies compared with years with encounters ($p< 2.2x10^{-16}$, Figure 4.7j). The proportion within eddies that were cyclonic was higher in years without encounters than in years with encounters ($p=0.0029$, Figure 4.7j).

4.4 Discussion

4.4.1 Baleen whales

In order to avoid competition, animals that occupy similar niches may further segregate through spatio-temporal habitat partitioning (García-Vernet et al., 2021). We found evidence of spatial as well as temporal habitat partitioning among three species of rorqual whales: fin, humpback, and blue whales. Blue and fin whale encounters were highest during the summer, while humpback whale encounters were highest in spring and generally low in the summer. Blue and fin whales were encountered in similar, but not identical, regions (Figure 4.3a and 4.3d): blue whales were encountered more often in the southern portion of the CalCOFI region while fin whales were encountered more often in the northern portion. Almost no blue or fin whale encounters occurred inshore on the northernmost line (76.7), where the majority of summertime humpback whale encounters occurred (Figure 4.3g). In fall, the other season in which we have two baleen whale species with greater than 30 encounters, there is clear geographic separation between fin and humpback whales. Fin whales were encountered offshore and at the shelf break, whereas

humpback whale encounters were confined to the inshore region (Figure 4.4a and 4.4d). Acoustic records of baleen whale calls recorded during CalCOFI cruises showed broadly similar temporal and spatial results to ours—aside from fin whale 20-Hz pulses which were detected both inshore and offshore in the fall (Vu, 2015). Our results are consistent with existing habitat models that predict high blue and fin whale densities throughout the CalCOFI region but predict that areas of high humpback whale density are confined to the inshore region (Becker et al., 2019).

Blue whales are obligate krill foragers, but both fin and humpback whales can forage on krill as well as other zooplankton and small pelagic fish (García-Vernet et al., 2021; Pauly et al., 1998). Surveys of krill abundance in the California Current show that krill hotspots are spatially displaced from high upwelling locations (Santora et al., 2011). Although krill hotspots were found both to the south and north, at Point Conception—a high upwelling location—krill abundance was low (Santora et al., 2011). This might explain the lack of blue and fin whale encounters inshore on line 76.7, which terminates just north of Point Conception. Intriguingly, this area has the highest encounters of humpback whales, supporting the hypothesis that krill might not be an important prey source for humpback whales in the CalCOFI region during the summer. Similar spatial and prey partitioning has been found among rorqual whales occupying the same area off of Iceland and Monterrey Bay (Fossette et al., 2017; García-Vernet et al., 2021).

Large, lunge-feeding rorqual whales, such as blue and fin whales, need dense prey patches in order to offset the energetic cost of diving and lunge feeding (Goldbogen et al., 2010). Modelling has shown that LCS can be regions of plankton accumulation (Harrison et al., 2013), while field work has shown that in the Gulf of St. Lawrence, dense krill aggregations were associated with surface LCSs across multiple spatial scales (Maps et al., 2015). Such dense aggregations are

important foraging resources for rorqual whales: dense krill patches at LCSs near Monterey Bay attracted "supergroups" of foraging blue whales, and supergroups of humpback whales were found along FSLE ridges off South Africa (Cade et al., 2021).

We found that summertime encounters for both blue and fin whales occurred at locations with stronger (more negative) FSLE intensities relative to the available FSLE intensities along the cruise tracks, indicating a preference for LCSs (Figure 4.8). Summer is the most important foraging season for blue and fin whales (Romagosa et al., 2021; Širović et al., 2013; Szesciorka et al., 2020). Our results are consistent with a recent study by Fahlbusch et al. (2022) that showed that blue whales foraged at LCSs, with feeding rates increasing with feature strength. Fin whale encounters during the fall occurred at stronger FSLE intensities, although this was only statistically significant at the $p \leq 0.1$ level. This may be due to a shift in behavioral state that occurs during the fall from foraging to breeding: acoustic records show that foraging-associated calls decrease throughout the fall while calls associated with breeding increase (Romagosa et al., 2021; Širović et al., 2013). Years without fin whale fall encounters were less likely to have strong FSLE intensities from -0.1 to -.25 day^{-1}. Taken together, these results support habitat models showing that fin whale presence in the Southern California Bight is associated with strong surface FSLE intensities, and the interaction between FSLE intensities and seafloor topography (Scales et al., 2017).

While blue whales appeared to be randomly distributed relative to available eddies during the summer, fin whales, in contrast, were more likely to be found at eddies, with a clear preference for cyclonic eddies (Figure 4.8). This is consistent with fin whales targeting cyclonic eddies as a form of niche partitioning, perhaps as a method of reducing competition between the two species for shared prey resources (krill). In addition to krill, fin whales forage on other zooplankton and

small forage fish and are known to prey switch (Pauly et al., 1998; Scales et al., 2017). An alternative hypothesis is that fin whales in the CalCOFI region are foraging, at least in part, on non-krill prey that are more likely to be found in cyclonic eddies. Our results show that fin whales in the California Current share similar preferences for mesoscale features as fin whales in the Mediterranean, which were associated with both eddies and FSLE ridges (Cotte et al., 2011).

Interestingly, while fin whales were no more likely to be encountered in an eddy than the cruise track locations in the fall, when in an eddy they showed a preference for cyclonic eddies (Figure 4.8). This could be indicative of a seasonal shift in prey, or it could reflect a behavioral change such as a reduction in time spent foraging in favor of breeding or migration (Romagosa et al., 2021; Širović et al., 2013). Another possibility is that fin whales may no longer need to target eddies in response to a reduction in competition from blue whales, which are much less likely to be encountered in the CalCOFI region in the fall (just 13 on-effort, on-transect fall encounters).

Humpback whale encounters occurred in sufficient numbers in each season to meet the inclusion criterion in this study (≥ 30 encounters in a given season), and thus we can compare seasonal responses. In the fall and winter, humpback whale encounters occurred at stronger FSLE intensities than expected from the cruise track locations (Figure 4.8), and during the summer, the peak of the FSLE PDF for humpback whale encounters was more negative (approximately -0.12 day^{-1}) than that for the cruise track locations (approximately -.06 day^{-1}, Figure 4.3h). This is consistent with a recent study by Johannessen et al. (2022) that found humpback whales to be associated with FSLE intensities between -0.10 and -0.25 along the West Antarctic Penninsula. However, our results were only statistically significant at the $p \leq 0.1$ level. This may be due to a lack of statistical power resulting from relatively low humpback whale encounter rates (30-36

encounters per season). In spring—the season with the greatest number of humpback whale encounters—we found no difference in FSLE intensities between humpback whale encounters and cruise track locations. Furthermore, years when there were no humpback whale encounters did not have different PDFs of FSLE intensities along the cruise tracks than years with encounters. Why humpback whales do not target strong FSLE intensities in spring is unknown; there may be differences due to seasonal changes in humpback whale foraging strategies, prey type, or behavior.

None of the 36 summertime humpback whale encounters occurred within an eddy, compared to 16% of the cruise track locations within the humpback whale summer domain—a significant difference (Figure 4.3i). For each of the other seasons the proportion of humpback whale encounters within eddies was lower than the proportion of cruise track locations within eddies; however, these differences were not statistically significant. These results are counter-intuitive because eddies are known to aggregate planktonic and fish prey, and thus are attractive foraging hotspots for many animals (Condie & Condie, 2016; Godø et al., 2012; Sabarros et al., 2009). Humpback whales may be performing niche partitioning, avoiding foraging at eddies in order to reduce competition with fin whales.

Another hypothesis is that high eddy activity may reduce prey for humpback whales inshore. Eddies can advect nutrient-rich, upwelled water offshore, reducing primary productivity at the coast (Gruber et al., 2011) and increasing it offshore (Giddings et al., 2022). Periods of reduced eddy activity may lead to retention of primary production near the coast, resulting in more prey in the inshore region for humpback whales. This is thought to be the mechanism behind the recent appearance of large supergroups of humpback whales (20-200 individuals) foraging in the Southern Benguela Current; all supergroups appeared during years of extremely low eddy activity

(Dey et al., 2021). In our study, we found that years with humpback whale encounters had a smaller proportion of cruise tracks located within eddies than years without encounters, although this was not the case during the summer (Figure 4.8).

The vast majority of humpback whale encounters occurred inshore in a relatively restricted geographic space. In spring and summer, a handful of encounters occurred offshore; these increased the size of the humpback whale seasonal domain used in our analyses (Figures 4.2a and 4.3g). This larger domain may have had different FSLE intensities or eddy presence along the cruise tracks compared to the more restricted inshore region where most of the humpback whale encounters occurred. Thus, our conservative (large) estimate of the humpback whales' domain may have obscured significant relationships of humpbacks with FSLE intensities and eddies where they are most commonly found. An additional caveat is that both the FSLE and eddy datasets are derived from satellite altimetry products, which are not as accurate close to the coast; this may have impacted our analyses of humpback whale encounters during summer, the majority of which are found nearshore in a narrow band around Point Conception.

4.4.2 Dolphins

Two dolphin species were encountered more than 30 times in a given season: short-beaked common dolphins and Pacific white-sided dolphins. Short-beaked common dolphins are the most abundant cetacean species in the CalCOFI region (Chapter 3) with more than 30 encounters over our study period in each season, while Pacific white-sided dolphins met this inclusion criterion only in the spring.

Short-beaked common dolphins are widely distributed throughout the offshore area of the CalCOFI region; they were encountered farther offshore than any other species in this study. They were notably absent from the northern inshore area in every season aside from fall (Figure 4.4g). The results for the short-beaked common dolphin were mixed and no obvious pattern was seen across seasons. During the summer, short-beaked common dolphins were more likely to be encountered at an eddy than expected from the cruise track locations (Figure 4.8) but not in any other season. During the fall, short-beaked common dolphin encounters occurred at slightly stronger FSLE intensities than the intensities along the cruise tracks, while in the winter they were less likely to be encountered at weak or strong FSLE intensities relative to the cruise track; spring and summer were not statistically significant for FSLE intensities.

These inconclusive results for short-beaked common dolphins might be due to limitations with our study design. Short-beaked common dolphins in the Southern California Bight forage predominantly at night (Simonis et al., 2017); marine mammal visual surveys are conducted only during daylight hours. We are therefore unable to see whether mobile nocturnal foragers, such as short-beaked common dolphins, use fronts and eddies for foraging based on the methodology used in this study. This methodological limitation is exacerbated with fast swimming cetaceans that can cover large distances within a few hours. Short-beaked common dolphins, for example, can swim up to 8.0 m/s in short bursts and sustain speeds of approximately 2.5-3 m/s (Rohr et al., 2002; Wiggins et al., 2013; Williams, 2018). Therefore, information recorded during the day about FSLE intensity or eddies may not accurately reflect the conditions at the foraging grounds for short-beaked common dolphins. Additional research with tools such as acoustic recordings or satellite tags can help to overcome these limitations.

Pacific white-sided dolphins were less likely to be encountered at an eddy than expected based on the cruise track locations (Figure 4.8). This result is similar to humpback whales in the summer that were encountered primarily inshore on the northernmost line (76.7)—the same line with the most Pacific white-sided dolphin spring encounters. This could potentially indicate that humpback whales and Pacific white-sided dolphins are exploiting similar prey resources in that area (both species are known to forage on small pelagic fish such as anchovy and sardine (Pauly et al., 1998; Rechsteiner et al., 2013). The result could also be an artifact of the inshore oceanography north of Point Conception having fewer eddies than the broader CalCOFI region.

There are two populations of genetically and morphologically distinct Pacific white-sided dolphins in the California Current: a northern population off the west coast of the US and Canada, and a southern population found primarily off Mexico; both populations are thought to overlap in the CalCOFI region (Henderson et al., 2011; Lux, 1997; Walker et al., 1986). The two populations appear to have different temporal foraging behavior: acoustic and visual evidence suggests that Pacific white-sided dolphins thought to be in the northern population forage primarily at night, whereas dolphins thought to be from the southern population forage during the day and night (Henderson et al., 2011; Soldevilla et al., 2010). If LCSs and eddies are foraging hotspots, we might expect to see an increased affinity for these features during our daytime visual surveys by the population that forages during the day, but not from the nighttime-foraging population. Unfortunately, we are unable to test this hypothesis with our visual survey data, as the two populations cannot be visually distinguished at sea. This makes it difficult to interpret our results, as our Pacific white-sided dolphin encounters cannot be attributed to one population or the other. Additional data such as acoustics or genetic information could provide the data necessary to test our hypothesis.

4.4.3 Dall's porpoise

In the CalCOFI region, Dall's porpoises are encountered most often in winter and spring. Dall's porpoises were encountered more frequently at higher FSLE intensities than we would expect based on the PDF of FSLE intensities along the cruise tracks, indicating a preference for LCSs (Figure 4.2k and 4.5h). This is particularly true of strong FSLE ridges with intensities ≤ -0.2 day^{-1}: 22% of Dall's porpoise spring encounters and 14% of winter encounters occurred at FSLE ridges with intensities of -0.2 day^{-1} or stronger (more negative). FSLE intensities ≤ -0.2 day^{-1} along the cruise tracks occurred just 3.5% of the time in spring and 5.0% in winter within the Dall's porpoise domain. In contrast to the FSLE intensities, no significant difference was found between the proportion of Dall's porpoise encounters within eddies and the proportion of cruise track locations within eddies (Figure 4.8). Although Dall's porpoises were more likely to be encountered within a cyclonic eddy versus an anticyclonic eddy in the winter relative to the proportion of cyclonic eddies on the cruise tracks, there was no evidence of such a preference in the spring.

Dall's porpoises are a cold water-associated species (Becker et al., 2017; Fleming et al., 2018; Jefferson, 2018); fewer sightings have occurred since 2014, possibly due to warmer-than-average oceanic conditions (Chapter 3). Interestingly, although Dall's porpoises were associated with stronger FSLE intensities, FSLE intensities along the cruise tracks did not differ between years when Dall's porpoises were encountered and years when they were not (Figure 4.8). This suggests that while Dall's porpoises may select for LCSs when they are within the CalCOFI region, the presence or strength of LCSs within the region is not the key factor determining whether Dall's porpoise are present.

4.5 Conclusions

We found distributions consistent with habitat partitioning by closely related baleen whale species (blue, fin, and humpback whales) in the CalCOFI region in the summer and fall seasons. This habitat partitioning included geographic separation between humpback whales and fin whales in the fall, and between blue, fin and humpback whales in the summer. The three species of baleen whale also had different preferences for mesoscale features during the summer season: blue whales showed a preference for LCS but no selection for or against eddies; fin whales showed a preference for LCS and a preference for cyclonic eddies; for humpback whales we found weak evidence of a preference for LCS and a strong preference for the areas outside of eddies.

In contrast, we found that toothed whales had a more complex relationship with mesoscale features. Dall's porpoises showed a preference for LCSs, especially strong convergence zones with FSLE intensities $\leq$ -0.2 day^{-1}. However, two delphinid species, Pacific white-sided dolphin and short-beaked common dolphin, showed inconclusive results—potentially due to nocturnal foraging (short-beaked common dolphin, some Pacific white-sided dolphins) and difficulties with differentiating different populations at sea. Further research using techniques such as satellite tagging, passive acoustics, or genetic analysis can help to clarify the relationship of these species and mesoscale features.

Chapter 4, in part, is currently being prepared for submission for publication of the material. Giddings, A., Franks, P. J. S. & Baumann-Pickering, S. The dissertation author was the primary investigator and author of this paper.

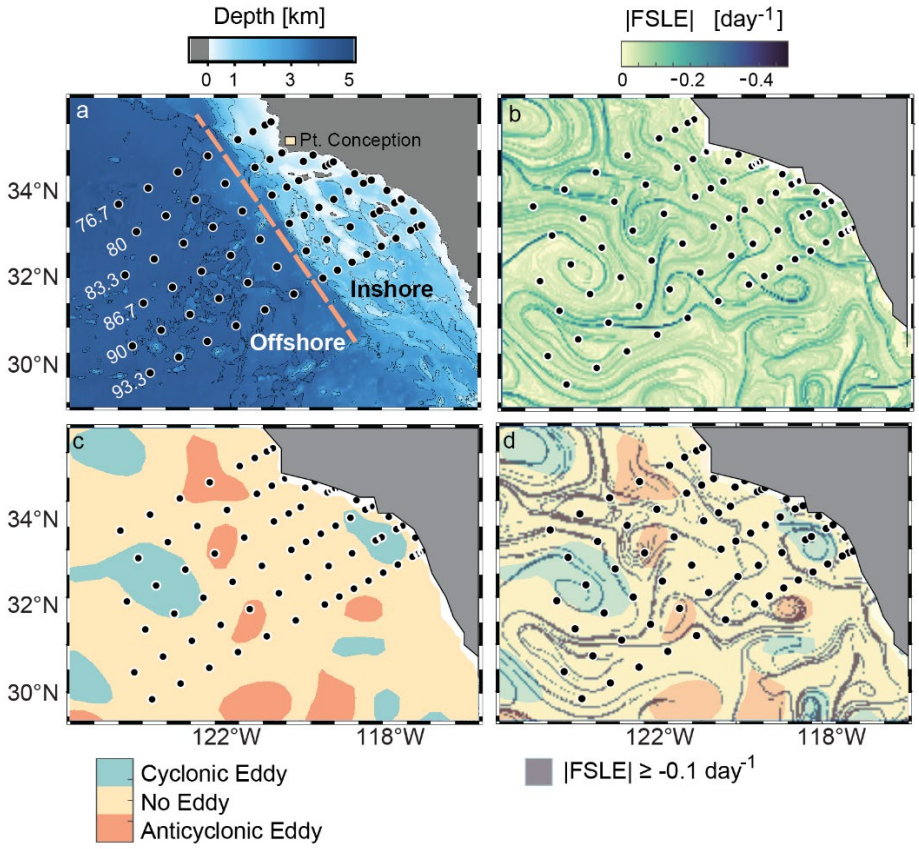

Figure 4.1: The CalCOFI sampling grid and example data from 2021-07-29. Black dots indicate CalCOFI sampling stations. (a) Map of the study region. CalCOFI line numbers are given next to the line. Whale observations occurred while transiting between stations along each line (perpendicular to the coast). (b) Finite-size Lyapunov exponents (FSLEs) from 2021-07-29. Darker colors (more negative) show stronger convergence. (c) Eddy data from 2021-07-29. Blue regions indicate cyclonic eddies, orange indicates anticyclonic eddies, and yellow indicates the area is outside of an eddy. White regions (near the coast) indicate where eddy data is unavailable. (d) FSLEs superimposed on the eddy field, 2021-07-29. Only FSLE ridges (defined as FSLEs ≤ -0.01) are shown.

Figure 4.2: Spring encounters, FSLE distributions, and proportion of locations with eddies. Column 1 (a, d, g, and j): Maps of on-effort, on transect encounters during the season. Orange dots are encounter locations. Black dots are CalCOFI sampling stations. The thick black line outlines the season- and species-specific domain. Background is the average FSLE intensity for every cruise in this season. Column 2 (b ,e, h, and k): Kernel density plots for FSLE intensities at cetacean encounter locations (green) and along cruise tracks within the season and species-specific domain (black). To test whether the FSLE distributions are significantly different, the p-values resulting from two-sample Kolmogorov-Smirnov tests are shown. Column 3 (c, f, i, and l): Proportion of encounters or cruise track locations within eddies (pink) or outside of eddies (yellow) and proportion of encounters or cruise track locations within eddies that were cyclonic (blue) or anticyclonic (orange). Results from the binomial proportion tests are given, showing whether the proportions are significantly different between encounters and cruise track locations. Cetacean illustrations by Freya Hammar.

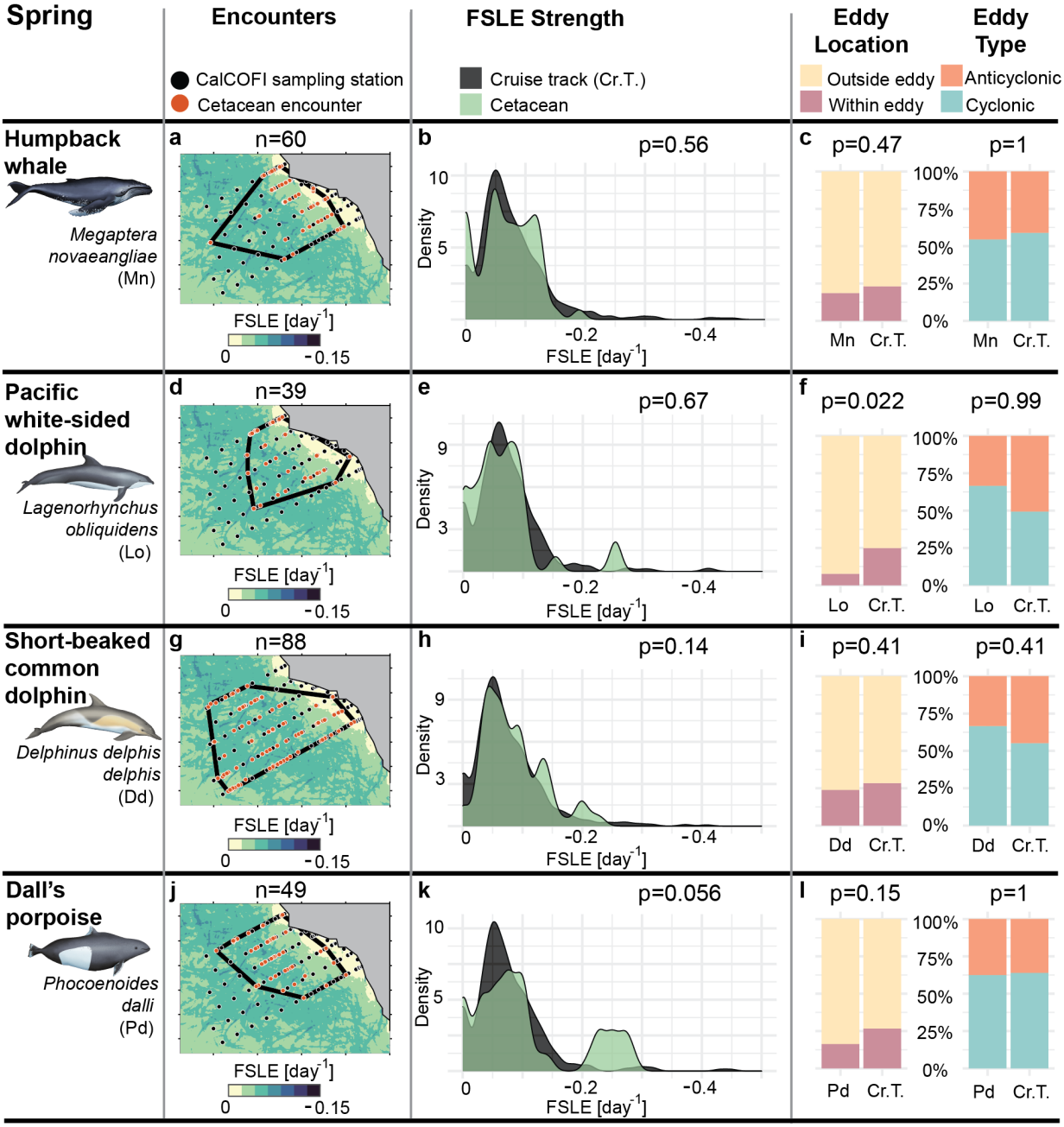
Spring
Encounters
CalCOFI sampling station
Cetacean encounter
FSLE Strength
Cruise track (Cr.T.)
Cetacean
Eddy Location
Outside eddy
Within eddy
Eddy Type
Anticyclonic
Cyclonic
Humpback whale
Megaptera novaeangliae (Mn)
a
n=60
FSLE [day-1]
0
-0.15
b
p=0.56
Density
10
5
0
-0.2
-0.4
FSLE [day-1]
c
p=0.47
p=1
100%
75%
50%
25%
0%
Mn
Cr.T.
Pacific white-sided dolphin
Lagenorhynchus obliquidens (Lo)
d
n=39
e
p=0.67
9
3
f
p=0.022
p=0.99
Lo
Short-beaked common dolphin
Delphinus delphis delphis (Dd)
g
n=88
h
p=0.14
i
p=0.41
p=0.41
Dd
Dall's porpoise
Phocoenoides dalli (Pd)
j
n=49
k
p=0.056
l
p=0.15
p=1
Pd

Figure 4.3: Summer encounters, FSLE distributions, and proportion of locations with eddies. Column 1 (a, d, g, and j): Maps of on-effort, on transect encounters during the season. Orange dots are encounter locations. Black dots are CalCOFI sampling stations. The thick black line outlines the season- and species-specific domain. Background is the average FSLE intensity for every cruise in this season. Column 2 (b, e, h, and k): Kernel density plots for FSLE intensities at cetacean encounter locations (green) and along cruise tracks within the season and species-specific domain (black). To test whether the FSLE distributions are significantly different, the p-values resulting from two-sample Kolmogorov-Smirnov tests are shown. Column 3 (c, f, i, and l): Proportion of encounters or cruise track locations within eddies (pink) or outside of eddies (yellow) and proportion of encounters or cruise track locations within eddies that were cyclonic (blue) or anticyclonic (orange). Results from the binomial proportion tests are given, showing whether the proportions are significantly different between encounters and cruise track locations. Cetacean illustrations by Freya Hammar.

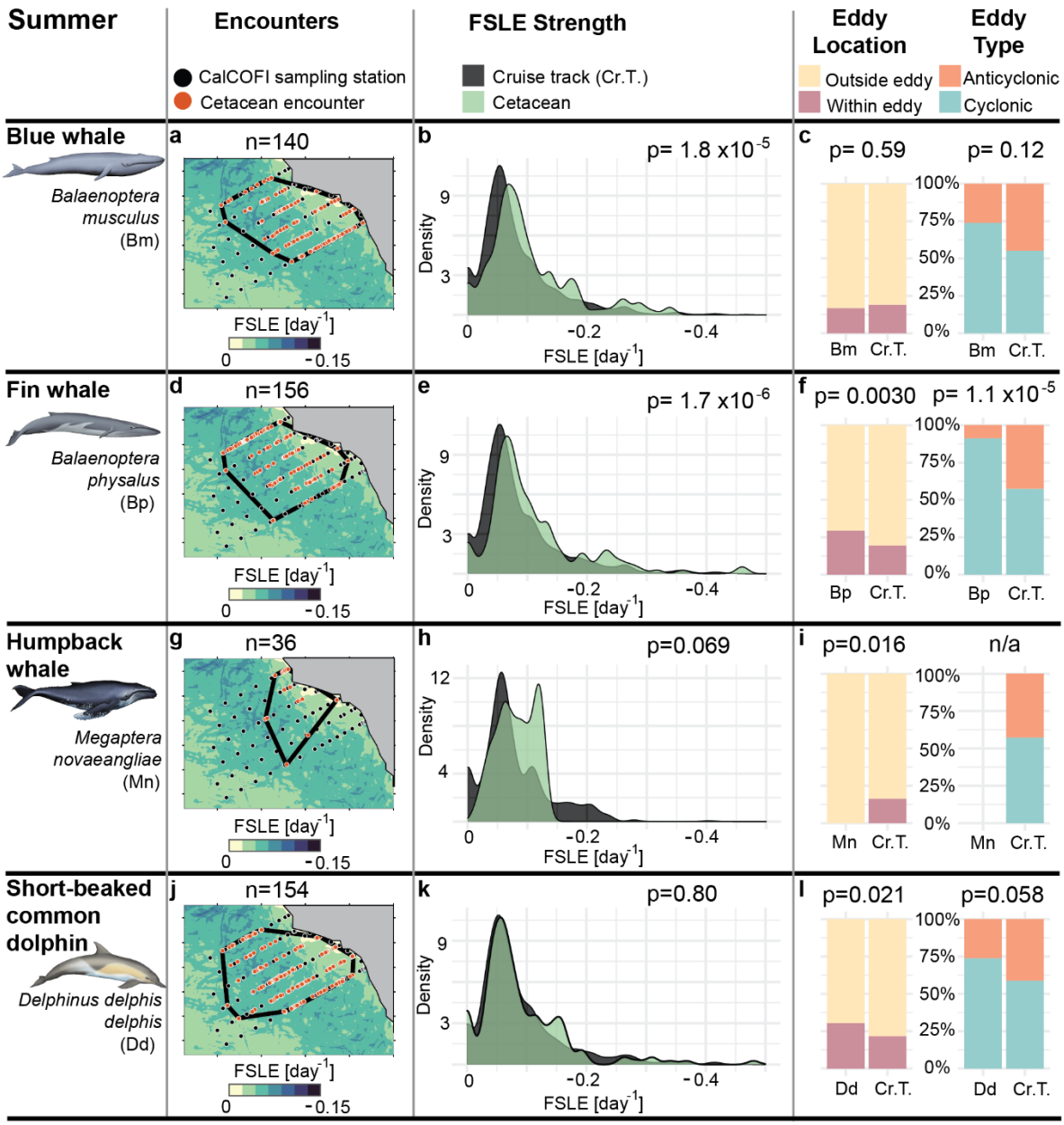
Summer
Encounters
CalCOFI sampling station
Cetacean encounter
FSLE Strength
Cruise track (Cr.T.)
Cetacean
Eddy Location
Outside eddy
Within eddy
Eddy Type
Anticyclonic
Cyclonic
Blue whale
Balaenoptera musculus (Bm)
a
n=140
FSLE [day-1]
0
-0.15
b
p= 1.8 x10-5
Density
9
3
0
-0.2
-0.4
FSLE [day-1]
c
p= 0.59
p= 0.12
100%
75%
50%
25%
0%
Bm
Cr.T.
Bm
Cr.T.
Fin whale
Balaenoptera physalus (Bp)
d
n=156
FSLE [day-1]
0
-0.15
e
p= 1.7 x10-6
Density
9
3
0
-0.2
-0.4
FSLE [day-1]
f
p= 0.0030
p= 1.1 x10-5
100%
75%
50%
25%
0%
Bp
Cr.T.
Bp
Cr.T.
Humpback whale
Megaptera novaeangliae (Mn)
g
n=36
FSLE [day-1]
0
-0.15
h
p=0.069
Density
12
4
0
-0.2
-0.4
FSLE [day-1]
i
p=0.016
n/a
100%
75%
50%
25%
0%
Mn
Cr.T.
Mn
Cr.T.
Short-beaked common dolphin
Delphinus delphis delphis (Dd)
j
n=154
FSLE [day-1]
0
-0.15
k
p=0.80
Density
9
3
0
-0.2
-0.4
FSLE [day-1]
l
p=0.021
p=0.058
100%
75%
50%
25%
0%
Dd
Cr.T.
Dd
Cr.T.

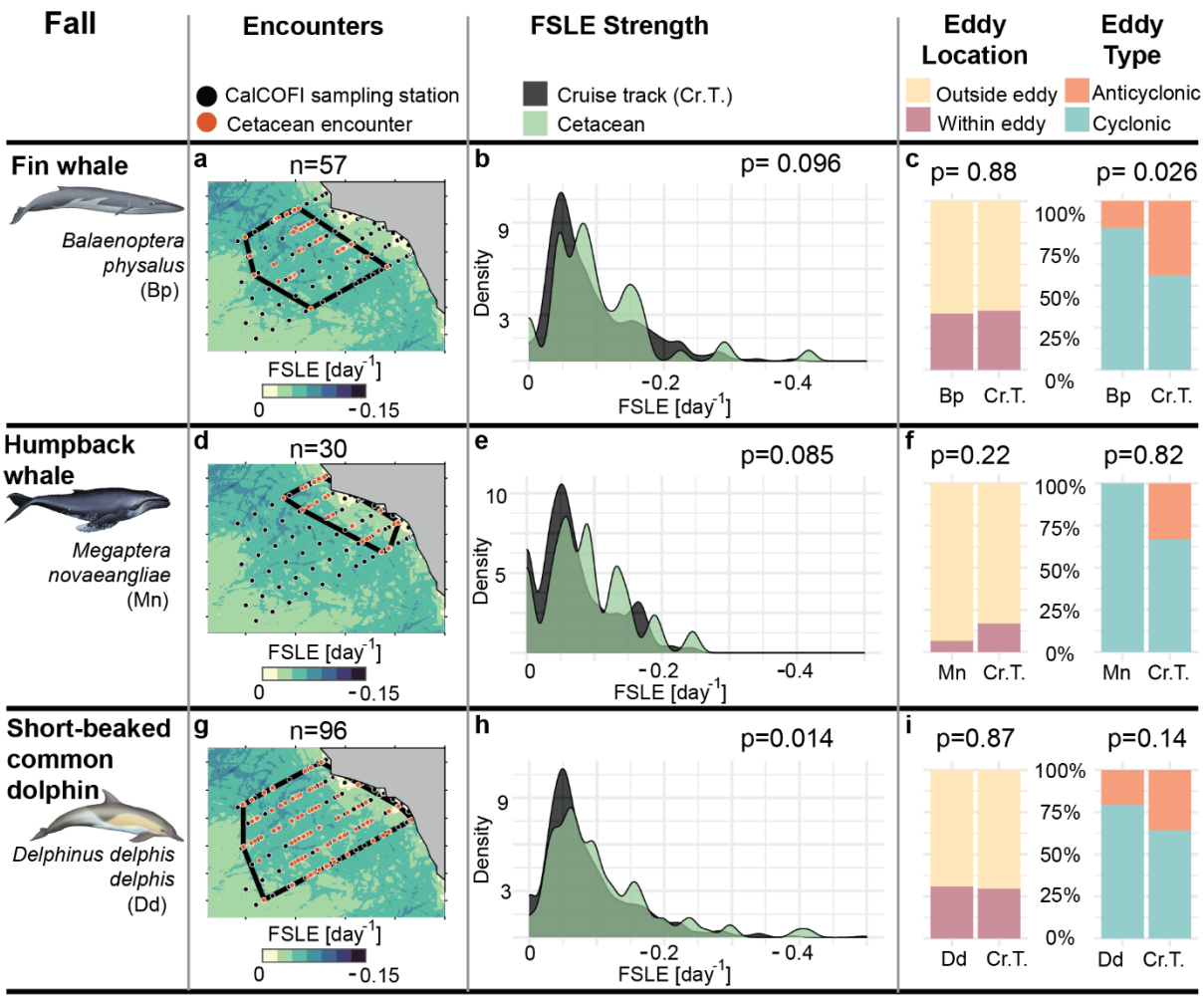

Figure 4.4: Fall encounters, FSLE distributions, and proportion of locations with eddies. Column 1 (a, d, and g): Maps of on-effort, on transect encounters during the season. Orange dots are encounter locations. Black dots are CalCOFI sampling stations. The thick black line outlines the season- and species-specific domain. Background is the average FSLE intensity for every cruise in this season. Column 2 (b ,e, and h): Kernel density plots for FSLE intensities at cetacean encounter locations (green) and along cruise tracks within the season and species-specific domain (black). To test whether the FSLE distributions are significantly different, the p-values resulting from two-sample Kolmogorov-Smirnov tests are shown. Column 3 (c, f, and i): Proportion of encounters or cruise track locations within eddies (pink) or outside of eddies (yellow) and proportion of encounters or cruise track locations within eddies that were cyclonic (blue) or anticyclonic (orange). Results from the binomial proportion tests are given, showing whether the proportions are significantly different between encounters and cruise track locations. Cetacean illustrations by Freya Hammar.

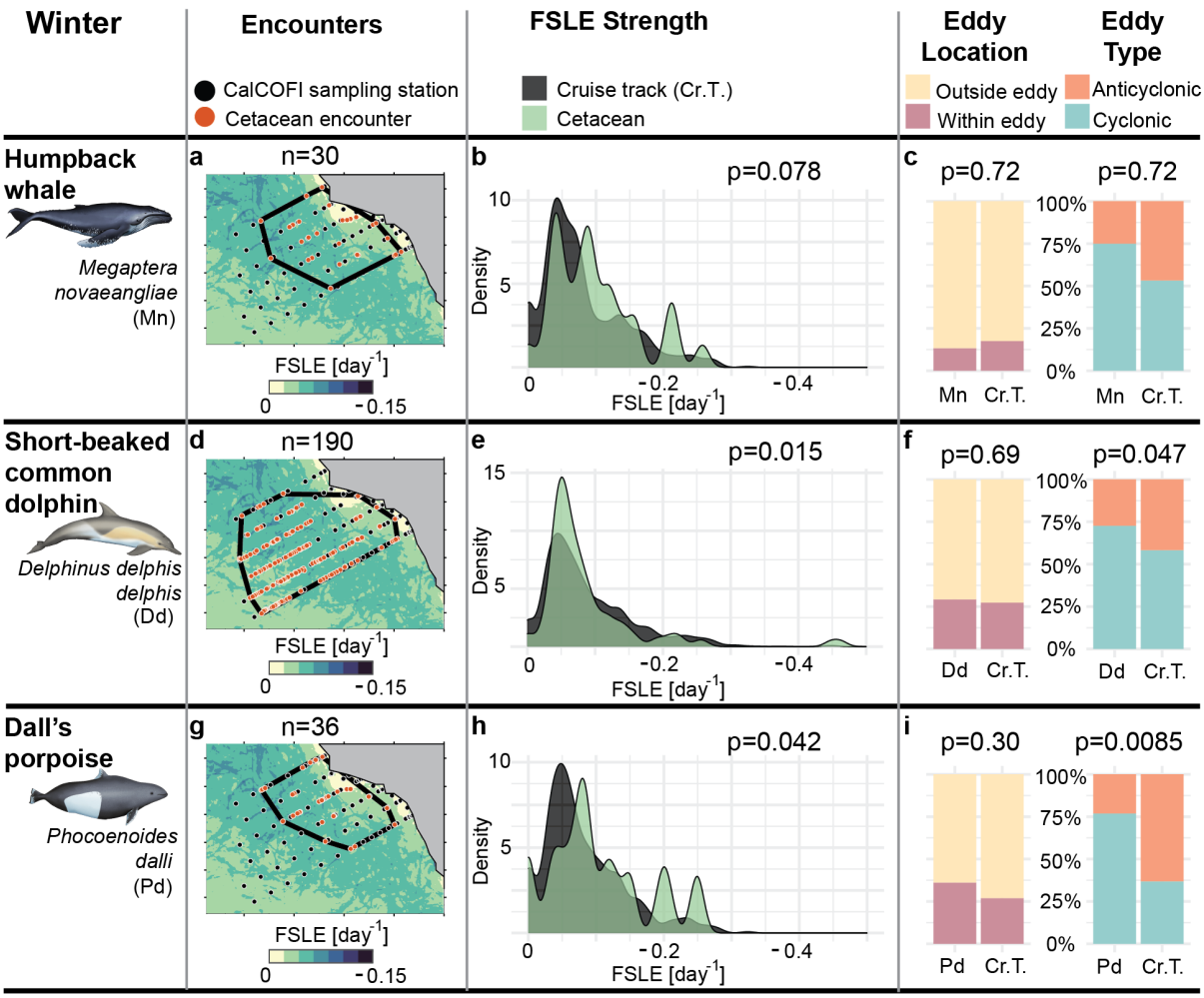

Figure 4.5: Winter encounters, FSLE distributions, and proportion of locations with eddies. Column 1 (a, d, and g): Maps of on-effort, on transect encounters during the season. Orange dots are encounter locations. Black dots are CalCOFI sampling stations. The thick black line outlines the season- and species-specific domain. Background is the average FSLE intensity for every cruise in this season. Column 2 (b ,e, and h): Kernel density plots for FSLE intensities at cetacean encounter locations (green) and along cruise tracks within the season and species-specific domain (black). To test whether the FSLE distributions are significantly different, the p-values resulting from two-sample Kolmogorov-Smirnov tests are shown. Column 3 (c, f, and i): Proportion of encounters or cruise track locations within eddies (pink) or outside of eddies (yellow) and proportion of encounters or cruise track locations within eddies that were cyclonic (blue) or anticyclonic (orange). Results from the binomial proportion tests are given, showing whether the proportions are significantly different between encounters and cruise track locations. Cetacean illustrations by Freya Hammar.

Figure 4.6: Spring and summer environmental conditions in years with encounters versus years without encounters. Column 1 (a ,c, e, g, i, and k): Kernel density plots for FSLE intensities along cruise tracks within the season and species-specific domain in years with encounters (black) and without encounters (light grey). To test whether the FSLE distributions are significantly different, the p-values resulting from two-sample Kolmogorov-Smirnov tests are shown. Column 2 (b, d, f, h, j, and l): Proportion of cruise track locations for years with encounters and years without encounters that were within eddies (pink) or outside of eddies (yellow) and proportion of cruise track locations within eddies that were cyclonic (blue) or anticyclonic (orange). Results from the binomial proportion tests are given, showing whether the proportions are significantly different between years with encounters and years without.

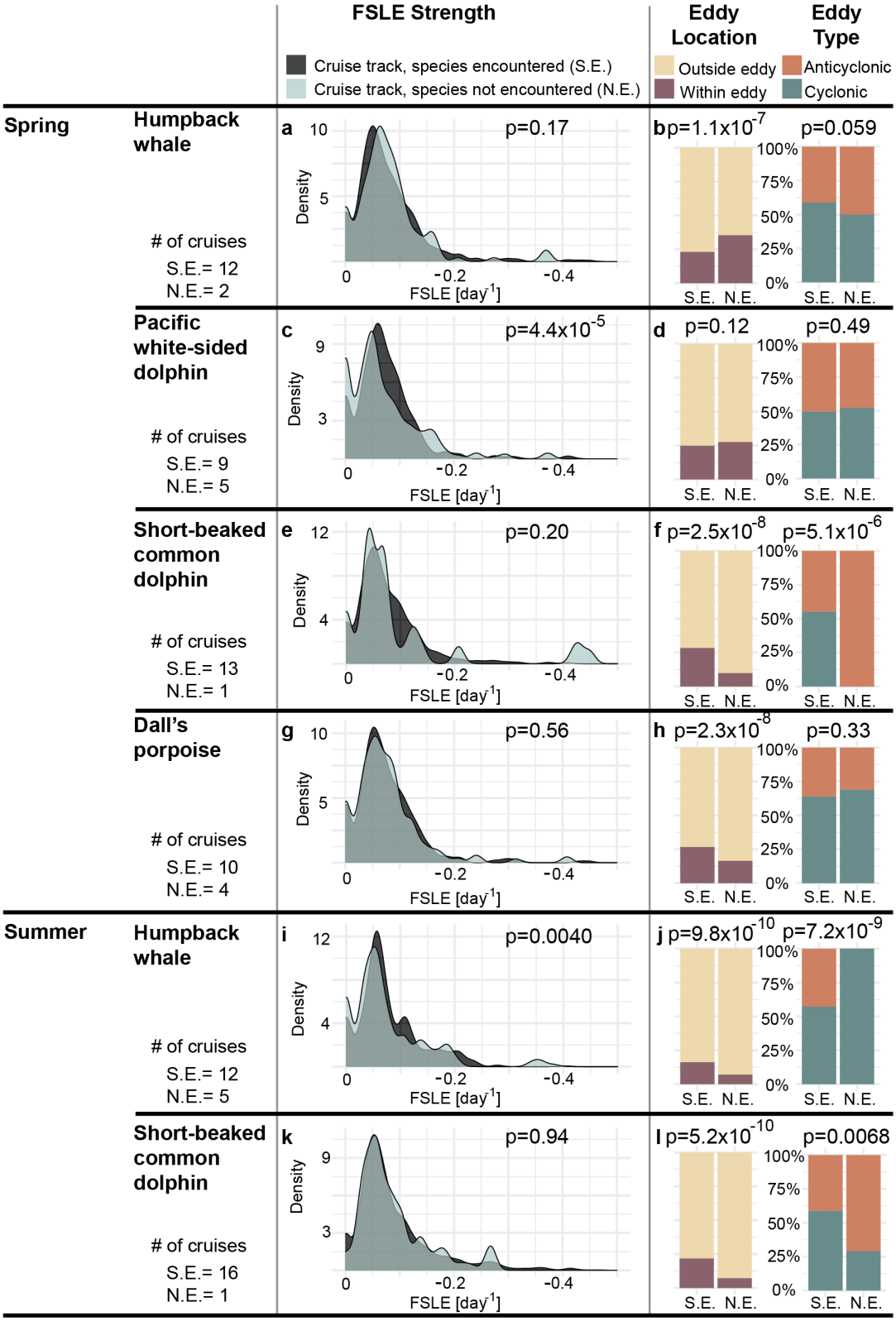
FSLE Strength
Cruise track, species encountered (S.E.)
Cruise track, species not encountered (N.E.)
Eddy Location
Outside eddy
Within eddy
Eddy Type
Anticyclonic
Cyclonic
Spring
Humpback whale
# of cruises
S.E.= 12
N.E.= 2
a
p=0.17
b p=1.1x10-7
p=0.059
Pacific white-sided dolphin
# of cruises
S.E.= 9
N.E.= 5
c
p=4.4x10-5
d
p=0.12
p=0.49
Short-beaked common dolphin
# of cruises
S.E.= 13
N.E.= 1
e
p=0.20
f p=2.5x10-8
p=5.1x10-6
Dall's porpoise
# of cruises
S.E.= 10
N.E.= 4
g
p=0.56
h p=2.3x10-8
p=0.33
Summer
Humpback whale
# of cruises
S.E.= 12
N.E.= 5
i
p=0.0040
j p=9.8x10-10
p=7.2x10-9
Short-beaked common dolphin
# of cruises
S.E.= 16
N.E.= 1
k
p=0.94
l p=5.2x10-10
p=0.0068
Density
FSLE [day-1]
S.E.
N.E.
100%
75%
50%
25%
0%

Figure 4.7: Fall and winter environmental conditions in years with encounters versus years without encounters. Column 1 (a ,c, e, g, and i,): Kernel density plots for FSLE intensities along cruise tracks within the season and species-specific domain in years with encounters (black) and without encounters (light grey). To test whether the FSLE distributions are significantly different, the p-values resulting from two-sample Kolmogorov-Smirnov tests are shown. Column 2 (b, d, f, h, and j: Proportion of cruise track locations for years with encounters and years without encounters that were within eddies (pink) or outside of eddies (yellow) and proportion of cruise track locations within eddies that were cyclonic (blue) or anticyclonic (orange). Results from the binomial proportion tests are given, showing whether the proportions are significantly different between years with encounters and years without.

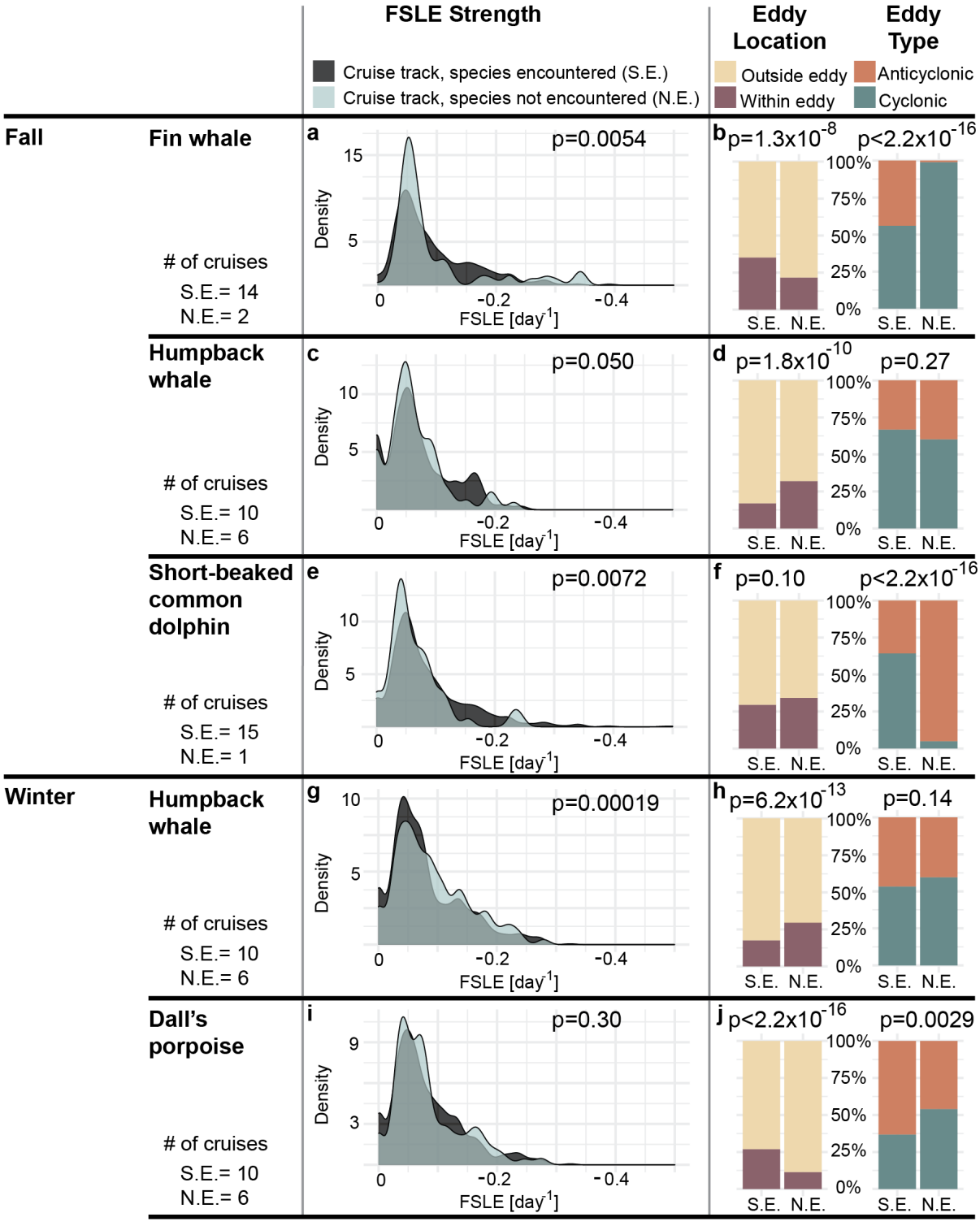
FSLE Strength
Cruise track, species encountered (S.E.)
Cruise track, species not encountered (N.E.)
Eddy Location
Outside eddy
Within eddy
Eddy Type
Anticyclonic
Cyclonic
Fall
Fin whale
# of cruises
S.E.= 14
N.E.= 2
a
p=0.0054
b p=1.3x10-8
p<2.2x10-16
Humpback whale
# of cruises
S.E.= 10
N.E.= 6
c
p=0.050
d p=1.8x10-10
p=0.27
Short-beaked common dolphin
# of cruises
S.E.= 15
N.E.= 1
e
p=0.0072
f p=0.10
p<2.2x10-16
Winter
Humpback whale
# of cruises
S.E.= 10
N.E.= 6
g
p=0.00019
h p=6.2x10-13
p=0.14
Dall's porpoise
# of cruises
S.E.= 10
N.E.= 6
i
p=0.30
j p<2.2x10-16
p=0.0029
Density
FSLE [day-1]
S.E.
N.E.

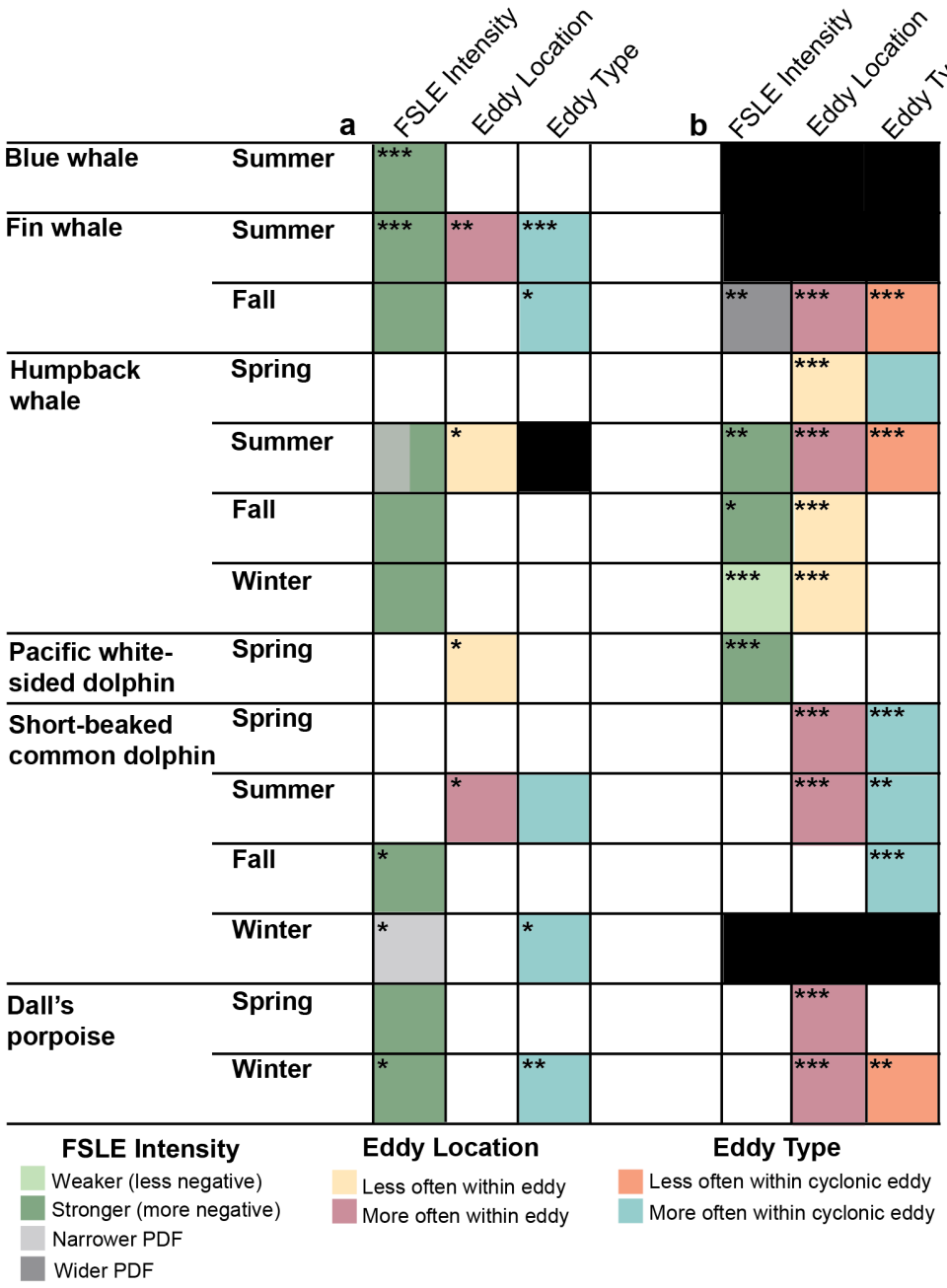

Figure 4.8 Summary of statistically significant differences between (a) encounters and cruise track locations and (b) environmental conditions between years with encounters and years without. (a) Differences in FSLE intensity, eddy location, and eddy type for cetacean encounters relative to the conditions along cruise tracks within the season and species-specific domain. Summarizes figures 2-5. (b) Differences in FSLE intensity, eddy location, and eddy type for conditions along cruise tracks for years with encounters relative to years without encounters. Summarizes figures 6-7. Asterisks indicate statistical significance: no asterisk ($0.05 < p < 0.1$), one asterisk ($0.01 < p < 0.05$), two asterisks ($0.001 < p < 0.01$) , or three asterisks ($p < 0.001$) White indicates results were not statistically significant. Black boxes indicate not applicable.

Table 4.1: Mean FSLE intensities and 95% confidence intervals. Confidence intervals were estimated using bootstrapping with 10,000 iterations. If the 95% confidence intervals do not overlap, we consider them significantly different (bold).

Season	*Species*	*Mean FSLE intensity, encounter locations [day^{-1}]*	*Mean FSLE intensity, cruise track locations, years with encounters [day-^{1}]*	*Mean FSLE intensity, cruise track locations, years without encounters [day-^{1}]*
Spring	Humpback whale	-0.066 (-0.055 – - 0.078)	-0.077 (-0.073 – - 0.081)	-0.079 (-0.069 – -0.090)
	Pacific white-sided dolphin	-0.08 (-0.054 – -0.118)	-0.072 (-0.068 – -0.076)	-0.070 (-0.063 – -0.077)
	Short-beaked common dolphin	-0.084 (-0.072 – -0.078)	-0.075 (-0.072 – -0.078)	-0.092 (-0.070 – -0.118)
	Dall's porpoise	-0.103 (-0.079 – -0.129)	-0.075 (0.071 – -0.080)	-0.075 (-0.068 – -0.083)
Summer	Blue whale	**-0.101 (-0.090 – -0.114)**	**-0.083 (-0.080 – -0.086)**	-
	Fin whale	**-0.107 (-0.095 – -0.120)**	**-0.086 (-0.083 – -0.089)**	-
	Humpback whale	-0.081 (-0.071 – -0.092)	-0.077 (-0.072 – -0.082)	-0.074 (-0.066 – -0.083)
	Short-beaked common dolphin	-0.089 (-0.077 – -0.101)	-0.088 (-0.085 – -0.092)	-0.087 (-0.076 – -0.099)
Fall	Fin whale	-0.101 (-0.083 – -0.121)	-0.092 (-0.088 – -0.096)	-0.094 (-0.081 – -0.108)
	Humpback whale	-0.086 (-0.066 – -0.109)	-0.070 (-0.065 – -0.075)	-0.064 (-0.057 – -0.071)
	Short-beaked common dolphin	-0.103 (-0.088 – -0.119)	-0.086 (-0.082 – -0.089)	-0.065 (-0.056 – -0.076)
Winter	Humpback whale	-0.099 (-0.077 – -0.122)	-0.080 (-0.075 – -0.085)	-0.090 (-0.083 – -0.096)
	Short-beaked common dolphin	-0.086 (-0.077 – -0.097)	-0.088 (-0.085 – -0.091)	-
	Dall's porpoise	-0.103 (0.081 – 0.126)	-0.080 (-0.075 – -0.086)	-0.081 (-0.075 – -0.088)

References

Alexander, M. A., Bladé, I., Newman, M., Lanzante, J. R., Lau, N.-C., & Scott, J. D. (2002). The Atmospheric Bridge: The Influence of ENSO Teleconnections on Air–Sea Interaction over the Global Oceans. *Journal of Climate*, *15*(16), 2205–2231. https://doi.org/10.1175/1520-0442(2002)015<2205:tabtio>2.0.co;2

Banks, R. C., & Brownell, R. L. (1969). Taxonomy of the Common Dolphins of the Eastern Pacific Ocean. Journal of Mammalogy, 50(2), 262. https://doi.org/10.2307/1378342

Barlow, J, Kahru, M., & Mitchell, B. (2008). Cetacean biomass, prey consumption, and primary production requirements in the California Current ecosystem. *Marine Ecology Progress Series*, *371*, 285–295. https://doi.org/10.3354/meps07695

Barlow, J., & Forney, K. A. (2007). Abundance and population density of cetaceans in the California Current ecosystem. *Fishery Bulletin*, *105*(4), 509–526.

Barth, J. A., Pierce, S. D., & Smith, R. L. (2000). A separating coastal upwelling jet at Cape Blanco, Oregon and its connection to the California Current System. *Deep Sea Research Part II: Topical Studies in Oceanography*, *47*(5–6), 783–810. https://doi.org/10.1016/s0967-0645(99)00127-7

Becker, E. A., Forney, K. A., Fiedler, P. C., Barlow, J., Chivers, S. J., Edwards, C. A., Moore, A.M., & Redfern, J.V. (2016). Moving Towards Dynamic Ocean Management: How Well Do Modeled Ocean Products Predict Species Distributions? *Remote Sensing*, *8*(2), 149. https://doi.org/10.3390/rs8020149

Becker, E. A., Forney, K. A., Thayre, B. J., Debich, A. J., Campbell, G. S., Whitaker, K., Douglas, A. B., Gilles, A., Hoopes, R., & Hildebrand, J. A. (2017). Habitat-Based Density Models for Three Cetacean Species off Southern California Illustrate Pronounced Seasonal Differences. *Frontiers in Marine Science*, *4*, 121. https://doi.org/10.3389/fmars.2017.00121

Becker, E. A., Forney, K. A., Redfern, J. V., Barlow, J., Jacox, M. G., Roberts, J. J., & Palacios, D. M. (2019). Predicting cetacean abundance and distribution in a changing climate. *Diversity and Distributions*, *25*(4), 626–643. https://doi.org/10.1111/ddi.12867

Becker, E. A., Carretta, J. V., Forney, K. A., Barlow, J., Brodie, S., Hoopes, R., Jacox, M. G., Maxwell, S. M., Redfern, J. V., Sisson, N. B., Welch, H., & Hazen, E. L. (2020). Performance evaluation of cetacean species distribution models developed using generalized additive models and boosted regression trees. *Ecology and Evolution*, *10*(12), 5759–5784. https://doi.org/10.1002/ece3.6316

Becker, E. A., Forney, K. A., Miller, D. L., Barlow, J., Rojas-Bracho, L., R, J. U., & Moore, J. E. (2022). Dynamic Habitat Models Reflect Interannual Movement of Cetaceans Within the California Current Ecosystem. *Frontiers in Marine Science*, *9*, 829523. https://doi.org/10.3389/fmars.2022.829523

Beron-Vera, F. J., Olascoaga, M. J., & Goni, G. J. (2008). Oceanic mesoscale eddies as revealed by Lagrangian coherent structures. *Geophysical Research Letters*, *35*(12), n/a-n/a. https://doi.org/10.1029/2008gl033957

Blondeau-Patissier, D., Gower, J. F. R., Dekker, A. G., Phinn, S. R., & Brando, V. E. (2014). A review of ocean color remote sensing methods and statistical techniques for the detection, mapping and analysis of phytoplankton blooms in coastal and open oceans. *Progress in Oceanography*, *123*, 123–144. https://doi.org/10.1016/j.pocean.2013.12.008

Bograd, S. J., Schroeder, I., Sarkar, N., Qiu, X., Sydeman, W. J., & Schwing, F. B. (2009). Phenology of coastal upwelling in the California Current. *Geophysical Research Letters*, *36*(1). https://doi.org/10.1029/2008gl035933

Buckland, S. T., Anderson, D. R., Burnham, K. P., Laake, J. L., Borchers, D. L., & Thomas, L. (2001). *Introduction to Distance Sampling: Estimating Abundance of Biological Populations*. Oxford, UK: Oxford University Press.

Cade, D. E., Fahlbusch, J. A., Oestreich, W. K., Ryan, J., Calambokidis, J., Findlay, K. P., Friedlaender, A. S., Hazen, E. L., Seakamela, S. M., & Goldbogen, J. A. (2021). Social exploitation of extensive, ephemeral, environmentally controlled prey patches by supergroups of rorqual whales. *Animal Behaviour*, *182*, 251–266. https://doi.org/10.1016/j.anbehav.2021.09.013

Campbell, G. S., Thomas, L., Whitaker, K., Douglas, A. B., Calambokidis, J., & Hildebrand, J. A. (2015). Inter-annual and seasonal trends in cetacean distribution, density and abundance off southern California. *Deep Sea Research Part II: Topical Studies in Oceanography*, *112*, 143–157. https://doi.org/10.1016/j.dsr2.2014.10.008

Capet, X., Colas, F., Mcwilliams, J. C., Penvan, P., & Marchesoello, P. (2008). Eddies in Eastern Boundary Subtropical Upwelling Systems. In M. W. Hecht & H. Hasumi (Eds.), *Ocean Modeling in an Eddying Regime*. AGU. https://doi.org/10.1029/177gm10

Carr, M.-E. (2001). Estimation of potential productivity in Eastern Boundary Currents using remote sensing. *Deep Sea Research Part II: Topical Studies in Oceanography*, *49*(1–3), 59–80. https://doi.org/10.1016/s0967-0645(01)00094-7

Cavole, L., Demko, A., Diner, R., Giddings, A., Koester, I., Pagniello, C., Paulsen, M.-L., Ramirez-Valdez, A., Schwenck, S., Yen, N., Zill, M., & Franks, P. (2016). Biological Impacts of the 2013–2015 Warm-Water Anomaly in the Northeast Pacific: Winners, Losers, and the Future. *Oceanography*, *29*(2). https://doi.org/10.5670/oceanog.2016.32

Chabert, P., d'Ovidio, F., Echevin, V., Stukel, M. R., & Ohman, M. D. (2021). Cross-Shore Flow and Implications for Carbon Export in the California Current Ecosystem: A Lagrangian Analysis. *Journal of Geophysical Research: Oceans*, *126*(2). https://doi.org/10.1029/2020jc016611

Checkley, D. M., & Barth, J. A. (2009). Patterns and processes in the California Current System. *Progress in Oceanography*, *83*(1–4), 49–64. https://doi.org/10.1016/j.pocean.2009.07.028

Chelton, D. B., & Schlax, M. G. (1996). Global Observations of Oceanic Rossby Waves. *Science*, *272*(5259), 234–238. https://doi.org/10.1126/science.272.5259.234

Chelton, D. B., Schlax, M. G., & Samelson, R. M. (2011). Global observations of nonlinear mesoscale eddies. *Progress in Oceanography*, *91*(2), 167–216. https://doi.org/10.1016/j.pocean.2011.01.002

Chenillat, F., Rivière, P., Capet, X., Lorenzo, E. D., & Blanke, B. (2012). North Pacific Gyre Oscillation modulates seasonal timing and ecosystem functioning in the California Current upwelling system. *Geophysical Research Letters*, *39*(1), n/a-n/a. https://doi.org/10.1029/2011gl049966

Chenillat, F., Franks, P. J. S., Rivière, P., Capet, X., Grima, N., & Blanke, B. (2015). Plankton dynamics in a cyclonic eddy in the Southern California Current System. *Journal of Geophysical Research: Oceans*, *120*(8), 5566–5588. https://doi.org/10.1002/2015jc010826

Chenillat, F., Franks, P. J. S., & Combes, V. (2016). Biogeochemical properties of eddies in the California Current System. *Geophysical Research Letters*, *43*(11), 5812–5820. https://doi.org/10.1002/2016gl068945

Chenillat, F., Franks, P. J. S., Capet, X., Rivière, P., Grima, N., Blanke, B., & Combes, V. (2018). Eddy properties in the Southern California Current System. *Ocean Dynamics*, *68*(7), 761–777. https://doi.org/10.1007/s10236-018-1158-4

Chereskin, T. K. (1995). Direct evidence for an Ekman balance in the California Current. *Journal of Geophysical Research: Oceans*, *100*(C9), 18261–18269. https://doi.org/10.1029/95jc02182

Cimino, M. A., Santora, J. A., Schroeder, I., Sydeman, W., Jacox, M. G., Hazen, E. L., & Bograd, S. J. (2020). Essential krill species habitat resolved by seasonal upwelling and ocean circulation models within the large marine ecosystem of the California Current System. *Ecography*, *43*(10), 1536–1549. https://doi.org/10.1111/ecog.05204

Combes, V., Chenillat, F., Lorenzo, E. D., Rivière, P., Ohman, M. D., & Bograd, S. J. (2013). Cross-shore transport variability in the California Current: Ekman upwelling vs. eddy dynamics. *Progress in Oceanography*, *109*, 78–89. https://doi.org/10.1016/j.pocean.2012.10.001

Condie, S., & Condie, R. (2016). Retention of plankton within ocean eddies. *Global Ecology and Biogeography*, *25*(10), 1264–1277. https://doi.org/10.1111/geb.12485

Cordero-Quirós, N., Miller, A. J., Subramanian, A. C., Luo, J. Y., & Capotondi, A. (2019). Composite physical-biological El Niño and La Niña conditions in the California Current System in CESM1-POP2-BEC. *Ocean Modelling*, *142*, 101439. https://doi.org/10.1016/j.ocemod.2019.101439

Cotte, C., d'Ovidio, F., Chaigneau, A., Lèvy, M., Taupier-Letage, I., Mate, B., & Guinet, C. (2011). Scale-dependent interactions of Mediterranean whales with marine dynamics. *Limnology and Oceanography*, *56*(1), 219–232. https://doi.org/10.4319/lo.2011.56.1.0219

Cullen, J. J. (2015). Subsurface Chlorophyll Maximum Layers: Enduring Enigma or Mystery Solved? *Annual Review of Marine Science*, *7*(1), 1–33. https://doi.org/10.1146/annurev-marine-010213-135111

Cunha, H. A., Castro, R. L. de, Secchi, E. R., Crespo, E. A., Lailson-Brito, J., Azevedo, A. F., Lazoski, C., & Solé-Cava, A. M. (2015). Molecular and Morphological Differentiation of Common Dolphins (Delphinus sp.) in the Southwestern Atlantic: Testing the Two Species Hypothesis in Sympatry. *PLoS ONE*, *10*(11), e0140251. https://doi.org/10.1371/journal.pone.0140251

d'Ovidio, F., Fernández, V., Hernández-García, E., & López, C. (2004). Mixing structures in the Mediterranean Sea from finite-size Lyapunov exponents. *Geophysical Research Letters*, *31*(17), n/a-n/a. https://doi.org/10.1029/2004gl020328

d'Ovidio, F., Isern-Fontanet, J., López, C., Hernández-García, E., & García-Ladona, E. (2009). Comparison between Eulerian diagnostics and finite-size Lyapunov exponents computed from altimetry in the Algerian basin. *Deep Sea Research Part I: Oceanographic Research Papers*, *56*(1), 15–31. https://doi.org/10.1016/j.dsr.2008.07.014

d'Ovidio, F., Monte, S. D., Alvain, S., Dandonneau, Y., & Lévy, M. (2010). Fluid dynamical niches of phytoplankton types. *Proceedings of the National Academy of Sciences*, *107*(43), 18366–18370. https://doi.org/10.1073/pnas.1004620107

Della Penna, A., Monte, S. D., Kestenare, E., Guinet, C., & d'Ovidio, F. (2015). Quasi-planktonic behavior of foraging top marine predators. *Scientific Reports*, *5*(1), 18063. https://doi.org/10.1038/srep18063

Dey, S. P., Vichi, M., Fearon, G., Seyboth, E., Findlay, K. P., Meynecke, J.-O., de Bie, J., Lee, S. B., Samanta, .S, Barraqueta, J. M., Roychoudhury, A. N., & Mackey B.. (2021).

Oceanographic anomalies coinciding with humpback whale super-group occurrences in the Southern Benguela. *Scientific Reports*, *11*(1), 20896. https://doi.org/10.1038/s41598-021-00253-2

Di Lorenzo, E., Schneider, N., Cobb, K. M., Franks, P. J. S., Chhak, K., Miller, A. J., McWilliams, J. C., Bograd, S. J., Arango, H., Curchitser, E., Powell, T. M., & Rivière, P. (2008). North Pacific Gyre Oscillation links ocean climate and ecosystem change. *Geophysical Research Letters*, *35*(8). https://doi.org/10.1029/2007gl032838

Doniol-Valcroze, T., Berteaux, D., Larouche, P., & Sears, R. (2007). Influence of thermal fronts on habitat selection by four rorqual whale species in the Gulf of St. Lawrence. *Marine Ecology Progress Series*, *335*, 207–216. https://doi.org/10.3354/meps335207

Fahlbusch, J. A., Czapanskiy, M. F., Calambokidis, J., Cade, D. E., Abrahms, B., Hazen, E. L., & Goldbogen, J. A. (2022). Blue whales increase feeding rates at fine-scale ocean features. *Proceedings of the Royal Society B*, *289*(1981), 20221180. https://doi.org/10.1098/rspb.2022.1180

Ferrari, R., & Wunsch, C. (2009). Ocean Circulation Kinetic Energy: Reservoirs, Sources, and Sinks. *Annual Review of Fluid Mechanics*, *41*(1), 253–282. https://doi.org/10.1146/annurev.fluid.40.111406.102139

Fleming, A. H., Clark, C. T., Calambokidis, J., & Barlow, J. (2015). Humpback whale diets respond to variance in ocean climate and ecosystem conditions in the California Current. *Global Change Biology*, *22*(3), 1214–1224. https://doi.org/10.1111/gcb.13171

Fleming, A. H., Yack, T., Redfern, J. V., Becker, E. A., Moore, T. J., & Barlow, J. (2018). Combining acoustic and visual detections in habitat models of Dall's porpoise. *Ecological Modelling*, *384*, 198–208. https://doi.org/10.1016/j.ecolmodel.2018.06.014

Fossette, S., Abrahms, B., Hazen, E. L., Bograd, S. J., Zilliacus, K. M., Calambokidis, J., Burrows, J. A., Goldbogen, J. A., Harvey, J. T., Marinovic, B., Tershy, B., & Croll, D. A. (2017). Resource partitioning facilitates coexistence in sympatric cetaceans in the California Current. *Ecology and Evolution*, *7*(21), 9085–9097. https://doi.org/10.1002/ece3.3409

Francis, R. C., Hare, S. R., Hollowed, A. B., & Wooster, W. S. (1998). Effects of interdecadal climate variability on the oceanic ecosystems of the NE Pacific. *Fisheries Oceanography*, *7*(1), 1–21. https://doi.org/10.1046/j.1365-2419.1998.00052.x

Freeland, H. J. (2006). What proportion of the north pacific current finds its way into the Gulf of Alaska? *Atmosphere-Ocean*, *44*(4), 321–330. https://doi.org/10.3137/ao.440401

Frischknecht, M., Münnich, M., & Gruber, N. (2015). Remote versus local influence of ENSO on the California Current System. *Journal of Geophysical Research: Oceans*, *120*(2), 1353–1374. https://doi.org/10.1002/2014jc010531

Frölicher, T. L., & Laufkötter, C. (2018). Emerging risks from marine heat waves. *Nature Communications*, *9*(1), 650. https://doi.org/10.1038/s41467-018-03163-6

Frölicher, T. L., Fischer, E. M., & Gruber, N. (2018). Marine heatwaves under global warming. *Nature*, *560*(7718), 360–364. https://doi.org/10.1038/s41586-018-0383-9

García-Vernet, R., Borrell, A., Víkingsson, G., Halldórsson, S. D., & Aguilar, A. (2021). Ecological niche partitioning between baleen whales inhabiting Icelandic waters. *Progress in Oceanography*, *199*, 102690. https://doi.org/10.1016/j.pocean.2021.102690

Gause, G. F. (1934). *The Struggle for Existence*. Baltimore, Maryland, USA: The Williams & Wilkins Company.

Gerrodette, T., Perryman, W. L., & Oedekoven, C. S. (2019). Accuracy and precision of dolphin group size estimates. *Marine Mammal Science*, *35*(1), 22–39. https://doi.org/10.1111/mms.12506

Giddings, A., Franks, P. J. S., & Baumann-Pickering, S. (2022). Monthly to Decadal Variability of Mesoscale Stirring in the California Current System: Links to Upwelling, Climate Forcing, and Chlorophyll Transport. *Journal of Geophysical Research: Oceans*, *127*(6). https://doi.org/10.1029/2021jc018180

Godø, O. R., Samuelsen, A., Macaulay, G. J., Patel, R., Hjøllo, S. S., Horne, J., , Kaartvedt, S., & Johannessen, J. A. (2012). Mesoscale Eddies Are Oases for Higher Trophic Marine Life. *PLoS ONE*, *7*(1), e30161. https://doi.org/10.1371/journal.pone.0030161

Goldbogen, J. A., Calambokidis, J., Oleson, E., Potvin, J., Pyenson, N. D., Schorr, G., & Shadwick, R. E. (2010). Mechanics, hydrodynamics and energetics of blue whale lunge feeding: efficiency dependence on krill density. *Journal of Experimental Biology*, *214*(1), 131–146. https://doi.org/10.1242/jeb.048157

Greene, C. A., Thirumalai, K., Kearney, K. A., Delgado, J. M., Schwanghart, W., Wolfenbarger, N. S., Thyng, K. M., Gwyther, D. E, Gardner, A. S., & Blankenship, D. D. (2019). The Climate Data Toolbox for MATLAB. *Geochemistry, Geophysics, Geosystems*, *20*(7), 3774–3781. https://doi.org/10.1029/2019gc008392

Grinsted, A., Moore, J. C., & Jevrejeva, S. (2004). Application of the cross wavelet transform and wavelet coherence to geophysical time series. *Nonlinear Processes in Geophysics*, *11*(5/6), 561–566. https://doi.org/10.5194/npg-11-561-2004

Grinsted, Aslak. (2021). Cross wavelet and wavelet coherence. Retrieved May 19, 2021, from https://github.com/grinsted/wavelet-coherence

Gruber, N., Lachkar, Z., Frenzel, H., Marchesiello, P., Münnich, M., McWilliams, J. C., Nagai, T., & Plattner, G.-K. (2011). Eddy-induced reduction of biological production in eastern

boundary upwelling systems. *Nature Geoscience*, *4*(11), 787–792. https://doi.org/10.1038/ngeo1273

Gygax, L. (2002). Evolution of group size in the dolphins and porpoises: interspecific consistency of intraspecific patterns. *Behavioral Ecology*, *13*(5), 583–590. https://doi.org/10.1093/beheco/13.5.583

Haller, G. (2015). Langrangian Coherent Structures. *Annual Review of Fluid Mechanics*, *47*(1), 1–25. https://doi.org/10.1146/annurev-fluid-010313-141322

Hardin, G. (1960). The Competitive Exclusion Principle. *Science*, *131*(3409), 1292–1297. https://doi.org/10.1126/science.131.3409.1292

Harrison, C. S., & Glatzmaier, G. A. (2012). Lagrangian coherent structures in the California Current System – sensitivities and limitations. *Geophysical & Astrophysical Fluid Dynamics*, *106*(1), 22–44. https://doi.org/10.1080/03091929.2010.532793

Harrison, C., Siegel, D., & Mitarai, S. (2013). Filamentation and eddy−eddy interactions in marine larval accumulation and transport. *Marine Ecology Progress Series*, *472*, 27–44. https://doi.org/10.3354/meps10061

Hartman, K. L. (2018). Risso's dolphins. In B. Würsig, J. G. M. Thewissen, & K. M. Kovacs (Eds.), *Encyclopedia of Marine Mammals Third Edition*. https://doi.org/https://doi.org/10.1016/C2015-0-00820-6

Hermann, A. J., Curchitser, E. N., Haidvogel, D. B., & Dobbins, E. L. (2009). A comparison of remote vs. local influence of El Niño on the coastal circulation of the northeast Pacific. *Deep Sea Research Part II: Topical Studies in Oceanography*, *56*(24), 2427–2443. https://doi.org/10.1016/j.dsr2.2009.02.005

Hernández-Carrasco, I., López, C., Hernández-García, E., & Turiel, A. (2011). How reliable are finite-size Lyapunov exponents for the assessment of ocean dynamics? *Ocean Modelling*, *36*(3–4), 208–218. https://doi.org/10.1016/j.ocemod.2010.12.006

Hernández-Carrasco, I., Rossi, V., Hernández-García, E., Garçon, V., & López, C. (2014). The reduction of plankton biomass induced by mesoscale stirring: A modeling study in the Benguela upwelling. *Deep Sea Research Part I: Oceanographic Research Papers*, *83*, 65–80. https://doi.org/10.1016/j.dsr.2013.09.003

Henderson, E. E., Hildebrand, J. A., & Smith, M. H. (2011). Classification of behavior using vocalizations of Pacific white-sided dolphins (*Lagenorhynchus obliquidens*). *The Journal of The Acoustical Society of America*, *130*(1), 557–567. https://doi.org/10.1121/1.3592213

Heyning, J. E., & Perrin, W. F. (1994). Evidence for two species of common dolphins (genus Delphinus) from the eastern North Pacific. *Contributions in Science*, *442*, 1–35. https://doi.org/10.5962/p.226804

Hickey, B. M. (1979). The California current system – hypotheses and facts. *Progress in Oceanography*, *8*(4), 191–279. https://doi.org/10.1016/0079-6611(79)90002-8

Hobday, A. J., Alexander, L. V., Perkins, S. E., Smale, D. A., Straub, S. C., Oliver, E. C. J., Benthuysen, J.A., Burrows, M.T., Donat, M.G., Feng, M., Holbrook, N.J., Moore, P.J., Scannell, H.A., Gupta, A.S., & Wernberg, T. (2016). A hierarchical approach to defining marine heatwaves. *Progress in Oceanography*, *141*, 227–238. https://doi.org/10.1016/j.pocean.2015.12.014

Hristova, H. G., Ladd, C., & Stabeno, P. J. (2019). Variability and Trends of the Alaska Gyre From Argo and Satellite Altimetry. *Journal of Geophysical Research: Oceans*, *124*(8), 5870–5887. https://doi.org/10.1029/2019jc015231

Hubbs, C. L. (1948). Changes in the fish fauna of western North America correlated with changes in ocean temperature. *Journal of Marine Research*, *VII*(3), 459–481.

Jacox, M. G., Moore, A. M., Edwards, C. A., & Fiechter, J. (2014). Spatially resolved upwelling in the California Current System and its connections to climate variability. *Geophysical Research Letters*, *41*(9), 3189–3196. https://doi.org/10.1002/2014gl059589

Jacox, M.G., Alexander, M. A., Mantua, N. J., Scott, J. D., Hervieux, G., Webb, R. S., & Werner, F. E. (2018a). Forcing of multiyear extreme ocean temperatures that impacted california current living marine resources in 2016. *Bulletin of the American Meteorological Society*, *99*(1), S27–S33. https://doi.org/10.1175/bams-explainingextremeevents2016.1

Jacox, M. G., Edwards, C. A., Hazen, E. L., & Bograd, S. J. (2018b). Coastal Upwelling Revisited: Ekman, Bakun, and Improved Upwelling Indices for the U.S. West Coast. *Journal of Geophysical Research: Oceans*, *123*(10), 7332–7350. https://doi.org/10.1029/2018jc014187

Jefferson, T. A. (2018). Dall's porpoise *Phocoenoides dalli*. In B. Würsig, J. G. M. Thewissen, & K. M. Kovacs (Eds.), *Encyclopedia of Maine Mammals, 3rd edition* (pp. 239–242). London, United Kingdom: Academic Press. https://doi.org/10.1016/b978-0-12-804327-1.00004-2

Jiao, Y. (2009). Regime shift in marine ecosystems and implications for fisheries management, a review. *Reviews in Fish Biology and Fisheries*, *19*(2), 177–191. https://doi.org/10.1007/s11160-008-9096-8

Johannessen, J. E. D., Biuw, M., Lindstrøm, U., Ollus, V. M. S., López, L. M. M., Gkikopoulou, K. C., Oosthuizen, W.C., & Lowther, A. (2022). Intra-season variations in distribution and abundance of humpback whales in the West Antarctic Peninsula using cruise vessels as opportunistic platforms. *Ecology and Evolution*, *12*(2), e8571. https://doi.org/10.1002/ece3.8571

Kahru, M., Jacox, M. G., & Ohman, M. D. (2018). CCE1: Decrease in the frequency of oceanic fronts and surface chlorophyll concentration in the California Current System during the

2014–2016 northeast Pacific warm anomalies. *Deep Sea Research Part I: Oceanographic Research Papers*, *140*, 4–13. https://doi.org/10.1016/j.dsr.2018.04.007

Kai, E. T., Rossi, V., Sudre, J., Weimerskirch, H., Lopez, C., Hernandez-Garcia, E., Marsac, F., & Garçon, V. (2009). Top marine predators track Lagrangian coherent structures. *Proceedings of the National Academy of Sciences*, *106*(20), 8245–8250. https://doi.org/10.1073/pnas.0811034106

Keister, J. E., & Strub, P. T. (2008). Spatial and interannual variability in mesoscale circulation in the northern California Current System. *Journal of Geophysical Research: Oceans (1978–2012)*, *113*(C4). https://doi.org/10.1029/2007jc004256

Killeen, H., Dorman, J., Sydeman, W., Dibble, C., & Morgan, S. (2021). Effects of a marine heatwave on adult body length of three numerically dominant krill species in the California Current Ecosystem. *ICES Journal of Marine Science*, *79*(3), 761–774. https://doi.org/10.1093/icesjms/fsab215

Kiszka, J. J., Woodstock, M. S., & Heithaus, M. R. (2022). Functional Roles and Ecological Importance of Small Cetaceans in Aquatic Ecosystems. *Frontiers in Marine Science*, *9*. https://doi.org/10.3389/fmars.2022.803173

Koslow, J., McMonagle, H., & Watson, W. (2017). Influence of climate on the biodiversity and community structure of fishes in the southern California Current. *Marine Ecology Progress Series*, *571*, 193–206. https://doi.org/10.3354/meps12095

Kurian, J., Colas, F., Capet, X., McWilliams, J. C., & Chelton, D. B. (2011). Eddy properties in the California Current System. *Journal of Geophysical Research: Oceans (1978–2012)*, *116*(C8). https://doi.org/10.1029/2010jc006895

Leatherwood, S., Perrin, W. F., Kirby, V. L., Hubbs, C. L., & Dahlheim, M. (1980). Distribution and movements of risso's dolphin, grampus grzseus, in the eastern north pacific. *Fishery Bulletin*, *77*(4), 951–963.

Lehahn, Y., d'Ovidio, F., & Koren, I. (2017). A Satellite-Based Lagrangian View on Phytoplankton Dynamics. *Annual Review of Marine Science*, *10*(1), 1–21. https://doi.org/10.1146/annurev-marine-121916-063204

Litzow, M. A., Hunsicker, M. E., Bond, N. A., Burke, B. J., Cunningham, C. J., Gosselin, J. L., Norton, E. L., Ward, E. J., & Zador, S. G. (2020). The changing physical and ecological meanings of North Pacific Ocean climate indices. *Proceedings of the National Academy of Sciences*, *117*(14), 7665–7671. https://doi.org/10.1073/pnas.1921266117

Lowther, A. D., Lydersen, C., Biuw, M., Bruyn, P. J. N. de, Hofmeyr, G. J. G., & Kovacs, K. M. (2014). Post-breeding at-sea movements of three central-place foragers in relation to submesoscale fronts in the Southern Ocean around Bouvetøya. *Antarctic Science*, *26*(5), 533–544. https://doi.org/10.1017/s0954102014000170

Lusseau, D., Williams, R., Wilson, B., Grellier, K., Barton, T. R., Hammond, P. S., & Thompson, P. M. (2004). Parallel influence of climate on the behaviour of Pacific killer whales and Atlantic bottlenose dolphins. *Ecology Letters*, *7*(11), 1068–1076. https://doi.org/10.1111/j.1461-0248.2004.00669.x

Lux, C. (1997). Mitochondrial DNA population structure of the Pacific white-sided dolphin. *Report of the International Whaling Commission*, *47*, 645–652.

Mantua, N. J., Hare, S. R., Zhang, Y., Wallace, J. M., & Francis, R. C. (1997). A Pacific Interdecadal Climate Oscillation with Impacts on Salmon Production. *Bulletin of the American Meteorological Society*, *78*(6), 1069–1079. https://doi.org/10.1175/1520-0477(1997)078<1069:apicow>2.0.co;2

Maps, F., Plourde, S., McQuinn, I. H., St-Onge-Drouin, S., Lavoie, D., Chassé, J., & Lesage, V. (2015). Linking acoustics and finite-time Lyapunov exponents reveals areas and mechanisms of krill aggregation within the Gulf of St. Lawrence, eastern Canada. *Limnology and Oceanography*, *60*(6), 1965–1975. https://doi.org/10.1002/lno.10145

Marchesiello, P., McWilliams, J. C., & Shchepetkin, A. (2003). Equilibrium Structure and Dynamics of the California Current System. *Journal of Physical Oceanography*, *33*(4), 753–783. https://doi.org/10.1175/1520-0485(2003)33<753:esadot>2.0.co;2

Marques, T. A., Thomas, L., Fancy, S. G., & Buckland, S. T. (2007). Improving Estimates of Bird Density Using Multiple- Covariate Distance Sampling. *The Auk*, *124*(4), 1229–1243. https://doi.org/10.1093/auk/124.4.1229

Martínez-Moreno, J., Hogg, A. McC., England, M. H., Constantinou, N. C., Kiss, A. E., & Morrison, A. K. (2021). Global changes in oceanic mesoscale currents over the satellite altimetry record. *Nature Climate Change*, *11*(5), 397–403. https://doi.org/10.1038/s41558-021-01006-9

McCabe, R. M., Hickey, B. M., Kudela, R. M., Lefebvre, K. A., Adams, N. G., Bill, B. D., Gulland, F. M. D., Thomson, R. E., Cochlan, W. P., & Trainer, V. L. (2016). An unprecedented coastwide toxic algal bloom linked to anomalous ocean conditions. *Geophysical Research Letters*, *43*(19), 10366–10376. https://doi.org/10.1002/2016gl070023

McClatchie, S., Goericke, R., Leising, A., Auth, T. D., Bjorkstedt, E., Robertson, R. R., Broadfur, R. D., Du, X., Daly, E. A., Morgan, C. A., Chavez, F. P., Debich, A. J., Hildebrand, J., Field, J., Sakuma, K., Jacox, M. G., Kahru, M., Kudela, R., Anderson, C., Lavaniegos, B. E., Gomez-Valdes, J., Jiméz-Rosenberg, S. P. A., McCabie, R., Melin, S. R., Ohman, M. D., Sala, L. M., Peterson, B., Fisher, J., Schroeder, I. D., Bograd, S,.J., Hazen, E. I., Schneider, S. R., Golightlly, R. T., Suryan, R. M., Gladics, A. J., Loredo, S., Proquez, J. M., Thompson, A. R., Weber, E. D., Watson, W., Trainer, V., Warzybok, P., Bradley, R., & Jahncke, J. (2016). State of the California Current 2015-2016: Comparisons with the 1997-98 El Niño. *CalCOFI Reports*, *57*, 1–57.

McGillicuddy, D. J. (2014). Mechanisms of Physical-Biological-Biogeochemical Interaction at the Oceanic Mesoscale. *Annual Review of Marine Science*, *8*(1), 1–35. https://doi.org/10.1146/annurev-marine-010814-015606

Meyer-Gutbrod, E. L., Greene, C. H., Davies, K. T. A., & Johns, D. G. (2021). Ocean regime shift is driving the collapse of the north Atlantic right whale population. *Oceanography*, *34*(3), 22–31.

Miller, D. L., Rexstad, E., Thomas, L., Marshall, L., & Laake, J. L. (2019). Distance Sampling in R. *Journal of Statistical Software*, *89*(1). https://doi.org/10.18637/jss.v089.i01

Nagai, T., Gruber, N., Frenzel, H., Lachkar, Z., McWilliams, J. C., & Plattner, G. (2015). Dominant role of eddies and filaments in the offshore transport of carbon and nutrients in the California Current System. *Journal of Geophysical Research: Oceans*, *120*(8), 5318–5341. https://doi.org/10.1002/2015jc010889

Narimousa, S., & Maxworthy, T. (1989). Application of a laboratory model to the interpretation of satellite and field observations of coastal upwelling. *Dynamics of Atmospheres and Oceans*, *13*(1–2), 1–46. https://doi.org/10.1016/0377-0265(89)90032-8

Nielsen, J. M., Rogers, L. A., Brodeur, R. D., Thompson, A. R., Auth, T. D., Deary, A. L., Duffy-Anderson, J. T., Galbraith, M., Koslow, J. A., Perry, R. I. (2021). Responses of ichthyoplankton assemblages to the recent marine heatwave and previous climate fluctuations in several Northeast Pacific marine ecosystems. *Global Change Biology*, *27*(3), 506–520. https://doi.org/10.1111/gcb.15415

Ohizumi, H., Kuramochi, T., Kubodera, T., Yoshioka, M., & Miyazaki, N. (2003). Feeding habits of Dall's porpoises (Phocoenoides dalli) in the subarctic North Pacific and the Bering Sea basin and the impact of predation on mesopelagic micronekton. *Deep-Sea Research I*, 593–610.

Oliver, E. C. J., Donat, M. G., Burrows, M. T., Moore, P. J., Smale, D. A., Alexander, L. V., Benthuysen, J. A., Feng, M., Gupta, A. S., Hobday, A. J., Holbrook, N. J., Perkins-Kirkpatrick, S. E., Scannell, H. A., Straub, S. C., & Wernberg, T. (2018). Longer and more frequent marine heatwaves over the past century. *Nature Communications*, *9*(1), 1324. https://doi.org/10.1038/s41467-018-03732-9

Oliver, M. J., Kohut, J. T., Bernard, K., Fraser, W., Winsor, P., Statscewich, H., , Fredj, E., Cimino, M., Patterson-Fraser, D., & Carvalho, F. (2019). Central place foragers select ocean surface convergent features despite differing foraging strategies. *Scientific Reports*, *9*(1), 157. https://doi.org/10.1038/s41598-018-35901-7

Pauly, D., & Christensen, V. (1995). Primary production required to sustain global fisheries. *Nature*, *374*(6519), 255–257. https://doi.org/10.1038/374255a0

Pauly, D., Trites, A. W., Capuli, E., & Christensen, V. (1998). Diet composition and trophic levels of marine mammals. *ICES Journal of Marine Science*, *55*(3), 467–481. https://doi.org/10.1006/jmsc.1997.0280

Pawlowicz, R. (n.d.). M_Map: A mapping package for MATLAB (Version 1.4m). Retrieved from www.eoas.ubc.ca/~rich/map.html

Pegliasco, C., Busché, C., & Faugère, Y. (2022). Mesoscale Eddy Trajectory Atlas META3.2 Delayed-Time all satellites: version META3.2 DT allsat. Retrieved from https://doi.org/10.24400/527896/A01-2022.005.210802

Perrin, W. F. (2018). Common dolphin. In B. Würsig, J. G. M. Thewissen, & K. M. Kovacs (Eds.) *Encyclopedia of Maine Mammals, 3rd edition* (pp. 205–209). London, United Kingdom: Academic Press.

Perrin, W. F., Thieleking, J. L., Walker, W. A., Archer, F. I., & Robertson, K. M. (2011). Common bottlenose dolphins (Tursiops truncatus) in California waters: Cranial differentiation of coastal and offshore ecotypes. *Marine Mammal Science*, *27*(4), 769–792. https://doi.org/10.1111/j.1748-7692.2010.00442.x

Poloczanska, E. S., Burrows, M. T., Brown, C. J., Molinos, J. G., Halpern, B. S., Hoegh-Guldberg, O., Kappel, C. V., Moore, P.J., Richardson, A.J., Schoeman, D.S., & Sydeman, W.J.. (2016). Responses of Marine Organisms to Climate Change across Oceans. *Frontiers in Marine Science*, *3*, 62. https://doi.org/10.3389/fmars.2016.00062

Rechsteiner, E. U., Rosen, D. A. S., & Trites, A. W. (2013). Energy requirements of Pacific white-sided dolphins (*Lagenorhynchus obliquidens*) as predicted by a bioenergetic model. *Journal of Mammalogy*, *94*(4), 820–832. https://doi.org/10.1644/12-mamm-a-206.1

Rohr, J. J., Fish, F. E., & Gilpatrick, J. W. (2002). Maximum swim speeds of captive and free-ranging delphinids: critical analysis of extraordinary performance. *Marine Mammal Science*, *18*(1), 1–19. https://doi.org/10.1111/j.1748-7692.2002.tb01014.x

Romagosa, M., Pérez-Jorge, S., Cascão, I., Mouriño, H., Lehodey, P., Pereira, A., Marques, T. A., Matias, L., & Silva, M. A. (2021). Food talk: 40-Hz fin whale calls are associated with prey biomass. *Proceedings of the Royal Society B*, *288*(1954), 20211156. https://doi.org/10.1098/rspb.2021.1156

Roman, J., & McCarthy, J. J. (2010). The Whale Pump: Marine Mammals Enhance Primary Productivity in a Coastal Basin. *PLoS ONE*, *5*(10), e13255. https://doi.org/10.1371/journal.pone.0013255

Roman, J., Estes, J. A., Morissette, L., Smith, C., Costa, D., McCarthy, J., Nation, J., Nicol, S., Pershing, A., & Smetacek, V. (2014). Whales as marine ecosystem engineers. *Frontiers in Ecology and the Environment*, *12*(7), 377–385. https://doi.org/10.1890/130220

Rosel, P. E., Dizon, A. E., & Heyning, J. E. (1994). Genetic analysis of sympatric morphotypes of common dolphins (genus Delphinus). *Marine Biology*, *119*(2), 159–167. https://doi.org/10.1007/bf00349552

Rossi, V., López, C., Hernández-García, E., Sudre, J., Garçon, V., & Morel, Y. (2009). Surface mixing and biological activity in the four Eastern Boundary Upwelling Systems. *Nonlinear Processes in Geophysics*, *16*(4), 557–568. https://doi.org/10.5194/npg-16-557-2009

Rubio, A., Caballero, A., Orfila, A., Hernández-Carrasco, I., Ferrer, L., González, M.,, Solabarrieta, L., Made,r J.. (2018). Eddy-induced cross-shelf export of high Chl-a coastal waters in the SE Bay of Biscay. *Remote Sensing of Environment*, *205*, 290–304. https://doi.org/10.1016/j.rse.2017.10.037

Rykaczewski, R. R., & Checkley, D. M. (2008). Influence of ocean winds on the pelagic ecosystem in upwelling regions. *Proceedings of the National Academy of Sciences*, *105*(6), 1965–1970. https://doi.org/10.1073/pnas.0711777105

Sabarros, P., Ménard, F., Lévénez, J., Tew-Kai, E., & Ternon, J. (2009). Mesoscale eddies influence distribution and aggregation patterns of micronekton in the Mozambique Channel. *Marine Ecology Progress Series*, *395*, 101–107. https://doi.org/10.3354/meps08087

Santora, J. A., Sydeman, W. J., Schroeder, I. D., Wells, B. K., & Field, J. C. (2011). Mesoscale structure and oceanographic determinants of krill hotspots in the California Current: Implications for trophic transfer and conservation. *Progress in Oceanography*, *91*(4), 397–409. https://doi.org/10.1016/j.pocean.2011.04.002

Santora, J. A., Mantua, N. J., Schroeder, I. D., Field, J. C., Hazen, E. L., Bograd, S. J., , Sydeman, W. J., Wells, B. K., Calambokidis, J., Saez, L., Lawson, D., & Forney, K. A. (2020). Habitat compression and ecosystem shifts as potential links between marine heatwave and record whale entanglements. *Nature Communications*, *11*(1), 536. https://doi.org/10.1038/s41467-019-14215-w

Savoca, M. S., Czapanskiy, M. F., Kahane-Rapport, S. R., Gough, W. T., Fahlbusch, J. A., Bierlich, K. C., Segre, P.S., Clemente, J.D., Penry, G. S., Wiley, D. N., Calambokidis, J., Nowacek, D. P., Johnston, D. W., Pyenson, N. D., Friedlaender, A. S., Hazen, E. L., & Goldbogen, J. A. (2021). Baleen whale prey consumption based on high-resolution foraging measurements. *Nature*, *599*(7883), 85–90. https://doi.org/10.1038/s41586-021-03991-5

Scales, K. L., Miller, P. I., Hawkes, L. A., Ingram, S. N., Sims, D. W., & Votier, S. C. (2014). REVIEW: On the Front Line: frontal zones as priority at-sea conservation areas for mobile marine vertebrates. *Journal of Applied Ecology*, *51*(6), 1575–1583. https://doi.org/10.1111/1365-2664.12330

Scales, K. L., Schorr, G. S., Hazen, E. L., Bograd, S. J., Miller, P. I., Andrews, R. D., Zerbini, A. N., & Falcone, E. A. (2017). Should I stay or should I go? Modelling year-round habitat

suitability and drivers of residency for fin whales in the California Current. *Diversity and Distributions*, *23*(10), 1204–1215. https://doi.org/10.1111/ddi.12611

Scales, K. L., Hazen, E. L., Jacox, M. G., Castruccio, F., Maxwell, S. M., Lewison, R. L., & Bograd, S. J. (2018). Fisheries bycatch risk to marine megafauna is intensified in Lagrangian coherent structures. *Proceedings of the National Academy of Sciences*, *115*(28), 201801270. https://doi.org/10.1073/pnas.1801270115

Shane, S. H. (1995). Relationship between pilot whales and Risso's dolphins at Santa Catalina Island, California, USA. *Marine Ecology Progress Series*, *123*, 5–11. https://doi.org/10.3354/meps123005

Simonis, A., Roch, M., Bailey, B., Barlow, J., Clemesha, R., Iacobellis, S., Hildebrand, J., & Baumann-Pickering, S. (2017). Lunar cycles affect common dolphin *Delphinus delphis* foraging in the Southern California Bight. *Marine Ecology Progress Series*, *577*, 221–235. https://doi.org/10.3354/meps12247

Širović, A., Williams, L. N., Kerosky, S. M., Wiggins, S. M., & Hildebrand, J. A. (2013). Temporal separation of two fin whale call types across the eastern North Pacific. *Marine Biology*, *160*(1), 47–57. https://doi.org/10.1007/s00227-012-2061-z

Smale, D. A., Wernberg, T., Oliver, E. C. J., Thomsen, M., Harvey, B. P., Straub, S. C., Burrows, M. T., Alexander, L. V., Benthuysen, J. A., Donat, M. G., Feng, M., Hobday, A. J., Holbrook, N. J., Perkins-Kirkpatrick, S. E., Scannell, H. A., Gupta, A. S., Payne, B. L., & Moore, P. J. (2019). Marine heatwaves threaten global biodiversity and the provision of ecosystem services. *Nature Climate Change*, *9*(4), 306–312. https://doi.org/10.1038/s41558-019-0412-1

Smultea, M. A., & Jefferson, T. A. (2014). Changes in Relative Occurrence of Cetaceans in the Southern California Bight: A Comparison of Recent Aerial Survey Results with Historical Data Sources. *Aquatic Mammals*, *40*(1), 32–43. https://doi.org/10.1578/am.40.1.2014.32

Soldevilla, M., Wiggins, S., & Hildebrand, J. (2010). Spatio-temporal comparison of Pacific white-sided dolphin echolocation click types. *Aquatic Biology*, *9*, 49–62. https://doi.org/10.3354/ab00224

Sprintall, J., Cravatte, S., Dewitte, B., Du, Y., & Gupta, A. S. (2020). El Niño Southern Oscillation in a Changing Climate. *Geophysical Monograph Series*, 337–359. https://doi.org/10.1002/9781119548164.ch15

Stegmann, P. M., & Schwing, F. (2007). Demographics of mesoscale eddies in the California Current. *Geophysical Research Letters*, *34*(14). https://doi.org/10.1029/2007gl029504

Stukel, M. R., Aluwihare, L. I., Barbeau, K. A., Chekalyuk, A. M., Goericke, R., Miller, A. J., Ohman, M. D., Ruacho, A., Song, H., Stephens, B. M., & Landry, M. R. (2017). Mesoscale ocean fronts enhance carbon export due to gravitational sinking and subduction. *Proceedings*

of the National Academy of Sciences, *114*(6), 1252–1257. https://doi.org/10.1073/pnas.1609435114

Suryan, R. M., Arimitsu, M. L., Coletti, H. A., Hopcroft, R. R., Lindeberg, M. R., Barbeaux, S. J., Batten, S. D., Bur,t W. J., Bishop, M. A., Bodkin, J. L., Brenner, R., Campbell, R.,W., Cushing, D. A., Danielson, S. L., Dorn, M. W., Drummond, B., Esler, D., Gelatt ,T., Hanselman, D. H., Hatch, S. A., Haught, S., Holderied, K., Iken, K., Irons, D. B., Kettle, A. B., Kimmel, D. G., Konar, B., Kuletz, K. J., Laurel, B. J., Maniscalco, J. M., Matkin, C., McKinstry, C. A. E., Monson, D. H., Moran, J. R., Olsen, D., Palsson, W. A., Pegau, W. S., Piatt, J. F., Rogers, L. A., Rojek, N. A., Schaefer, A., Spies, I. B., Straley, J. M., Strom, S. L., Sweeney, K. L., Szymkowiak, M., Weitzman, B. P., Yasumiishi, E.M., & Zador, S. G.. (2021). Ecosystem response persists after a prolonged marine heatwave. *Scientific Reports*, *11*(1), 6235. https://doi.org/10.1038/s41598-021-83818-5

Sydeman, W. J., Santora, J. A., Thompson, S. A., Marinovic, B., & Lorenzo, E. D. (2013). Increasing variance in North Pacific climate relates to unprecedented ecosystem variability off California. *Global Change Biology*, *19*(6), 1662–1675. https://doi.org/10.1111/gcb.12165

Szesciorka, A. R., Ballance, L. T., Širović, A., Rice, A., Ohman, M. D., Hildebrand, J. A., & Franks, P. J. S. (2020). Timing is everything: Drivers of interannual variability in blue whale migration. *Scientific Reports*, *10*(1), 7710. https://doi.org/10.1038/s41598-020-64855-y

Taylor, B. L., Martinez, M., Gerrodette, T., Barlow, J., & Hrovat, Y. N. (2007). Lessons from monitoring trends in abundance of marine mammals. *Marine Mammal Science*, *23*(1), 157–175. https://doi.org/10.1111/j.1748-7692.2006.00092.x

Torrence, C., & Compo, G. P. (1998). A Practical Guide to Wavelet Analysis. *Bulletin of the American Meteorological Society*, *79*(1), 61–78. https://doi.org/10.1175/1520-0477(1998)079<0061:apgtwa>2.0.co;2

Toste, R., Assad, L. P. de F., & Landau, L. (2019). Changes in the North Pacific Current divergence and California Current transport based on HadGEM2-ES CMIP5 projections to the end of the century. *Deep Sea Research Part II: Topical Studies in Oceanography*, *169*, 104641. https://doi.org/10.1016/j.dsr2.2019.104641

Vignudelli, S., Birol, F., Benveniste, J, Fu, L.L., & Picot, N. (2019). Satellite Altimetry Measurements of Sea Level in the Coastal Zone. *Surv Geophys* 40, 1319–1349 https://doi.org/10.1007/s10712-019-09569-1 Waugh, D. W., & Abraham, E. R. (2008). Stirring in the global surface ocean. *Geophysical Research Letters*, *35*(20). https://doi.org/10.1029/2008gl035526

Vu, E. T. A. (2015). *Habitat use of calling baleen whales in the southern California Current Ecosystem*. Doctoral dissertation. University of California San Diego.

Walker, W. A., Leatherwood, S., Goodrich, K. R., Perrin, W. F., & Stroud, R. K. (1986). Geographical variation and biology of the Pacific white-sided dolphin, Lagenorhynchus

obliquidens, in the north-eastern Pacific. In M. M. Bryden & R. Harrison (Eds.), *Research on Dolphins* (pp. 441–465). Oxford: Claredon Press.

Walker, H. J., Hastings, P. A., Hyde, J. R., Lea, R. N., Snodgrass, O. E., & Bellquist, L. F. (2020). Unusual occurrences of fishes in the Southern California Current System during the warm water period of 2014–2018. *Estuarine, Coastal and Shelf Science*, *236*, 106634. https://doi.org/10.1016/j.ecss.2020.106634

Warlick, A. J., Huggins, J. L., Lambourn, D. M., Duffield, D. A., D'Alessandro, D. N., Rice, J. M., , Calambokidis, J., Hanson, M. B., Gaydos, J. K., Jeffries, S. J., Olson, J. K., Scordino, J. J., Akmajian, A. M., Klope, M., Berta, S., Dubpernell, S., Carlson, B., Riemer, S., Hodder, J., Souze, V., Elsby, A., King, C., Wilkinson, K., Boothe, T., & Norman, S. A. (2022). Cetacean Strandings in the US Pacific Northwest 2000–2019 Reveal Potential Linkages to Oceanographic Variability. *Frontiers in Marine Science*, *9*. https://doi.org/10.3389/fmars.2022.758812

Watson, J. R., Fuller, E. C., Castruccio, F. S., & Samhouri, J. F. (2018). Fishermen Follow Fine-Scale Physical Ocean Features for Finance. *Frontiers in Marine Science*, *5*, 46. https://doi.org/10.3389/fmars.2018.00046

Weber, E. D., Auth, T. D., Baumann-Pickering, S., Baumgartner, T. R., Bjorkstedt, E. P., Bograd, S. J., Burke, B.J., Cadena-Ramírez, J. L., Daly, E. A., de la Cruz, M., Dewar, H., Field, J. C., Fisher, J. L., Giddings, A., Goericke, R., Gomez-Ocampo, E., Gomez-Valdes, J., Hazen, E. L., Hildebrand, J., Horton, C. A., Jacobson, K. C., Jacox, M. G., Jahncke, J., Kahru, M., Kudela, R. M., Lavaniegos, B. E., Leising, A., Melin, S. R., Miranda-Bojorquez, L. E., Morgan, C.A., Nickels, C. F., Orben, R. A., Porquez, J. M,. Portner, E. J., Robertson, R. R., Rudnick, D. L., Sakuma, K. M., Santora, J. A., Schroeder, I. D., Snodgrass, O. E., Sydeman, W. J., Thompson, A. R., Thompson, S. A., Trickey, J. S., Villegas-Mendoza, J., Warzybok, P., Watson, W., & Zeman, S. M. (2021). State of the California Current 2019–2020: Back to the Future With Marine Heatwaves? *Frontiers in Marine Science*, *8*, 709454. https://doi.org/10.3389/fmars.2021.709454

Weelden, C. van, Towers, J. R., & Bosker, T. (2021). Impacts of climate change on cetacean distribution, habitat and migration. *Climate Change Ecology*, *1*, 100009. https://doi.org/10.1016/j.ecochg.2021.100009

Wiggins, S. M., Frasier, K. E., Henderson, E. E., & Hildebrand, J. A. (2013). Tracking dolphin whistles using an autonomous acoustic recorder array. *The Journal of the Acoustical Society of America*, *133*(6), 3813–3818. https://doi.org/10.1121/1.4802645

Williams, T. M. (2018). Swimming. In B. Würsig, K. M. Kovacs, & J. G. M. Thewissen (Eds.), *Encyclopedia of Marine Mammals, 3rd edition* (pp. 970–979). Academic Press.

Wisheu, I. C. (1998). How Organisms Partition Habitats: Different Types of Community Organization Can Produce Identical Patterns. *Oikos*, *83*(2), 246. https://doi.org/10.2307/3546836

Zaba, K. D., Franks, P. J. S., & Ohman, M. D. (2021). The California Undercurrent as a Source of Upwelled Waters in a Coastal Filament. *Journal of Geophysical Research: Oceans*, *126*(2). https://doi.org/10.1029/2020jc016602

Zhao, D., Xu, Y., Zhang, X., & Huang, C. (2021). Global chlorophyll distribution induced by mesoscale eddies. *Remote Sensing of Environment*, *254*, 112245. https://doi.org/10.1016/j.rse.2020.112245